

Die approbierte Originalversion dieser Diplom-/Masterarbeit ist an der
Hauptbibliothek der Technischen Universität Wien aufgestellt
(<http://www.ub.tuwien.ac.at>).

The approved original version of this diploma or master thesis is available at the
main library of the Vienna University of Technology
(<http://www.ub.tuwien.ac.at/englweb/>).



TECHNISCHE
UNIVERSITÄT
WIEN

Vienna University of Technology

Unterschrift des Betreuers

DIPLOMARBEIT

Impedance Spectroscopy on Resonant Systems

Ausgeführt am Institut für
Angewandte Physik
der Technischen Universität Wien

unter der Leitung von

Ao.Univ.Prof. Dipl.-Ing. Dr.techn. Martin Gröschl

durch

Ilgar Beniaminov
Matrikelnummer: 0425180
Handelskai 214/24/44
1020 Wien

Wien, 31. Jänner 2013

Unterschrift

Acknowledgements

I would like to thank my family for their love and support during my studies, especially my brother, Eldar Beniaminov, B.Sc., an engineer himself, who always encouraged and motivated me in many situations.

I also wish to thank my advisor, Prof. Martin Gröschl, for his guiding suggestions and interesting discussions. Further, I am very obliged to Prof. Michael Schmid, whose insights helped to implement the locus fit algorithm. Speaking of software, I'd like to thank the staff of SinePhase Instruments GmbH, particularly Dipl.-Ing. Plamen Kostov for his major support regarding the reprogramming of the hardware communication.

And finally, I'd like to thank my colleagues Dipl.-Ing. Stanislav Bocanski and Dipl.-Ing. Erwin Mayrhofer for their supporting discussions and for helping to create a great working environment in the *Sensors and Ultrasonics* work group.

Abstract

At the beginning of this study three different impedance analyzers, *QxSens* (developed at the Institute of Applied Physics, Vienna University of Technology), *Impedance Analyzer 16777k* (SinePhase Instruments GmbH) and *Agilent 4395A* were evaluated with regards to mobility, accuracy and long term maintenance. The prime aim was to analyse the dynamic frequency scan algorithm of the *QxSens* system, which uses small frequency steps when resonances are detected and large steps between resonances in admittance spectra. Then to implement it within an elementary version of the *Impedance Analyzer 16777k* software. Finally, a least-squares fit procedure had to be found for accurate data evaluation.

It was discovered that the *QxSens* algorithm did not produce the same measurement results on the *Impedance Analyzer 16777k*, thus leading the focus of this work on alternative methods for resonance peak detection, such as the area change algorithm. It uses a purely geometric approach, where the difference between the areas of the last two triangles, that are built out of three admittance vectors in the locus representation, are compared to empirically found multiples of the moving average of the last 28 area differences as decision criteria to dynamically change the frequency steps for admittance measurements. The applied least-squares fit algorithm is based on the locus data, where in the first step the differences of the locus radii are minimised in order to calculate the centre coordinates and radius of a fitted admittance circle and in the second step the differences tangential to the admittance circle are minimised. Thus yielding accurate values for the resonance frequency f_s , the quality factor Q and the Butterworth-Van-Dyke equivalent circuit parameters. The algorithms were implemented in a version of the original software of the *Impedance Analyzer 16777k* and equipped with easy to use data analysing possibilities.

The results indicated that the new area detection algorithm in combination with the impedance analyzer from SinePhase measures the resonances of ceramic type sensors as well as quartz crystal resonators with high point densities and produces fit results with similar accuracy as the high end, but expensive reference device *Agilent 4395A*. The principal conclusion was that the *Impedance Analyzer 16777k* with the new software offers a truly mobile, small-sized, light, low-cost and easy to use measurement device to dynamically scan admittance spectra of various piezoelectric sensors with high accuracy and considerably short measurement times.

Kurzfassung

Zu Beginn dieser Arbeit wurden die drei Impedanz - Messgeräte *QxSens* (entwickelt am Institut für Angewandte Physik der Technischen Universität Wien), *Impedance Analyzer 16777k* (SinePhase Instruments GmbH) und *Agilent 4395A* hinsichtlich ihres mobilen Einsatzes, Messgenauigkeit und Langzeitwartung verglichen. Das Hauptziel bestand darin, den Resonanzsuch-Algorithmus des *QxSens* Systems, welches die Frequenzschrittweite bei Resonanzen eines Admittanz-Spektrums verkleinert und zwischen diesen vergrößert, zu analysieren und in eine Basissoftware des *Impedance Analyzer 16777k* zu implementieren. Schließlich musste eine Methode der kleinsten Fehlerquadrate gefunden werden, um die gemessenen Daten zu fitten und genau zu evaluieren.

Es wurde festgestellt, dass der *QxSens*-Algorithmus mit dem *Impedance Analyzer 16777k* Messresultate lieferte, die mit jenen des *QxSens* Messsystems nicht vergleichbar waren. Daher musste andere Lösungen für die dynamische Resonanzsuche gefunden werden. Einer dieser Algorithmen nutzt einen geometrischen Ansatz, indem die Flächenunterschiede zweier Dreiecke, die sich aus drei Admittanz-Vektoren in der Ortskurve zusammensetzen, mit empirisch gefundenen Vielfachen des gleitenden Mittelwerts der jeweils letzten 28 Flächendifferenzen verglichen werden, um ein Entscheidungskriterium für die Frequenzschrittweitenänderung zu liefern. Der angewandte Fit-Algorithmus verwendet die Daten in der Ortskurvendarstellung. Im ersten Schritt werden die Unterschiede in den Radien für den Fit einer Ortskurve minimiert, um die Mittelpunktskordinaten eines Admittanzkreises und dessen Radius zu bestimmen. Darüber hinaus werden in einem zweiten Schritt die Differenzen tangential zum Admittanzkreis minimiert. Dies führt in weiterer Folge zur genauen Bestimmung der Resonanzfrequenz f_s , der Güte Q und der Werte des Butterworth-Van-Dyke Ersatzschaltbilds des Resonators. Die beschriebenen Prozeduren wurden in einer Softwareversion des *Impedance Analyzer 16777k* implementiert und mit leicht handzuhabenden Datenanalyse-Möglichkeiten ausgestattet.

Die Ergebnisse der Messungen zeigen, dass die neue Methode mit dem Impedanz-Messgerät von SinePhase, Flächenunterschiede in der Ortskurve zu detektieren, für Keramiksensoren als auch für Quarze hohe Messgenauigkeit im Bereich der Resonanzen und vergleichbare Fit-Parameter wie das High-end-Messgerät *Agilent 4395A* liefert. Aufgrund der Messdaten konnte die Schlussfolgerung gezogen werden, dass der *Impedance Analyzer 16777k* mit den neuen Softwarefeatures ein Admittanz-Messsystem mit schneller dynamischer Resonanzsuche darstellt, welches aufgrund der sehr kleinen und leichten Bauweise des kostengünstigen Gerätes, sehr gut für den mobilen Einsatz geeignet ist und eine hohe Genauigkeit für die Analyse von Resonanzen aufweist.

Contents

1	Introduction	6
2	Theory	10
2.1	Basics of admittance measurement	10
2.2	Probe compensation	12
2.3	Concept of the Locus-fit	13
3	Methodology	17
3.1	Description of the problem	17
3.2	Admittance measurement devices	18
3.2.1	QxSens	18
3.2.2	SinePhase Impedance Analyzer 16777k	21
3.2.3	Agilent 4395A Impedance Analyzer	24
3.2.4	Overview	26
3.3	Development of the resonance peak detection algorithm	27
3.3.1	The QxSens algorithm	27
3.3.2	”Zero-crossing” method	32
3.3.3	Phase angle detection in the admittance locus	35
3.3.4	Detection of the area change in the admittance locus	37
3.4	Locus-fit and accurate data evaluation	44
4	Admittance scan software	56
4.1	Software state diagram and procedures	56
4.1.1	Overview	56
4.1.2	Measurement procedure	57
4.1.3	Locus-fit procedure	58
4.2	Software user interface	59
4.2.1	User manual	60
4.2.2	Usability aspects	62
5	Results and Discussion	64
5.1	Ceramic type PZT	64
5.1.1	PIC 255	64
5.1.2	PIC 181	70
5.2	Quartz crystal resonators	76

<i>CONTENTS</i>	2
5.3 Discussion	81
6 Conclusion and Recommendations	85
Bibliography	86

List of Figures

2.1	Admittance locus and characteristic frequencies	11
2.2	Butterworth-Van-Dyke equivalent circuit	12
2.3	Admittance measurement set-up and probe compensation	13
2.4	Term definitions of an admittance circle	15
3.1	QxSens schematic diagram of signal conditioning	19
3.2	QxSens hardware concept	20
3.3	QxSens software user interface	21
3.4	SinePhase Impedance Analyzer 16777k hardware	22
3.5	SinePhase Impedance Analyzer 16777k measurement example	23
3.6	Agilent 4395A hardware	25
3.7	Agilent 4395A admittance measurement example	25
3.8	SinePhase's elementary demo software	27
3.9	QxSens basic idea behind the moving average of $ \Delta Y^2 $	29
3.10	Flow chart of the QxSens algorithm	30
3.11	Measurement of a ceramic type sensor with QxSens algorithm	32
3.12	Measurement of a quartz sensor with <i>QxSens</i> algorithm	33
3.13	Basic idea behind the "zero-crossing" algorithm	34
3.14	Admittance scan with the "zero-crossing" algorithm	34
3.15	Measurement showing the limits of the "zero-crossing" algorithm	35
3.16	Admittance phase angle plot	35
3.17	Using admittance phase angle for resonance detection	36
3.18	Basic idea behind the area change detection in the admittance locus	37
3.19	Strict monotonic increase of admittance values	39
3.20	Measurement example with the so called "Noise-Level" parameter	40
3.21	Flow chart of the area detection algorithm	42
3.22	Measurement of a ceramic type sensor with area detection algorithm	44
3.23	Measurement of a quartz crystal resonator with area detection algorithm	45
3.24	Initial fit procedure of the original SinePhase software	46
3.25	Determination of the frequency interval for the Locus-Fit	47
3.26	Extending the Butterworth-Van-Dyke model with the parameter R_p	50
3.27	Shifting the admittance circle into the origin	51
3.28	Flow chart of the Locus-Fit algorithm	54
3.29	Demonstration of the Locus-Fit algorithm	55

4.1	Software state diagram	57
4.2	Data flow diagram of the measurement procedure	58
4.3	Data flow diagram of the Locus-Fit procedure	59
4.4	Software user interface	60
5.1	PIC 255: Admittance spectrum - overview	64
5.2	PIC 255 - Admittance scan of resonance A	66
5.3	PIC 255 - Admittance scan of resonance B	67
5.4	PIC 255 - Admittance scan of resonance C	68
5.5	PIC 181: Admittance spectrum - overview	70
5.6	PIC 181 - Admittance scan of resonance A	72
5.7	PIC 181 - Admittance scan of resonance B	73
5.8	PIC 181 - Admittance scan of resonance C	74
5.9	Admittance scan - Quartz A	77
5.10	Admittance scan - Quartz B	78
5.11	Admittance scan - Quartz C	79

List of Tables

3.1	Pros and cons QxSens measurement system	22
3.2	Pros and cons Impedance Analyzer 16777k	24
3.3	Pros and cons Agilent 4395A	26
3.4	Device overview	26
3.5	Measurement comparison of a ceramic PZT with QxSens algorithm .	31
3.6	Measurement comparison of a quartz sensor with QxSens algorithm .	31
5.1	PIC 255 - Measurement input parameters	65
5.2	PIC 255 - Fit results of resonances A-C	69
5.3	PIC 181 - Measurement input parameters	71
5.4	PIC 181 - Fit results of resonances A-C	75
5.5	Measurement input parameters for the quartz crystal resonators A-C	76
5.6	Fit results of the quartz crystal resonators A-C	80

Chapter 1

Introduction

Piezoelectric resonators have become a very reliable and universal measurement tool to control quality in many industrial production processes as well as used in many fields of research to determine different physical quantities. The applications range from temperature control, measurement of viscosity, density, speed of sound in liquids to film thickness, humidity, pressure, etc. The basis of these measurements is the inverse piezoelectric effect, which occurs when resonant sensors, vibrate due to applied AC voltage. Generally speaking the change of resonance frequency and his Q factor between two measurement environments such as air and liquids is used to calculate physical quantities. A common and needfully example is the measurement of viscosity of specific oils.

These mechanical resonant systems can be seen as a series resonant circuit in electrical terms with a parallel capacitance due to the electrodes of the sensors. The inductance L and capacitance C in the equivalent circuit leads to a phase shift of the current and the voltage which again leads to a complex impedance of the resonator. Moreover the inverse of the impedance, the admittance, is an indicator for the resonances. By measuring the real and imaginary part of the piezoelectric sensor's admittance, it is possible to analyse the vibrations in the frequency spectrum. These resonance frequencies are important, because their knowledge determine how to design new measurement applications. Therefore the admittance spectrum of a piezoelectric sensor is vital to get the information of the resonance frequencies and their quality factors (Q factor).

Theoretical approaches of piezoelectric structures based on a general transfer matrix description allows through simple matrix multiplications the calculation of the electrical admittance for any frequency and the entire resonance frequency spectrum [1]. In personal talks with the work group of Dr. Nowotny and Dr. Gröschl further developments of the above theoretical attempts, whereby the resonator at its both boundary surfaces is in contact with boundary media of infinite thickness, the need for a admittance measurement device with dynamically adjustable frequency steps with high frequency resolution for resonances for experimental verification was discussed. Measurement applications with quartz viscosity sensors and quartz temperature sensors presented in [2] and the described test measurements for cellulosic liquids (e.g. Lyocell) illustrate the demand for admittance measurement systems

such as the *QxSens* especially for rough industry environments used for on-line controlling of viscosity. An other application example is the assembling of a sensor in bioreactors, whereby ultrasonic particle manipulation is combined with infra-red spectroscopy for bioprocess monitoring [3],[4]. The ultrasonic wave generation is created by an piezoelectric resonator made of PZT (a composition of lead, zirconate and titanate). To optimize the particle manipulation, where they are forced in the nodal regions of the standing wave, exact resonance frequency of the sensor must be measured prior particularly it depends on the thickness of every single PZT.

Each application uses different type of sensors and it is essential to know the exact resonance frequencies in the admittance spectrum to design the measurement application. The problem lies in scanning these resonance spectra with high frequency resolution for typical frequency bandwidths of two MHz or more and in a reasonable time. The frequency half width of the resonance is usually many magnitudes smaller than the distance between the resonances. Therefore when the measurement is done with a linear frequency step width then depending on the frequency half width of the resonances two disadvantages can occur. In the first case, when the frequency step width is much smaller than the resonance's frequency half width, then the measurement can take considerable time. The second disadvantage may arise, when the frequency step width is much higher then the resonance's half width and therefore resonances can be skipped over. The first objective lies therefore the dynamic change of the frequency step width during the admittance measurement. This will lead on the one hand to the decisive reduction of measurement time and on the other hand to an accurate scan of most relevant resonances with high frequency resolution. The second goal is to implement a fitting procedure, so that it is able to fit the measured data within the locus curve of the admittance and calculate resonance frequency, Q factor and the parameters of the equivalent series resonance circuit.

In [5] a measurement system is presented especially for recording the resonances of piezoelectric quartz crystal resonators with high Q factors. It is important to point out that the algorithm needed four input parameters to vary the frequency steps dynamically. That means using small frequency steps when a resonance is detected and large steps between the resonances. The four input parameters are Δf_{min} , Δf_{max} , ΔY_{min} and ΔY_{max} and the algorithm compares the last two to the change of admittance, which is the absolute value $|Y_2 - Y_1|$. If the change is larger than ΔY_{max} , usually because of a resonance, then the last measurement is discarded and the frequency step reduced by 20%, but considering the lower limit of Δf_{min} . After passing a resonance for example the change in admittance is usually smaller than ΔY_{min} . Therefore the measured point is discarded again and the frequency step increased by 20%, but not beyond its upper limit Δf_{max} . Furthermore the calculation of the equivalent circuit parameters is the result of a least-squares fit of the measured data in the admittance locus. On the one hand the advantage with this method is that it can detect great number of resonance (300) for a plan-convex AT-cut quartz crystals with high quality factor of 10^6 and even resonance couplings, but on the other hand the measurement time is considerably long and the parameters have to be chosen very carefully for each sensor for the algorithm to find the harmonic and an-harmonic overtones.

The *QxSens* is another measurement system that was developed over the course of Schnitzer's PhD-thesis [2] to support various sensor types, using also a frequency scanning algorithm for resonance peaks detection. In contrast to [5] the criteria for decreasing or increasing the frequency steps were the moving average of $|Y_n^2 - Y_{n-1}^2|$ of the last 15 measured admittance values compared to empirically found values. Besides tested results with different resonant piezoelectric crystal sensors for viscosity of liquids (e.g. lubricating oils) and their calibration methods, this work also promises a reduction of spurious influence of the sensor's parallel capacitance due to the electrodes. A disadvantage of the electronics is that because it is based on a voltage divider principle with a conventional ohmic resistor to measure the voltage change of the sensors, the resistance of the piezoelectric resonator has to be at the same order of magnitude to avoid spurious effects. Hence the voltage divider resistor must be changed for various sensor types for great resistance differences. The *QxSens* system was developed for a PC-based and mobile version that can be used via USB connection. The software was implemented on a virtual instrument interface software called LabVIEW®.

One of the commercial devices to measure the admittance spectrum is the Agilent 4595A in impedance analyser mode from the company Agilent Technologies Japan, Ltd. The advantages of this system is the high accuracy therefore it will be used as reference apparatus over the course of this work. In spite of a great variety of features such as averaging the measurement over 16 times [6] or calculating the Butterworth-Van Dyke equivalent circuit [5] for resonances, the frequency scanning is just done linearly. Furthermore the calibration procedures must be elaborated carefully prior to a measurement and are very time-consuming. Incidentally due to the size and weight of the device it is not suitable for a mobile use, which is one of the main requirements we set out at the beginning.

Another admittance measurement device is the *Impedance Analyzer 16777k* from the company SinePhase Instruments GmbH, that performs a proprietary method for vector voltage multiplication using an accurate reference voltage. This leads therefore to high accuracy over a wide frequency range. It is a commercial apparatus and comes also with a PC-based software based on Labview® that provides probe compensation and offers basic data plot possibilities for impedance and admittance measurements [7]. The computer connection is done over USB cable. Moreover the conductance of resonances can be used to perform a fit based on the Lorentz-function. The advantages of this device may be summarised as follows, the size and weight of the apparatus is considerably small compared to all the above systems, therefore very suitable for mobile use in laboratories where the sensors may be incorporated in measuring equipment or immersed in liquids, and as well as the probe compensation and calibration is provided within the basis software for simple usage. It is true that these advantages outweigh the ones from all other presented devices, yet the fact remains that the software has only implemented a linear frequency scan method. Therefore the aim of this work is primarily to take the approach for the dynamic frequency scan of [2] and implement it in a elementary software version of the *Impedance Analyzer 16777k* from SinePhase. Depending on the measurement and implementation results, it is desirable to evaluate possible improvements of the

scan algorithm for the resonance peak detection. Furthermore a least-squares fit of the measured data according to the description of [5] is designated, with the result that resonance frequencies, Q factors and their equivalent circuit parameters can be evaluated. The offspring of this work is planned to be an admittance measurement software for various piezoelectric sensors provided that the frequency ranges of the resonance frequencies are usually unknown. The question is, how can a scan algorithm be designed that needs as few input parameters as possible, can be applied for various types of resonators with big quality factor differences, simultaneously is working faster as the presented devices, but with the same or even better frequency resolution? Since this software is first and foremost scheduled to be implemented in the original application of the commercial device *Impedance Analyzer 16777k*, but also for the use in the work group *Sensors and Ultrasonics* at the Institute of Applied Physics (IAP), there must be put some efforts to improve the usability for the users. On the whole the aim of this work is to combine the advantages of the *Impedance Analyzer 16777k* device, the algorithm of the *QxSens* with possible improvements and the fitting procedures of [5] to create a universal admittance measurement system for various piezoelectric resonators assuming unknown resonance frequencies and Q factors that is ease to use, mobile, light and doesn't require any maintenance work.

Chapter 2

Theory

2.1 Basics of admittance measurement

It is a well-known that for the determination of the electrical properties of piezoelectric resonators, the admittance is an important parameter for characterising the sensor's behaviour. The electronic measurement systems to govern the electric impedance or admittance spectra are the so called impedance analyzers. In order to derive physical measured variables, such as force, temperature, viscosity etc., which have varyingly strong influences on piezoelectric resonator vibrations, there is a necessity to measure the electrical parameters of the sensors with high precision.

The admittance \mathbf{Y} is a complex quantity and can be defined as the reciprocal of the total resistance a resonator has at a the flow of an alternating current at a given frequency. The complex plane, in which the admittance is represented as a vector, is called locus. It consists of a real part or conductance G and the an imaginary part or susceptance B (see fig. 2.1). The mathematical relations for G , B , \mathbf{Y} and the vector's phase angle φ is given by the following equations:

$$\begin{aligned}\mathbf{Y} &= G + jB = (Y, \varphi) \\ G &= Y \cos(\varphi) \\ B &= Y \sin(\varphi) \\ Y &= \sqrt{G^2 + B^2} \\ \varphi &= \arctan\left(\frac{B}{G}\right)\end{aligned}\tag{2.1}$$

Admittance circle of a resonance and its characteristic points

The resonance phenomenon on resonant systems can be seen as a periodical exchange between two energy forms, characterised by a resonance frequency. The Butterworth-Van-Dyke equivalent circuit (see fig. 2.2) is used to model this for piezoelectric resonators [8]. The motional branch is a series circuit with a resistor, an inductor and a capacitor. The energy, stored in the electrical field across the capacitor, is exchanged trough current, that flows into the inductor, storing magnetic energy associated with the magnetic field produced by that current in the inductor.

The losses are considered by the motional resistance R_1 and the parallel capacitor C_p characterises the fixed dielectric capacitance of the resonator, which must be compensated. This circuit models the electrical behaviour of a piezoelectric sensor near one of its fundamental or overtone resonances. Each resonance is represented by an admittance circle in the locus graph (fig. 2.1), where the curve is passed clockwise with increasing frequency. Moreover, it is important to distinguish three characteristic admittance points and their associated frequencies on the circle. The frequencies $f_{-1/2}$ and $f_{+1/2}$ [9] respectively denote the local maximum and minimum susceptance value. Finally the point at maximum conductance is at the series resonance frequency and can be calculated as

$$f_s = \frac{1}{2\pi\sqrt{L_1 C_1}} \quad (2.2)$$

The quality factor indicates the ratio of the mean stored energy in the resonant cycle to the mean energy dissipated per cycle [5] [8] and can be expressed as

$$Q = \frac{1}{R_1} \sqrt{\frac{L_1}{C_1}} \cong \frac{f_s}{f_{+1/2} - f_{-1/2}} \quad (2.3)$$

High Q factors imply low loss in resonance, which is the case for quartz crystal sensors (typically 10^5).

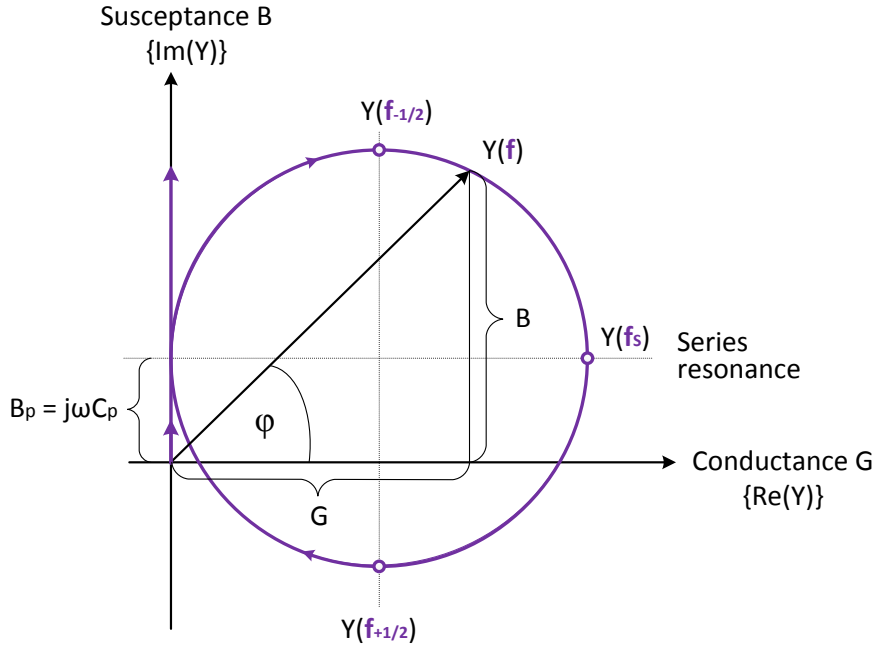


Figure 2.1: Admittance locus describing a series resonance by a circle; characteristic frequencies points; susceptance offset B_p is associated with the parallel capacitance C_p

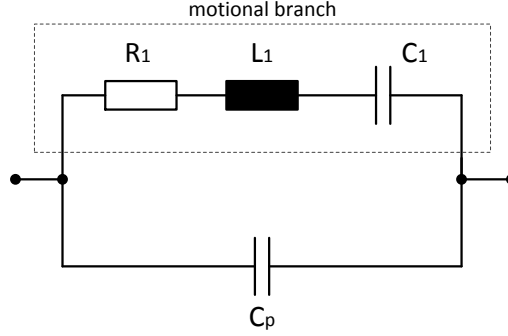


Figure 2.2: Butterworth-Van-Dyke equivalent circuit of a piezoelectric sensor

Transient effect

Frequency scan measurements on resonant systems are sensitive to transient effects, especially when the frequency values change discretely or at sudden jumps in ranges [2]. This means that impedance analyzers must allow to apply a delay time in order to abide the settling time for every frequency change, when measuring the admittance spectra of a sensor. This settling time and therefore the necessary delay time varies for different type of sensors and measurement systems. Typical values for ceramic type resonators are between $1ms$ and $10ms$, whereas for quartz crystals due to the high quality factors of typically 10^5 it can lie between $10ms$ and $100ms$.

2.2 Probe compensation

A principle admittance measurement set-up is shown in figure 2.3, whereby the probe is meant to be the cable that connects the piezoelectric resonator with an impedance analyzer. Since high accuracy is important to determine differences in physical quantities due to vibration changes of a sensor, a probe compensation (cable compensation) is required for every frequency range of interest. Since every cable has a finite inductance, capacitance and resistance, their influence can be modelled with a simple equivalent circuit (fig. 2.3). The effect of the inductance L_C and capacitance is significant at high frequencies. The series resistance R_C becomes important depending on the of resonators resistance at a certain frequency. The parameters R_C , L_C , G_C and C_C must be determine for every frequency range of interest prior to every measurement and included in the software's measurement and calculation procedures. The correction of the sensors admittance can be given as follows

$$\mathbf{Y}_{compensated} = \frac{1}{\frac{1}{\mathbf{Y}_{piezo} - \mathbf{Y}_C} - \mathbf{Z}_C} \quad (2.4)$$

with \mathbf{Y}_{piezo} being the original admittance value measured at the resonator. Further, \mathbf{Y}_C and \mathbf{Z}_C are the complex expressions of the probe compensation, which can be

written as

$$\mathbf{Y}_C = G_C + j\omega C_C \quad (2.5)$$

$$\mathbf{Z}_C = R_C + j\omega L_C \quad (2.6)$$

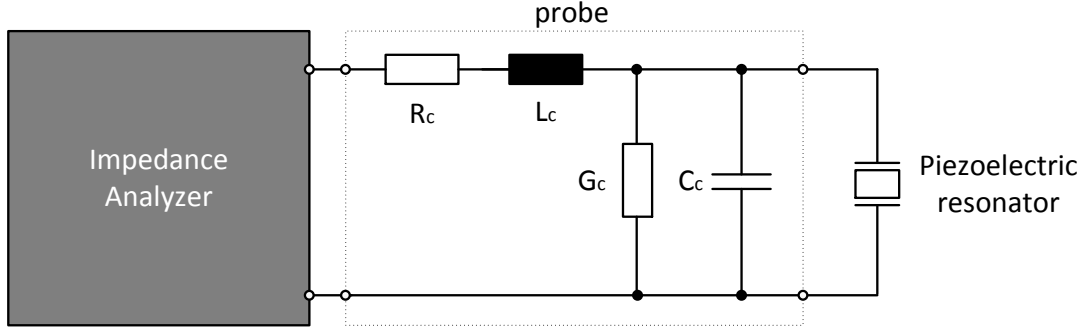


Figure 2.3: Admittance measurement set-up for a piezoelectric sensor; probe is meant here as the connection cable between the sensor and the impedance analyzer

2.3 Concept of the Locus-fit

In this chapter a least-squares fit procedure is presented, that uses the locus representation of measured admittance data in order to calculate the resonance frequency f_s , the quality factor Q and the parameters of the Butterworth-Van-Dyke equivalent circuit with increased accuracy. The concept outlined here is mainly based on the references [5], [10] and [11]. The following assumptions are necessary for the parameters of a resonance to be stated in a closed form:

$$2\pi f C_p \ll \frac{1}{R_1} \quad (2.7)$$

or

$$Q^2 \frac{C_1}{C_p} = QM \gg 1. \quad (2.8)$$

In other words the admittance circles are not distorted by the admittance change of the parallel capacitance C_p . In the above equation the figure of merit is denoted as M and defined as $M = Q \frac{C_1}{C_p}$ [12].

The fit procedure can be split into two parts, the first of which is to minimise the differences of the locus radii, therefore calculating the conductance G_c and susceptance B_c of the centre of an admittance circle and its radius. In other words G_c and B_c are circles center coordinates in the locus diagram. The second part is responsible for minimising the differences tangential to the admittance circle, yielding the parameters f_s , C_1 and Q [5, p 973 and 974].

Let us now turn to the first step. In order to fit an admittance circle to the measured admittance values, its radius

$$Y_{radius} = \left[\frac{1}{n} \left(\sum G^2 + \sum B^2 + n(G_c^2 + B_c^2) - 2(G_c \sum G + B_c \sum B) \right) \right]^{1/2} \quad (2.9)$$

and its centre coordinates

$$G_c = \frac{ab + cd}{2(ce - a^2)} \quad \text{and} \quad B_c = \frac{ad + eb}{2(ce - a^2)} \quad (2.10)$$

must be calculated by using the minimising formulae [11]

$$a = \sum GB - \sum G \sum B/n \quad (2.11)$$

$$b = \sum B/n \left(\sum G^2 + \sum B^2 \right) - \sum B^3 - \sum G^2 B \quad (2.12)$$

$$c = \left(\sum B \right)^2 / n - \sum B^2 \quad (2.13)$$

$$d = \sum G/n \left(\sum G^2 + \sum B^2 \right) - \sum G^3 - \sum GB^2 \quad (2.14)$$

$$e = \left(\sum G \right)^2 / n - \sum G^2. \quad (2.15)$$

The summation is done over the number of data points used for the fitting procedure, which is denoted as n here. The first equivalent circuit parameter, the resistance R_1 of the resonance is reciprocal to the circles diameter.

$$R_1 = 1 / (2Y_{radius}) \quad (2.16)$$

The next parameter is the parallel capacity C_p , which can be calculated through the susceptance B_c and the estimation of f_s within the measured data points.

$$2\pi f_s C_p = B_c \quad (2.17)$$

It is important to emphasize, that this way of determining C_p can be very inaccurate for high figure of merits, whereby the radius of the circle may be much larger than $2\pi C_p$. This is the case, when the centre of the circle has an offset of B_c that is in the magnitude of measurement noise or is distorted by mode couplings. The deviation of the conductance G_c is denoted as G_p and indicates the accuracy of the measurement. To illustrate the above term definitions, figure 2.4 gives an schematic example of a fitted admittance circle of a resonance with the deviation of the centre by G_p in the conductance and an offset of $B_p = B_c$ in the susceptance. We can now define Y_p under the assumption, that equation 2.8 is valid, as the admittance of the parallel capacitance C_p .

$$\begin{aligned} Y_p &= G_p + jB_p = G_c - Y_r + jB_c \\ G_p &= G_c - Y_r \\ B_p &= B_c \end{aligned} \quad (2.18)$$

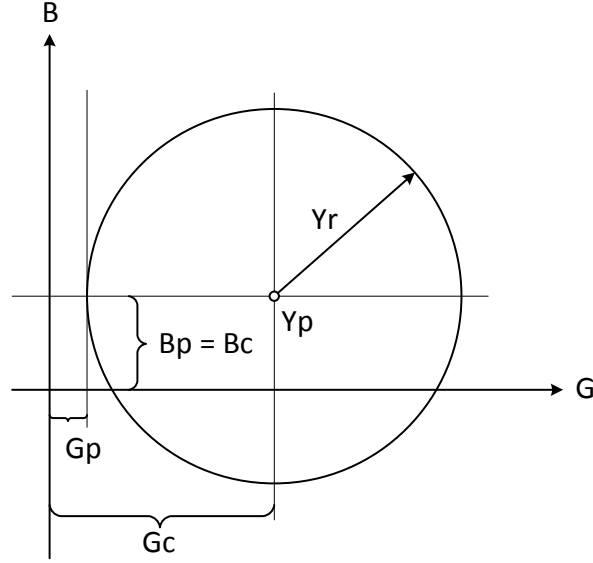


Figure 2.4: An schematic fitted admittance circle with its circle centre at (G_c/B_c) ; G_p denotes the deviation of G_c from its theoretical value Y_r (radius of the admittance circle)

In the second step of the fitting procedure the resonance frequency f_s of the series resonance, the quality factor Q and the second parameter C_1 of the equivalent circuit are calculated by minimising the sum of the squares of the error of admittance

$$\sum_m (\Delta_{\parallel} Y_m)^2 \approx \sum_m \left[|Y_m - Y_p|^2 \Delta_{\parallel} \left(\frac{1}{Y_m - Y_p} \right) \right]^2 \quad (2.19)$$

The difference between the measured data and the calculated values is denoted by the symbol Δ_{\parallel} . However, the parallel sign indicates, that only the component tangential to the admittance circle is used here. Using the assumption that $Q \gg 1$ and since small differences in Δ_{\parallel} is equivalent to a purely imaginary difference of the motional arm, we can express equation (2.19) as

$$\sum_m \Delta_{\parallel} Y^2 \approx \sum_m \left[\text{Im} \left(\frac{1}{Y_m - Y_p} - \frac{2jR_1Q}{f_s} f_m + 2jR_1Q \right) |Y_m - Y_p|^2 \right]^2 \quad (2.20)$$

By minimising (2.20) the wanted parameters are given as

$$f_s = \frac{u_1 v_1 - u_0 v_2}{u_1 v_0 - u_0 v_1} \quad (2.21)$$

$$C_1 = \frac{1}{\pi f_s} \frac{v_0 v_2 - v_1^2}{u_1 v_1 - u_0 v_2} \quad (2.22)$$

$$Q = \frac{1}{2\pi f_s C_1 R_1} \quad (2.23)$$

The coefficients u_i and v_i are defined as

$$\begin{aligned}
u_i = & - \sum B^3 f^i - \sum G^2 B f^i \\
& + B_p \left(3 \sum B^2 f^i + \sum G^2 f^i \right) \\
& + 2G_p \sum G B f^i - (3B_p^2 + G_p^2) \sum B f^i \\
& - 2B_p G_p \sum G f^i + (B_p^3 + G_p^2 B_p) \sum f^i
\end{aligned} \tag{2.24}$$

$$\begin{aligned}
v_i = & \sum G^4 f^i + \sum B^4 f^i - 4G_p \sum G^3 f^i - 4B_p \sum B^3 f^i \\
& + 6G_p^2 \sum G^2 f^i + 6B_p^2 \sum B^2 f^i - 4G_p^3 \sum G f^i \\
& - 4B_p^3 \sum B f^i + G_p^4 \sum f^i + B_p^4 \sum f^i + 2 \sum G^2 B^2 f^i \\
& + 2G_p^2 B_p^2 \sum f^i + 2G_p^2 \sum B^2 f^i + 2B_p^2 \sum G^2 f^i \\
& - 4B_p \sum G^2 B f^i - 4G_p \sum G B^2 f^i \\
& - 4G_p B_p^2 \sum G f^i - 4G_p^2 B_p \sum B f^i + 8G_p B_p \sum G B f^i
\end{aligned} \tag{2.25}$$

for $i = 0, 1$ and 2 .

The summation here is done also over the number of data points used for the fitting procedure. The last parameter L_1 of the equivalent circuit is determined by inserting (2.21) and (2.22) in the general expression of

$$f_s = \frac{1}{2\pi\sqrt{L_1 C_1}} \tag{2.26}$$

which yields the formula

$$L_1 = \frac{1}{4\pi^2 f_s^2 C_1} \tag{2.27}$$

Chapter 3

Methodology

3.1 Description of the problem

As we already discussed in the first chapter, it is essential to know the exact resonance and characteristic frequencies together with their quality factors to optimize measurement applications as well as to prove theoretical concepts such as the transfer matrix description of the piezoelectric structures experimentally. The problem lies thereby in the implementation of a dynamic admittance scan algorithm for various piezoelectric sensors, in general with unknown characteristics, that will be complemented in the original software of the *Impedance Analyzer 16777k* of the company SinePhase. Depending on the input parameters chosen from the user, the frequency steps near a resonance peak must be lowered automatically, that within the allowed range the frequency resolution is high enough to perform a data-fit afterwards and increased to a predetermined upper limit between resonances so that the overall measurement time lies in the range of a few minutes. The second main feature is to evaluate the measured data and to provide a least-squares fit procedure based on the equations discussed in chapter 2. The goal is to implement a fit algorithm that uses the conductance ($\text{Re}(Y)$) as well as the susceptance ($\text{Im}(Y)$) to achieve better results than the fit-feature of the SinePhase software that only fits a Lorentz function in the conductance. Furthermore usability aspects must be taken under consideration since the results of this work will be incorporated into the commercially available software of the *Impedance Analyzer 16777k* for future releases.

In this chapter I will first present admittance measurement devices, that was used during the course of this work, with their advantages and disadvantages. Then a detailed description of the development of the resonance peak detection algorithm with an significant improvements to the first approach of just implementing the *QxSens*-algorithm [2] will be given. The realization of the data evaluation through a so called Locus-fit will be outlined and finally a state diagram with all relevant procedures will give an overview of the software which was implemented in LabVIEW®.

3.2 Admittance measurement devices

To answer the questions stated in the introduction, we begin by taking a closer look at the measurement devices used in the course of this work and compare their advantages and disadvantages. The criteria that are interesting to us are the following:

- frequency range
- linear and/or dynamic frequency scan algorithm
- size, weight and usability that makes a device mobile and portable to use in different laboratory or industrial environments
- the measurement time to scan an admittance spectrum
- whether the devices have probe compensations and measurement calibrations to consider spurious effects of the sensors parallel capacitance. Furthermore, how time-consuming and complicated these steps are to set up.
- data evaluation and fitting procedures (e.g. Locus-fit)
- long term hard- and software maintenance aspects
- price of the device and its peripheral fixtures

3.2.1 QxSens

The admittance measurement principle of the *QxSens* system is based on a voltage divider, where the resonator is in series with an ohmic resistor Z_C (see figure 3.1). The figure shows the schematic circuit of the signal conditioning where also the cable compensation is outlined. The measurement test point is the resistor Z_C and not the sensor (RPC) itself. We can also see a second reference signal V_0 that is 90° phase shifted to the driving signal V_G . By using four analogue multiplier circuits it is possible to evaluate the resonator's signal, whereby the information about the sensor's complex admittance is carried by two of them and the other two are each proportional to the amplitude of V_G or V_0 . The results of the voltage multiplication are four signals and the idea here is to compensate possible offset errors of electronics devices by specifically dividing them to yield two normalized signals [2, p48 and p84]. It is important to point out one essential disadvantage of this signal conditioning method, that it will only work properly when the series resistor Z_C has the same order of magnitude as the piezoelectric sensor's ohmic resistance. Hence several kernel electronics for various types of sensors and scales of resistance has to be made or the resistor R_C has to be replaced for different measurements.

Figure 3.2 is showing the hardware components of the *QxSens* measurement system. Within the picture (a) is contained the kernel electronics that is connected through a individually pinned VGA cable to the interface electronics which is built-in into a conventional desktop PC board with further signal processing PC boards

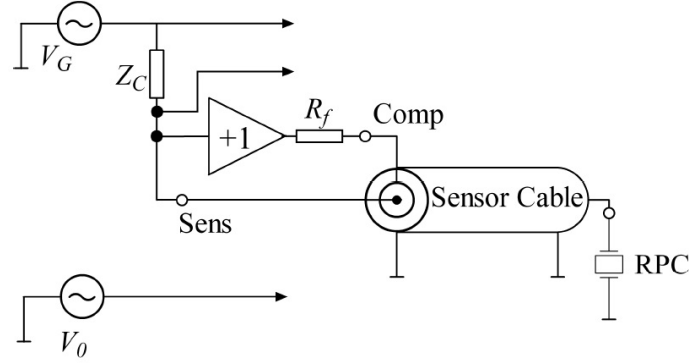
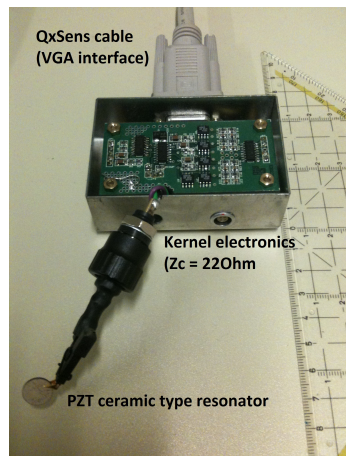


Figure 3.1: Schematic signal conditioning circuit of the *QxSens* kernel electronics [2, p32]

(figure (b)). According to the specifications of the kernel electronics a frequency range from 30 kHz to 50 MHz is specified.

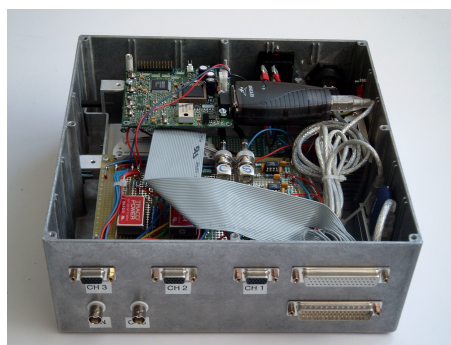
It is now clear that the hardware concept of the *QxSens* measurement system is split to several components and because of self designed electronics it is therefore likely to need in the long term high maintenance. Let us turn our attention to software part and technically speaking to the so called non-linear algorithm, that can adjust the frequency steps to detect resonance peaks. Besides the hardware parameters, the procedure needs two input parameters (minimal and maximal frequency step width), which has to be estimated by the user. A detailed description of the peak detection algorithm will be given later in chapter 3.3.1. A measurement example with this system for a dynamic scanned admittance spectrum of an PZT ceramic type resonator for a frequency range between 2 and 2.2 MHz can be seen in figure 3.3 (screen shot of the *QxSens* software user interface). The minimum frequency step is 10 Hz and the upper limit is determined here by a multiplication parameter called *Maximum factor*, which therefore yields a maximum step width of 1 kHz. The kernel electronics signal conditioning mode is set to $VDC - V_C$ (voltage divider principle whereby the voltage of the resistor R_C is measured) and the values of R_C and C_C can be specified, whereas C_C has to be set to zero, because *QxSens* system uses only ohmic values for Z_C [2]. Further input parameters are the averaging number, the delay time ($WAIT[ms]$) and the so called baseline compensation for subtracting spurious errors of a sensor cable, which will not be necessary for the measurements presented in this work due to short probe lengths of about 6cm (fig. 3.2(a)). Furthermore the software automatically performs a least-squares fit in the admittance locus for the resonance peak with the highest conductance amplitude and calculates its resonance frequency, Q factor and the parameters for the Butterworth-Van-Dyke equivalent circuit. One minus point here is that the locus-fit (plotted in red in fig. 3.3) is shifted to zero so that is difficult for the user to differentiate the results in case of resonances with similar conductance values and locus radii respectively.



(a) Showing a PZT ceramic type sensor that is connected to the *QxSens* kernel electronics.



(b) Desktop PC hardware set-up [2, p79]



(c) Mobile USB version [2, p81]

Figure 3.2: The *QxSens* kernel electronics (a) will be connected with an so called *QxSens* cable (individually pinned VGA cable) to a interface electronics either on a desktop PC board (b) or the USB version (c).

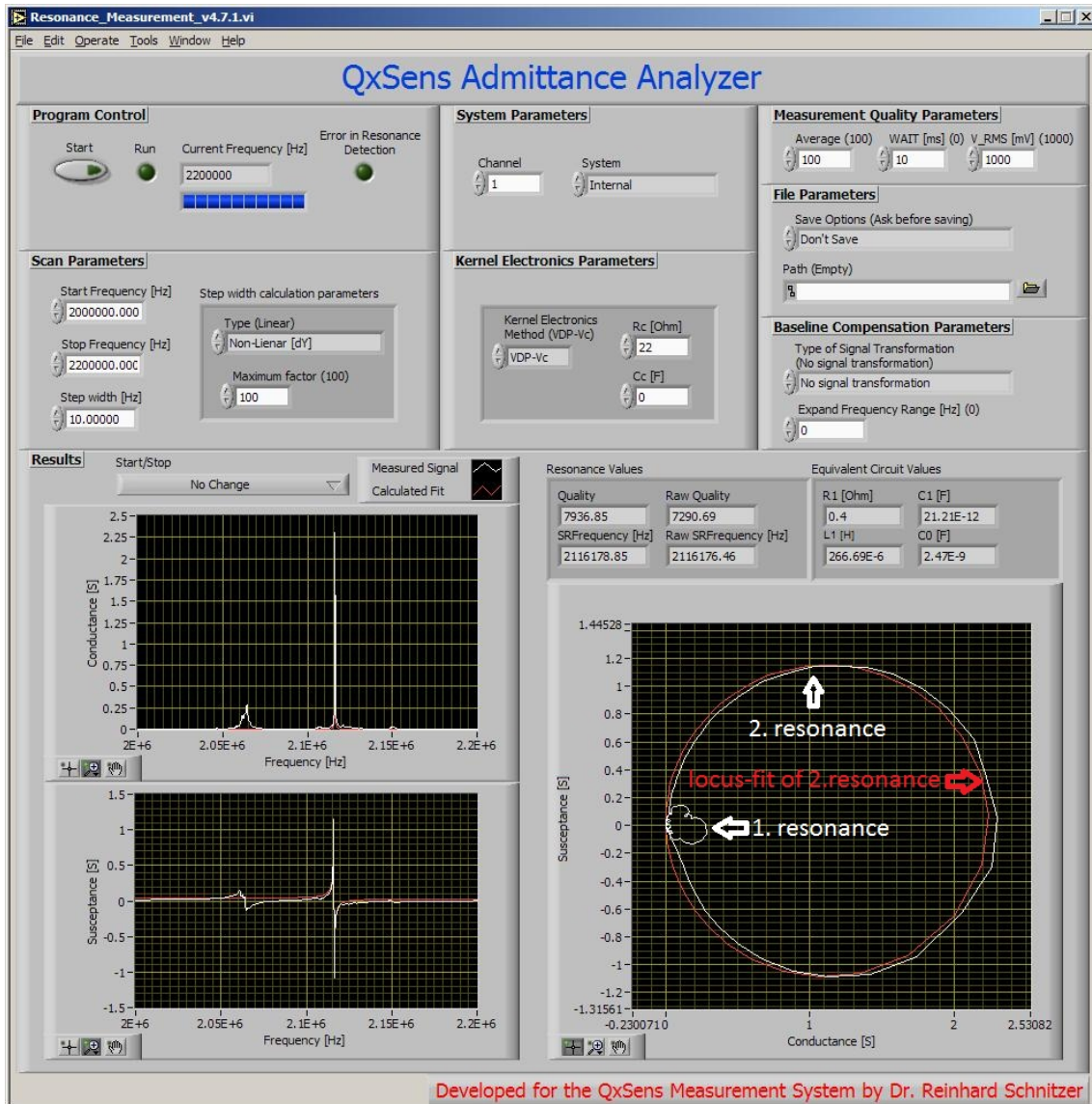


Figure 3.3: Showing a screen shot of an admittance measurement of a ceramic type PZT between 2 to 2.2 MHz with the *QxSens* admittance scan software; the conductance diagram is depicting a prominent resonance at 2.116 MHz with a quality factor around 8000 and the locus diagram is representing the least-squares fit (red curve).

3.2.2 SinePhase Impedance Analyzer 16777k

The *Impedance Analyzer 16777k* from the company SinePhase is the basis for the aim of this work. The goal is to implement the dynamic frequency scan algorithm and to replace the fit procedure with one that uses locus curve to calculate the resonance frequencies, quality factor and the equivalent circuit parameters. Within the picture in figure 3.4(a) we can see the hardware with a ceramic type PZT connected to a customized terminal also made by the company SinePhase for these types of sensors.

Advantages	Disadvantages
<ul style="list-style-type: none"> • linear and dynamic frequency scan mode • fit procedure and calculation of the equivalent circuit parameters • USB version • PC controlled and data export options (txt and MS-Excel format) 	<ul style="list-style-type: none"> • needs different kernel electronics because of R_C for various sensor types • fit procedure only for one resonance (highest conductance value) • highly distributed hardware concept with a lot self-made components (e.g. signal conditioning, <i>QxSens</i> cable etc.) • high long term hardware maintenance

Table 3.1: Pros and cons of the *QxSens* measurement system

A big advantage of this device is that it is powered and controlled via a standard USB connection. The specifications states for example a frequency range between 1kHz and 16.777MHz and a frequency resolution of 1Hz . Further details about the dimensions and weight (see fig 3.4(b)) makes this device truly mobile for the use in different laboratories and industrial environments, which is one of the big advantages of this measurement system.

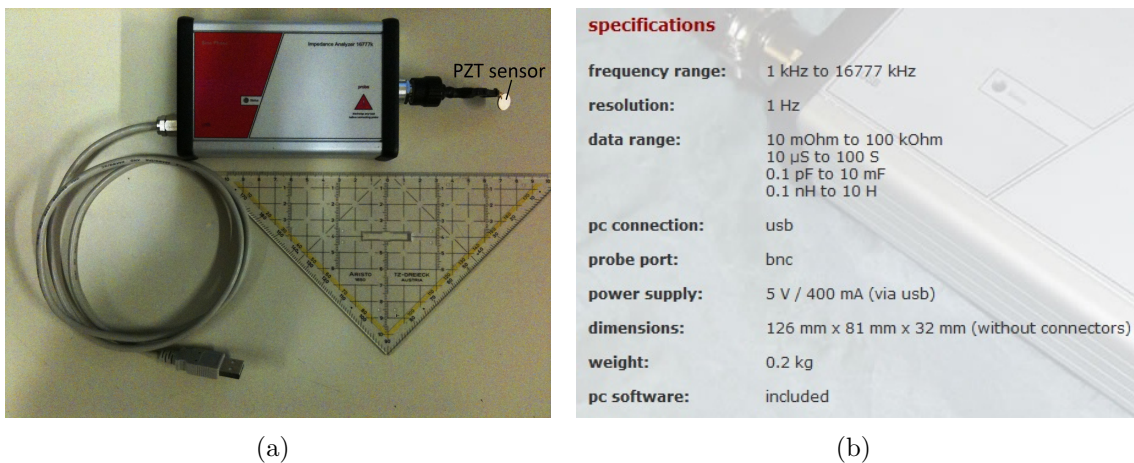
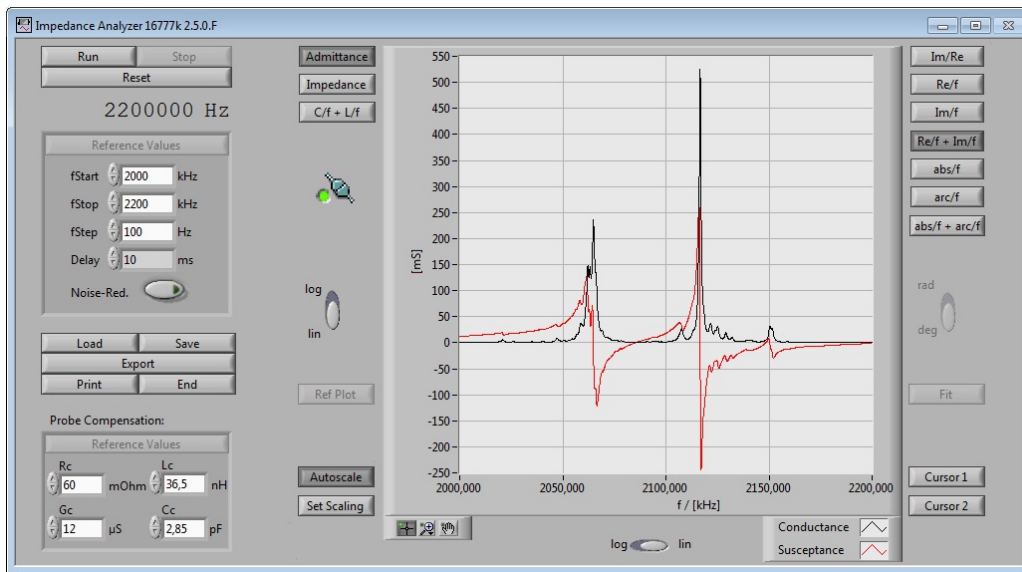


Figure 3.4: (a) showing the hardware of the Impedance Analyzer 16777k; the sensor is connected through a probe to the device; power supply and data communication works over a standard USB connection; (b) hardware specifications [13]

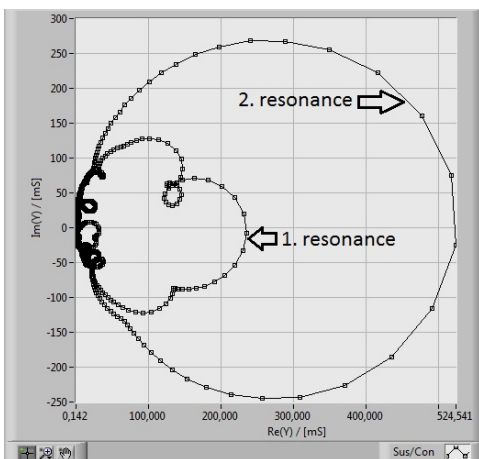
The measurement principle is based on a special proprietary voltage vector multiplication also with a reference signal which promises high accuracy over a wide frequency range and simultaneously with low hardware effort and small size. Let us now turn to the software part of this device. Figure 3.5(a) depicts a screen shot of the user interface with an admittance spectrum of a ceramic type PZT resonator from 2 to 2.2 MHz. To achieve high accuracy there is necessary to compensate the probe, whose parameters can be filled in the lower left corner. In the admittance diagram

one can see the real- and imaginary part and also an equivalent representation in the locus (fig. 3.5(b)).

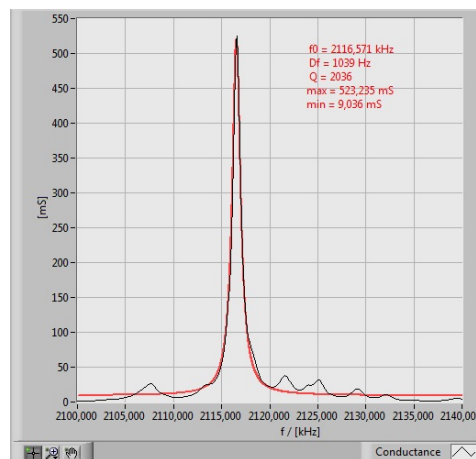
One of the big disadvantages of this system clearly is that it only performs a linear admittance scans with constant frequency steps, which means that with to big frequency steps resonances can be skipped over and with to small steps the measurement will take considerably long and produce data points of the irrelevant areas of the spectrum. Moreover the fit procedure takes only the conductance into consideration and matches a Lorentz function into resonance peak (fig. 3.5(c)).



(a) Screen shot of the software user interface



(b) Admittance locus curves



(c) Results of the Lorentz function fit

Figure 3.5: Presenting the admittance scan of an PZT ceramic type resonator between 2 and 2.2 MHz with an linear frequency scan ($f_{Step} = 100$ Hz); (a) admittance spectrum with two resonances; (b) locus curves; (c) fit results of the resonance at 2.116 MHz with $Q = 2036$

Advantages	Disadvantages
<ul style="list-style-type: none"> • truly mobile device (small and lightweight) • high measurement accuracy over a wide frequency range • no hardware maintenance required (commercially available product) • fully PC-controlled and data export options (txt, bmp, jpg, png and MS-Excel format) • probe compensation 	<ul style="list-style-type: none"> • no dynamic frequency scan algorithm • fit procedure uses only the conductance data instead of the locus curve • maximum frequency only till 16.777 MHz

Table 3.2: Pros and cons of the Impedance Analyzer 16777k from SinePhase

3.2.3 Agilent 4395A Impedance Analyzer

The *Agilent 4395A* is an extensive measurement device consisting of three analyzer types: Network-, Spectrum- and Impedance mode. Of course for our purpose we are applying here the third to scan admittance spectra. It has a high accuracy and therefore we will be using it as an reference system to compare measurement results (see chapter 5). Figure 3.6(a) is showing the measurement system, whereby a PZT sensor is connected trough a special test fixture (3.6(b)). From the mobility and usability point of view the disadvantages are firstly the relatively big size and high weight, secondly the calibration of the system and the test fixture with special terminations and lastly the outdated data storing possibility on floppy disks. Incidentally, the calibration procedure has to be done for every frequency range [6] and thus makes the measurement set-up very time consuming and inept for mobile use. However to compensate additional measurement cables and probes it is possible to enter the electrical length of these. One interesting difference to all the other systems is that the Agilent 4395A measures continuously after the set-up and builds an average (max. 16 times) of the spectrum.

Despite the high accuracy there is again the same problem as with the SinePhase device, there is only a linear frequency scan mode and in addition to that the selected frequency range is divided into 801 data points maximally. Hence the constant step width is yielded trough that number. In figure 3.7(a) we can see an admittance scan of a ceramic type PZT sensor between 2 and 2.2 MHz, which was also used for the other two measurement devices. In the locus representation in figure 3.7(b)) clearly shows that the resulting frequency step of approximately 250 Hz is too large for a high resolution scan of the second resonance.

Moreover, another argument to declare the Agilent 4395A as a reference device is the possibility to calculate the parameters of the Buttherworth-Van-Dyke equivalent circuit so that the results of the locus fit can be evaluated. A list of the equivalent circuit models is presented in figure 3.7(c), where we will use the model E during the course of this work.

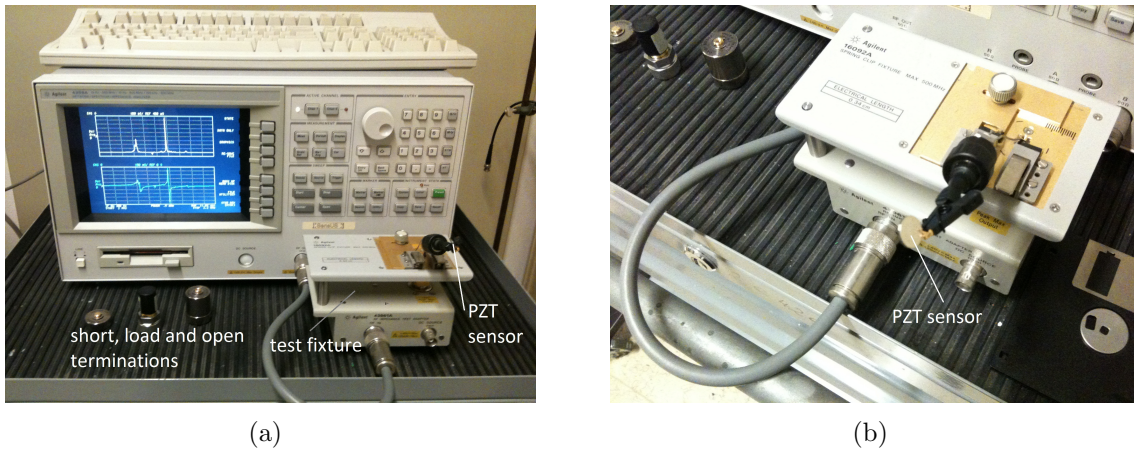


Figure 3.6: (a) showing the Agilent 4395A Network/Spectrum/Impedance Analyzer in admittance scanning mode; (b) a ceramic type PZT is connected to the Agilent 16092A test fixture

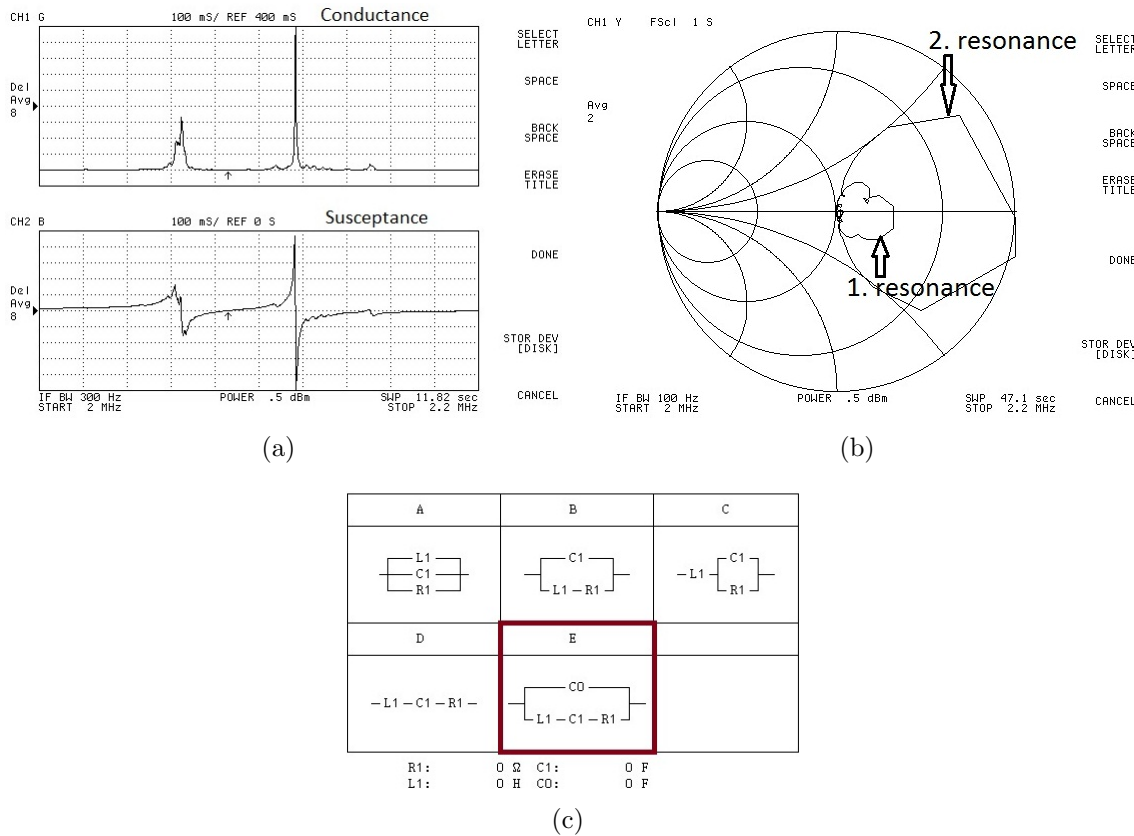


Figure 3.7: (a) admittance spectrum of a ceramic type PZT from 2 – 2.2MHz measured with the Agilent 4395A; Conductance and susceptance are displayed on different channels; (b) locus curve; constant frequency step $\approx 250Hz$; (c) equivalent circuit models of the Agilent 4395A system; Model E (Butterworth-Van-Dyke) will be used in this work

Advantages	Disadvantages
<ul style="list-style-type: none"> • high frequency accuracy ($< \pm 5.5 ppm$) • high resolution (1 mHz) • large frequency range (10 Hz to 500 MHz) • calculation of the equivalent circuit parameters • calibration and probe compensation available • low hardware maintenance (commercially available product) 	<ul style="list-style-type: none"> • no dynamic frequency scan algorithm • not applicable for mobile use • initial system and test fixture calibration very time consuming • out-dated data storing with floppy disks • relatively high price

Table 3.3: Pros and cons of the Agilent 4395A Impedance Analyzer; specifications [6, p11-1]

3.2.4 Overview

To recapitulate and compare all the relevant criteria for a admittance and impedance measurement device defined in the beginning of this subsection we can see an overview in table 3.4.

	QxSens	SinePhase Impedance Analyzer 16777k	Agilent 4395A
freq. range	30 kHz - 50 MHz	1 kHz - 16.777 MHz	10 Hz - 500 MHz
scan algorithm	linear, dynamic	linear	linear
mobile usability	partly	truly	no
scanning time (same minimum frequency step)	short	long	long
calibration and compensation	partly	yes	yes
fit procedure	locus fit	Lorentz function	equivalent circuit parameters
hardware maintenance	high	low	middle
price in relation to other devices	high	low	very high

Table 3.4: Comparison overview of all relevant criteria for admittance measurement devices

It is now the goal to take the advantages of true mobility, low hardware maintenance, low price, adequate calibration and compensation procedures from SinePhase's *Impedance Analyzer 16777k* and incorporate the benefits of the *QxSens* system,

which is the dynamic scanning of resonance peaks and enhanced locus fit, and improve respectively. The *Agilent 4395A* will serve as a reference device to compare the results.

3.3 Development of the resonance peak detection algorithm

In this section the steps and outcomes in the development and improvement of the resonance peak detection algorithm will be outlined. The starting point was a rudimentary version of the official software from SinePhase for the *Impedance Analyzer 16777k*, whereby at first the frequency step optimization algorithm from the *QxSens* software was implemented and further developed by using new approaches.

The elementary demo version of the SinePhase software has all the hardware drivers to control the *Impedance Analyzer 16777k* and could only perform a linear frequency scan measurements. In the screen shot in figure 3.8 we can see the frequency input parameters and graphs of the linearly scanned admittance spectrum as well as the impedance spectrum.

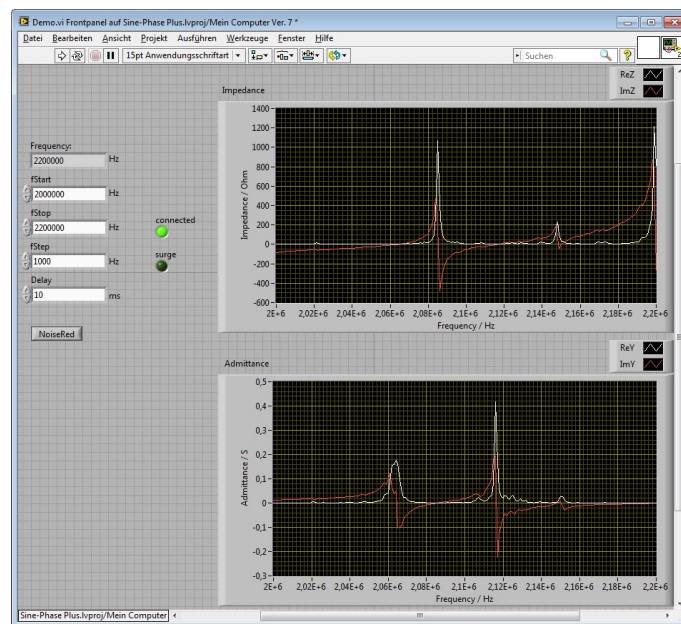


Figure 3.8: Showing the screen shot of the elementary demo version of the official SinePhase software for the *Impedance Analyzer 16777k*; impedance as well as admittance graphs are present and linear measurement is implemented

3.3.1 The QxSens algorithm

The first approach was to analyse the *QxSens* algorithm in order to implement a similar version in the SinePhase demo software. As we can depict from the user

interface of the *QxSens* software in figure 3.3 the frequency input parameters are as follows:

- Start frequency [Hz]
- Stop frequency [Hz]
- Step width [Hz] ... lower limit of $\Delta f =: \Delta f_{Min}$
- Maximum factor [1] ... is a multiplication factor to define the upper limit of $\Delta f = \text{Stop frequency} \cdot \text{Maximum factor} =: \Delta f_{Max}$
- Type: Non-linear[dY] ... scanning mode

Depending on the type of sensor and the frequency range, the user must choose appropriate values of the above parameters. Especially the minimum and maximum frequency step width is crucial for a fast and accurate admittance scan, whereby all relevant resonances of the wanted frequency range can be detected with high resolution. Before we go into the details of the dynamic frequency step optimization, we first discuss the basic ideas behind the criteria where the step width is reduced when approaching a resonance and increasing Δf when passing it. In figure 3.9 the lengths of Y^2 for the last 15 points of an ideal resonance peak in the admittance locus are shown schematically. Δ is the absolute difference between the last two lengths (see equation 3.1). This value is always calculated pairwise for the last 15 values and is then used to determine a moving average represented by equation 3.2. The number of 15 data points is found through empirical studies measuring noise levels and their effect for various resonators [14, p30 and p51], [2].

$$\Delta = |Y_n^2 - Y_{n-1}^2| \quad (3.1)$$

$$\overline{|\Delta Y^2|}_{\{\text{last 15 values}\}} = \sum_{i=n-14}^n \frac{\Delta_i}{14} = \sum_{i=n-14}^n \frac{|Y_{i+1}^2 - Y_i^2|}{14} =: MA \text{ (moving average)} \quad (3.2)$$

Let us now examine the details of the frequency step algorithm used in the *QxSens* software by looking at the flow chart in figure 3.10, which was derived by analysing the source code of the latest version. Beginning at the `Start frequency`, 15 measurements are done linearly so that it is possible to build the moving average, which then is used to define two important comparisons based on the values Δ and $\overline{|\Delta Y^2|}$ (MA). From the 16th measurement on the last 15 data points are saved and the calculation of Δ and MA is carried out. The first comparison is:

$$\boxed{\Delta > 4 \cdot MA}$$

In the yes-case the current frequency (f) will be reduced by twice the current frequency step width (Δf) and the step width itself reduced by approximately 20%.

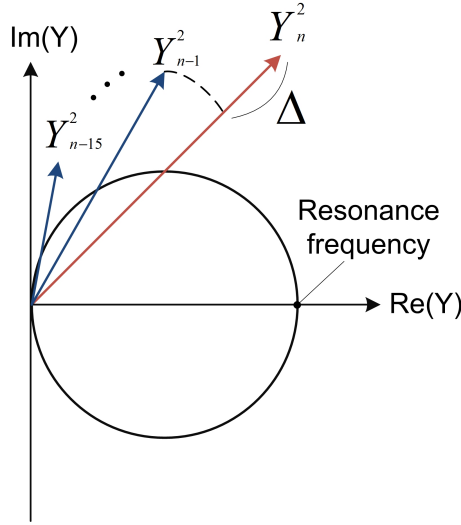


Figure 3.9: Schematic admittance locus showing the calculation of the moving average of $|\Delta Y^2|$ for the last 15 measurement points; it is a significant criteria for the detection of a resonance peak

This is necessary because, a resonance peak might be detected, when the admittance values are rising. Therefore the algorithm reduces the step width to measure in particular more data points around the half width of that resonance. If we follow the chart further, then Δf will be coursed into the frequency range defined by the minimum- and maximum frequency parameter (Δf_{Min} and Δf_{Max}) chosen by the user, in case it lies outside these limits. In the next procedure the current step width is added to the current frequency and the data points saved. Now because the step width was reduced it is better to delete the last two entries and perform new measurements with an reduced step width, that is 20% smaller and therefore increasing the frequency resolution around a possible resonance.

After passing a possible resonance the goal is now to increase the frequency step width. Hence the second criteria to trigger that is defined as follows:

$$\Delta < 2 \cdot MA$$

After this inquiry is yes, then the current frequency stays unaltered and the current step width is increased by 20%. This is done because the purpose here is to reduce the scanning time of admittance spectra by increasing the frequency steps between resonance peaks. When the current frequency exceeds the `Stop frequency` the program stops the scan and automatically performs a locus fit for the resonance with the highest conductance amplitude.

The two comparison criteria are used to define slope limits in the change of admittance to detect resonances. The values $2 \cdot MA$, $4 \cdot MA$ as well as the increase and decrease of Δf by 20% are empirically found and featured good results for various piezoelectric sensors ([2], [14]). It is important to stress out here that the performance of the scan algorithm is very much dependent on the chosen frequency input parameters, such as the minimum and maximum frequency step width and

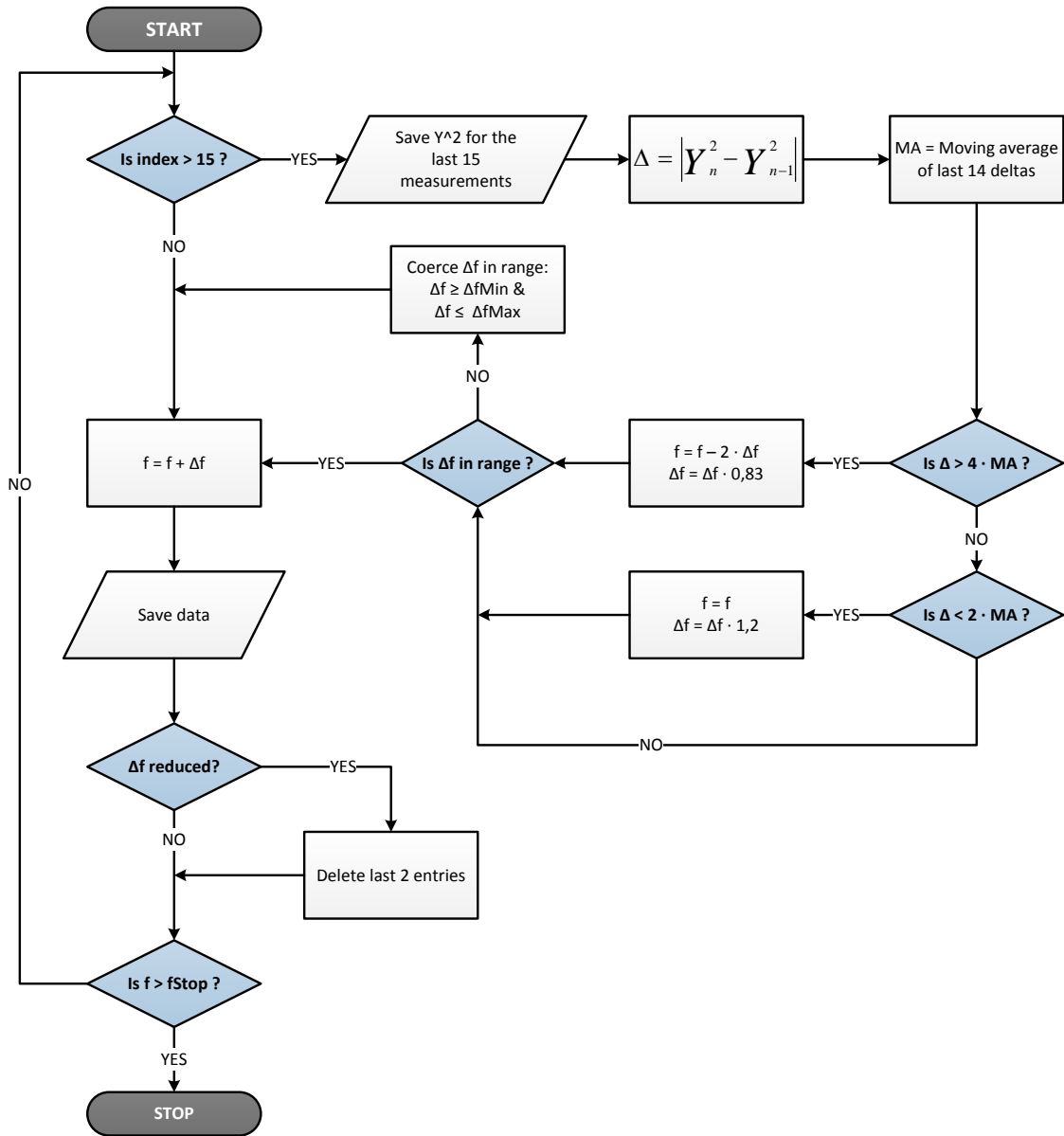


Figure 3.10: This flow chart describes the basic ideas behind the *QxSens* resonance peak detection algorithm

also the delay time for a specific resonator. On the contrary, it is possible to still detect peaks provided the upper frequency step limit is not greater than 10 times the smallest resonance half width appearing in the admittance spectrum [2].

Results of the *QxSens* algorithm implementation

Since measurements with the *QxSens* algorithm seemed promising, the first approach was to implement the ideas outlined in figure 3.10 into the demo version of the *Impedance Analyzer 16777k* software. All empirically found values were kept the same, but measurement results with the same algorithm indicated different outcomes in point density around the half width of resonance peaks. A comparison measurement of a ceramic type sensor between 2 and 2.2MHz can be depicted in figure 3.11 between the demo software of the *Impedance Analyzer 16777k* with the *QxSens* algorithm and the *QxSens* system itself. Furthermore the spectra of a quartz crystal with the resonance frequency at 6 MHz are shown in figure 3.12. By drawing comparisons for both cases, we can see that the point densities in particular for the ceramic type resonator is considerably smaller with the SinePhase software as with the *QxSens* system (tab. 3.5 and 3.6). Despite the similar results for a quartz sensor with only one resonance at 6 MHz and higher Q factor then the ceramic type resonator, the fact remained that with other combinations of the minimum and maximum step width the SinePhase demo software using the *QxSens* algorithm would get stuck in an endless loop deleting the last two entries and measuring new similar points with the same frequency step width over and over. One would assume similar results for the same scan algorithm since the criteria for changing Δf were equal, but admittedly the reasons for the big differences in measurement results could not be found. On the contrary, since the device are of different designs, it seems to me that these hardware varieties could have influenced the dynamic step width change. Moreover, changes in the set of parameters that would define new criteria for the slope of the peak detection, did not bring better results. Therefore it was important to develop alternative ideas that would ensure the same if not better resonance detection. These new concepts will be presented in the following subsections.

ceramic type PZT	measurement time [sec.]	number of points within resonance half width
SinePhase	31	6
QxSens	15	12

Table 3.5: Measurement comparison of the admittance scan in figure 3.11 with the *QxSens* algorithm; despite the same input parameters of $\Delta f_{Min} = 10Hz$ and $\Delta f_{Max} = 1000Hz$ the scanning time and frequency resolution differ considerably

quartz resonator	measurement time [sec.]	number of points within resonance half width
SinePhase	10	6
QxSens	6	7

Table 3.6: Measurement comparison of the admittance scan in figure 3.12 with the *QxSens* algorithm; also same input parameters of $\Delta f_{Min} = 10Hz$ and $\Delta f_{Max} = 1000Hz$, but still different scanning time and frequency resolution

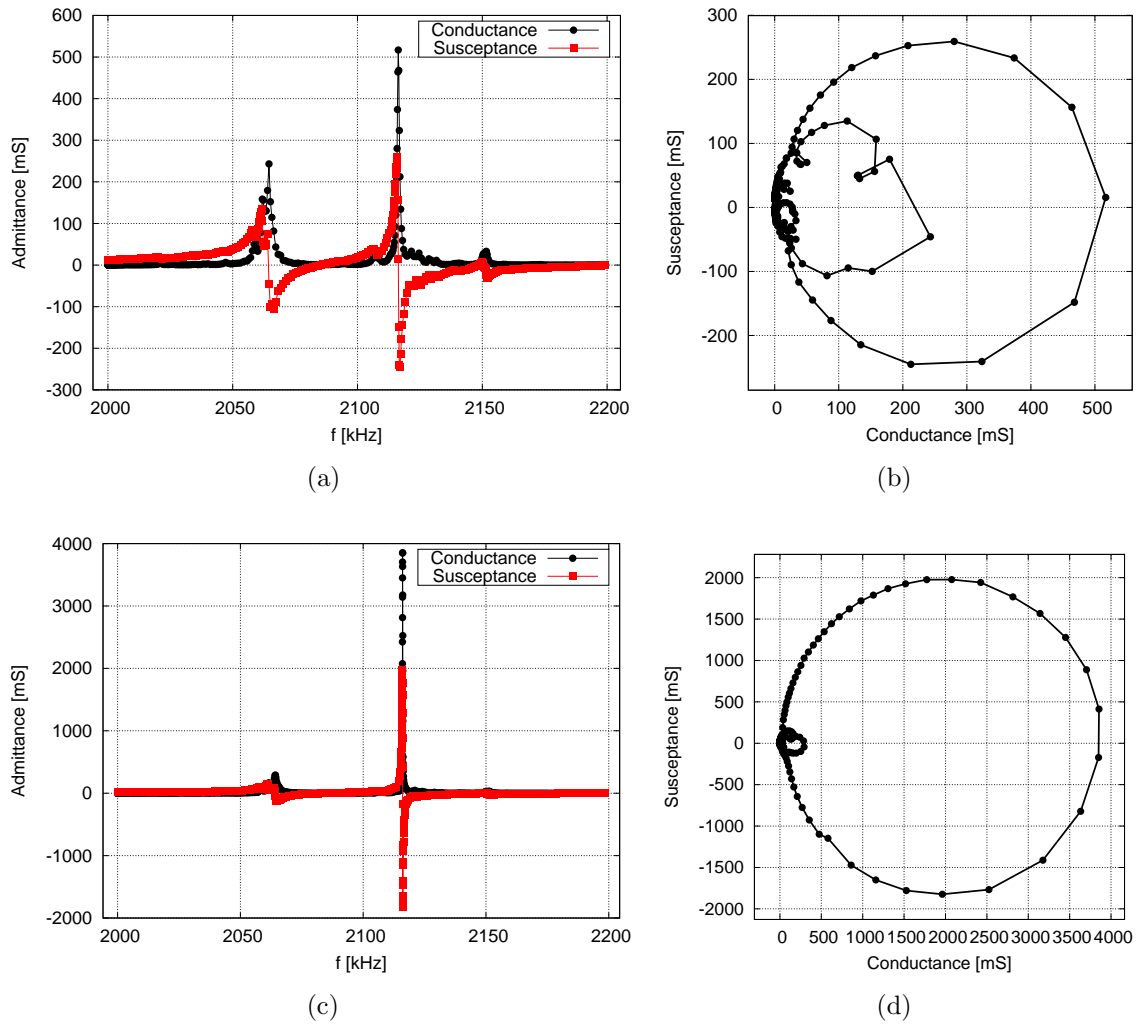


Figure 3.11: Admittance scan of an ceramic type sensor between 2 and 2.2 MHz measured with the *QxSens* algorithm implemented in the demo software of the *Impedance Analyzer 16777k* (a) and (b); *QxSens* system (c) and (d)

3.3.2 ”Zero-crossing” method

Due to the unsatisfying results of the implemented *QxSens* algorithm, which was discussed in the previous section, a new idea to increase the frequency resolution around resonance peaks was to detect the zero-crossing of the susceptance ($\text{Im}(Y)$). Figure 3.13 demonstrates the general concept behind this algorithm. The way this works is, that it uses the *QxSens* method with parameters that, which prevent endless loops for a first rough scan. In general at each resonance the imaginary part increases in the positive realm and becomes negative passing the resonance frequency, thus thus crossing the zero-level. The software is triggered in these cases and estimates the half width of the resonance with the measured points available. Then the frequency is set back to the beginning of the resonance, e.g. twice the half width to the left from the resonance frequency, which is the zero-crossing point,

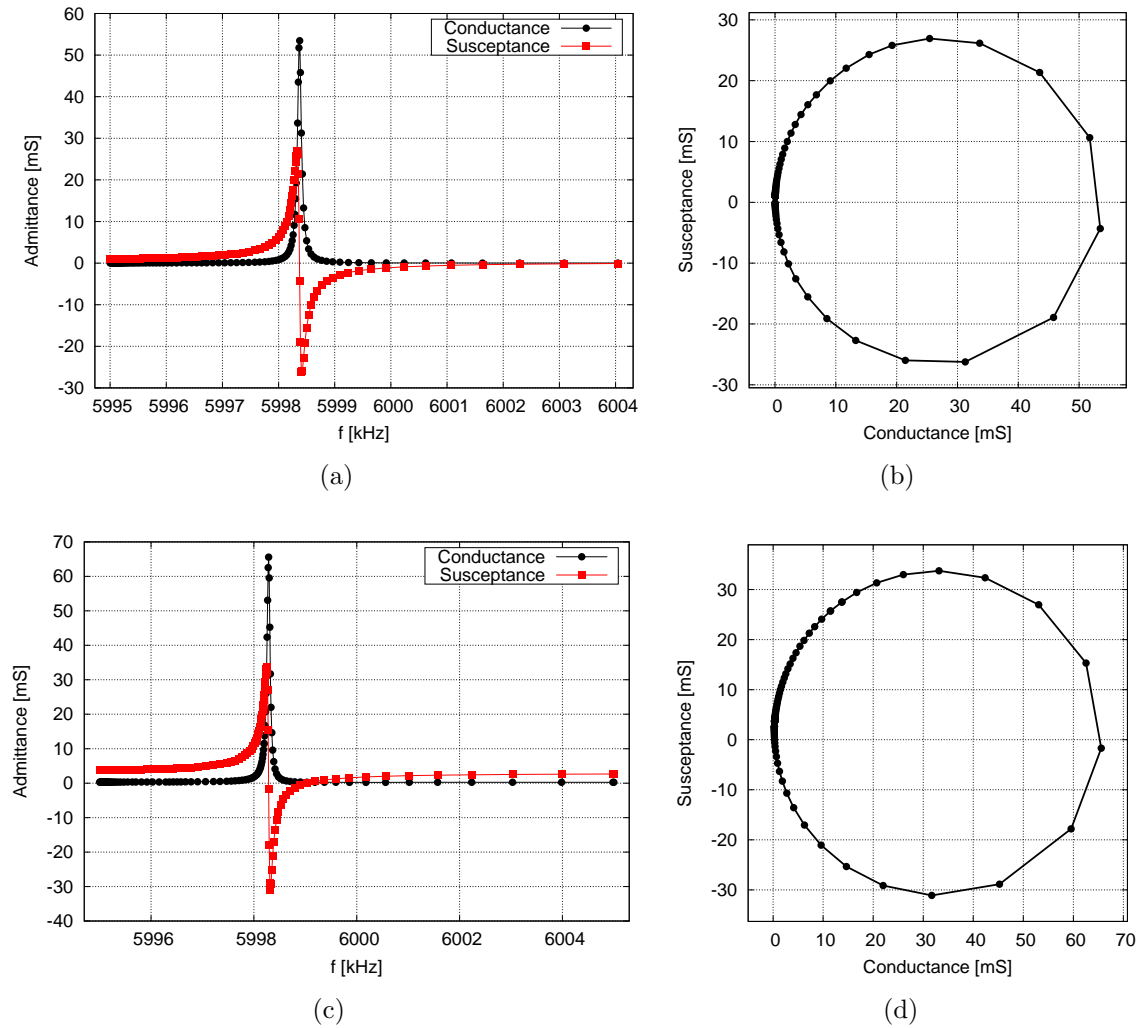


Figure 3.12: Admittance scan of a quartz sensor with the resonance frequency at 5.9985MHz , measured with the *QxSens* algorithm implemented in the demo software of the *Impedance Analyzer 16777k* (a) and (b); *QxSens* system (c) and (d)

deletes all data point as far as this value and starts a linear scan with a high frequency resolution up to twice the half width to the right. After passing this peak the susceptance becomes positive again and the algorithm continuous with the rough *QxSens* method.

A measurement example of a ceramic type PZT sensor in figure 3.14 can demonstrate the "zero-crossing" method, whereby the peak was scanned linearly after deleting the first roughly measured data points with a constant frequency step width of approximately 50 Hz in the range of four times the estimated half width symmetrically around the resonance frequency of 2.116 MHz. This was a promising method since the frequency resolution could be increased easily by defining a point density for the realm around a resonance frequency and furthermore the measurement time only increased slightly, but was still in the same magnitude compared to the original *QxSens* method.

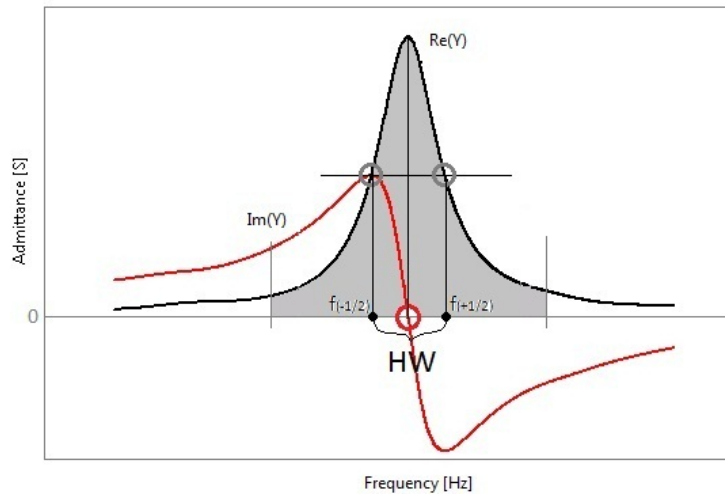


Figure 3.13: Illustrates the basic idea of the zero-crossing detection algorithm

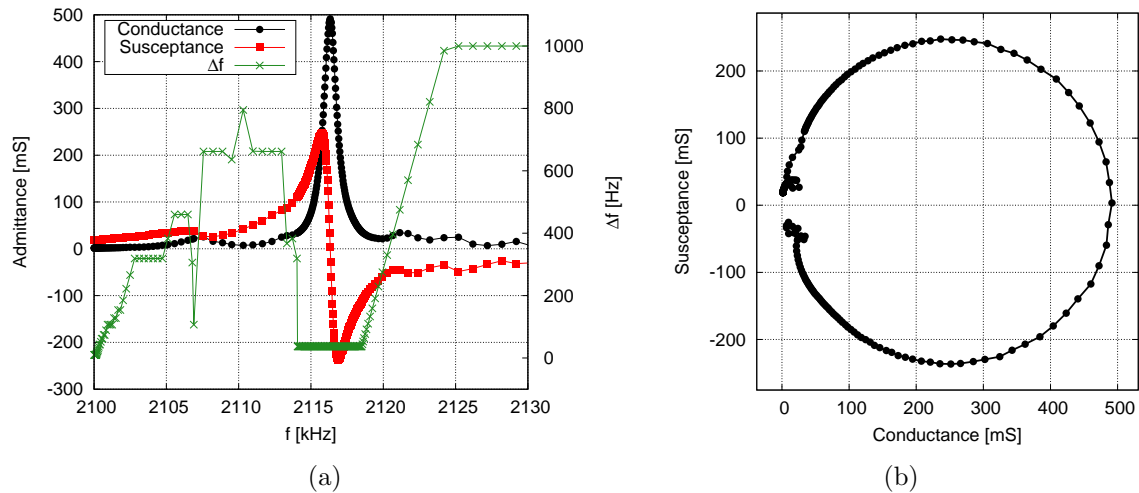


Figure 3.14: Showing a measurement with the "zero-crossing" algorithm of a ceramic type PZT between $2.1MHz$ and $2.13MHz$ with $\Delta f_{Min} = 10Hz$ and $\Delta f_{Max} = 1kHz$; (a) $\Delta f \simeq 40Hz$ in the range of four times the estimated half width around the resonance; (b) the locus indicates a high frequency resolution

In contrast to the first approach this algorithm indicated a great advantage, but when measuring at high frequency ranges the limits of the "zero-crossing" method became obvious. At this areas the spurious parallel capacitance can become so large that $Im(Y)$ does not switch to negative values any more, thus failing to detect a resonance peak and increase the resolution. Figure 3.15 is an example of a measurement at $11 - 11.8MHz$, where B_0 becomes so high that the zero-crossing could not be triggered. Hence the resolution is limited to the rough measurement of the $QxSens$ method. Due to this unreliability at high frequency ranges, the "zero-crossing" algorithm did not fulfil the goals for the resonance peak detection set out at the beginning.

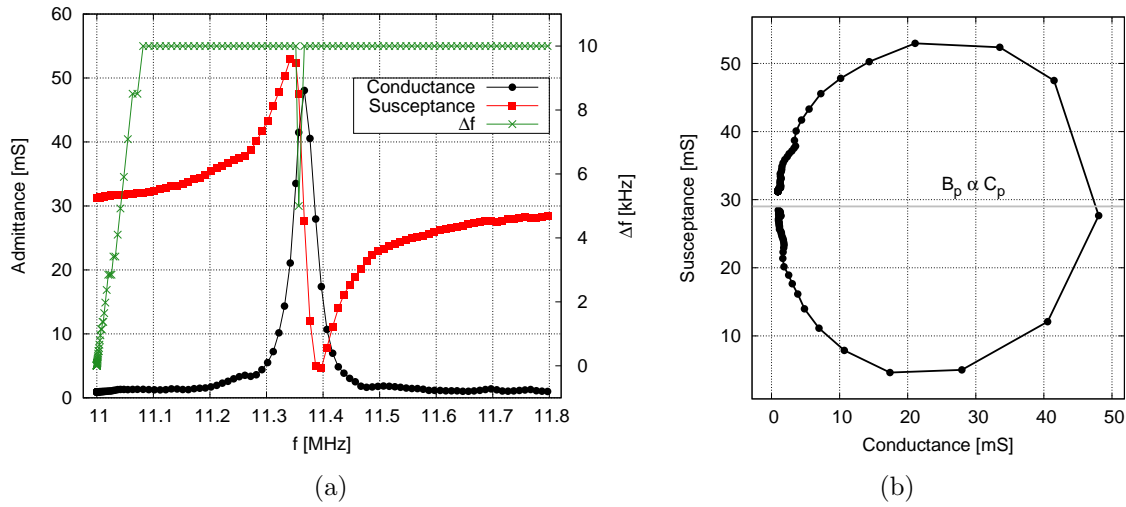


Figure 3.15: Showing the limits of the "zero-crossing" algorithm; (a) the result of the admittance scan is low frequency resolution; (b) the locus representation illustrates very well the large value of the spurious parallel capacitance $C_0 \propto B_0$

3.3.3 Phase angle detection in the admittance locus

In this subsection an idea is presented, whereby the phase angle of the admittance is used as a criterion to detect resonance peaks and increase the frequency resolution around them. For illustration purposes a plot of the phase angle distribution is shown in figure 3.16 for a quartz crystal resonator with a resonance frequency at approximately 6 MHz. As we can see, the phase angle φ of the admittance data point starts at 90° , decreases till -90° during the resonance peak and will return back to its initial value.

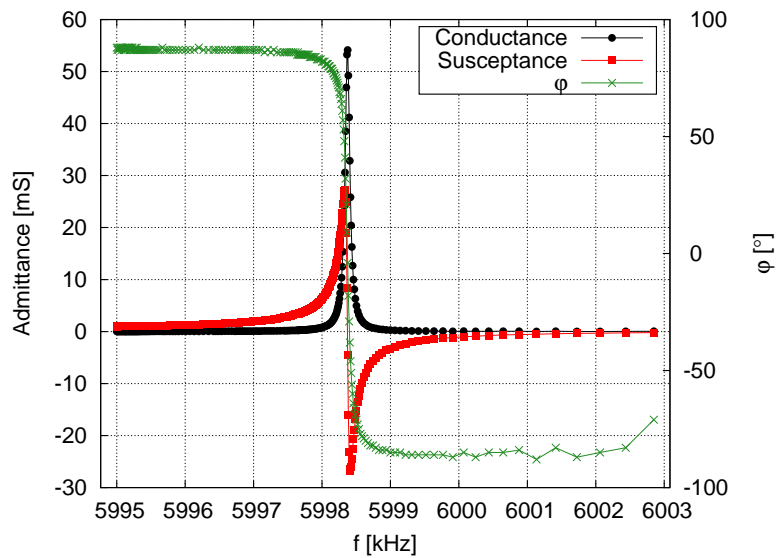


Figure 3.16: Plot of the admittance phase angle φ within a resonance peak

To explain the general notion how to use the phase angle to increase the frequency resolution around resonances we go into the locus representation, where three resonances with minimal influence of the parallel capacitance are shown in figure 3.17(a). One can interpret the graph in several ways. Firstly it shows that the frequency step width can be reduced to the minimal value of Δf_{Min} as long as the phase angle φ is for example between $+60^\circ$ and -60° and raised between the resonance. Thus increasing the resolution at relevant areas around the peaks. Secondly the great advantage would be that no matter how big the locus radii were, the criterion of $\varphi = \pm 60^\circ$ would always be triggered. Unfortunately as for the "Zero-crossing" method, which was discussed in the last subsection, this new concept works also only under the assumption that the spurious effects such as the parallel capacitance or resistance have negligible values of B_0 and G_0 . The graph in figure 3.17(b) can thus be used to predict problems with this method, which will arise when faced with realistic examples of an unknown piezoelectric resonator at high frequency ranges. The most important disadvantage here is firstly that after reducing the step width to the minimum, the second condition of -60° will not be triggered in this case, because the locus circles are lifted by different values of B_0 . Thus leading to a linear and slow scanning method with a constant frequency step width in some instances, which leads us to the conclusion that this detection method is not suitable for the scope of analysing all kind of various piezoelectric sensors with unknown properties if need be in desired frequency range between $1kHz$ and $16.777MHz$.

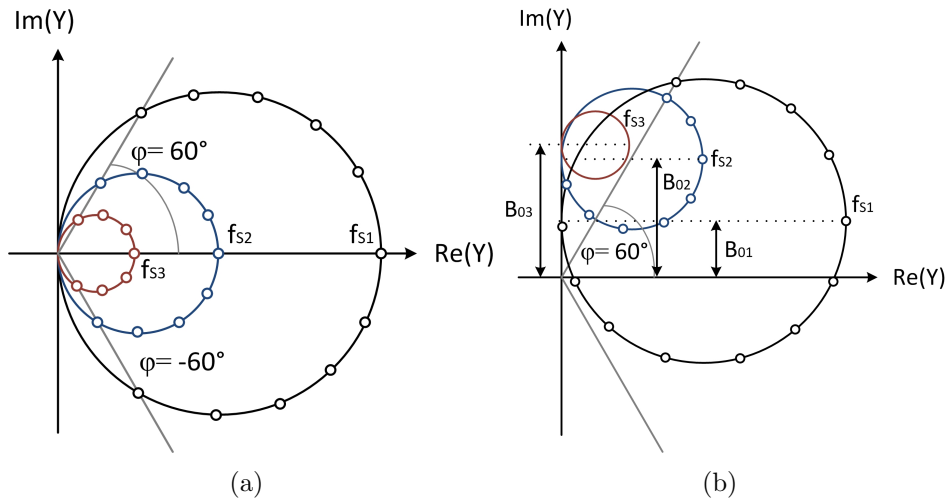


Figure 3.17: General idea to use the admittance phase angle to increase the frequency resolution within the area of $\varphi = \pm 60^\circ$ of a resonance; (a) locus of 3 resonance circles with neglect-able values of $B_0 \propto C_0$; (b) locus curves with high influence of C_0

3.3.4 Detection of the area change in the admittance locus

As we could conclude from the last alternative algorithms in previous subsections, the major difficulty was the influence of the parallel capacitance and the spurious effects that would move the position of the locus circle, so that the defined criteria would either not be triggered or not work efficiently. It is important to emphasize that the admittance values around a resonance is highly non-linear in relation to the frequency. Therefore the central question then becomes: how can we detect the fast change in spite of big influences of C_0 that may occur? A promising approach that also includes high sensitivity for phase angle changes, is to go into the locus representation and to treat this problem from a purely geometrical point of view. As can be depicted from figure 3.18(a) and (b) we can calculate the area change $\Delta A = A_1 - A_2$ in the locus curve by using the cross product computation for the area of a triangle between two admittance vectors respectively. This means for the frequency step width first and for most that area changes are far more sensitive to phase angle changes and that this is also nearly independent from the position of a resonance circle lifted by the error of B_0 . This subsection will present measurements, that gives a better alternative to all other concepts and compare it to the *QxSens* method. Before we go into the description of the are detection algorithm, a few definitions will be given in order to understand the flow chart better.

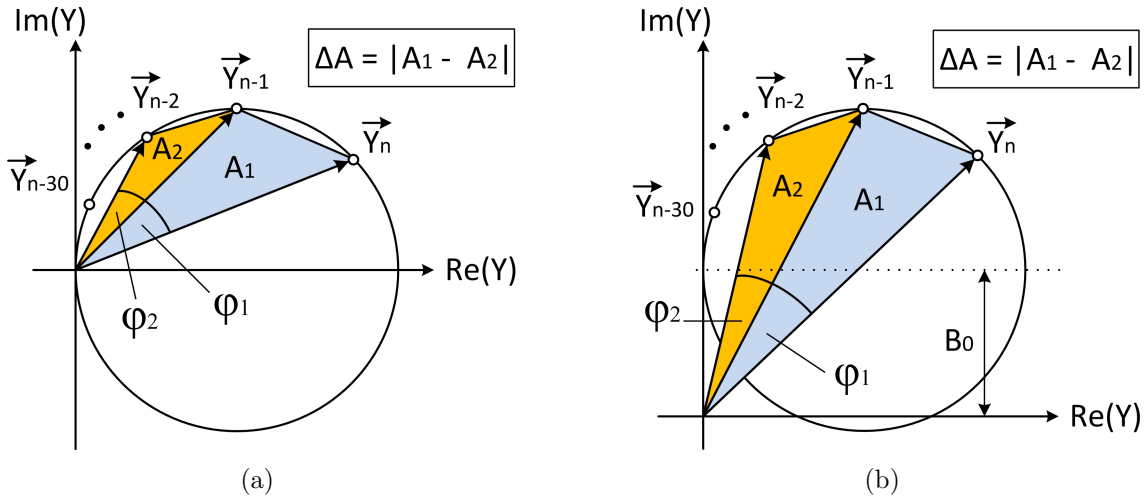


Figure 3.18: Basic idea to detect the are change in the admittance locus by calculating the triangle area between each two admittance vectors; (a) neglect-able influence of B_0 ; (b) for high values respectively

The triangle area formed by each two adjoining admittance vectors is calculated as follows:

$$A = \frac{|\vec{Y}_n \times \vec{Y}_{n-1}|}{2} \quad (3.3)$$

Further computing the area change build-up by a bundle of three contiguous vectors respectively:

$$\Delta A = |A_m - A_{m+1}| \quad (3.4)$$

Similar to the *QxSens* method, we also define a moving average of the latest 30 values of area differences ΔA

$$\overline{|\Delta A|}_{\{\text{last 30 values}\}} = \sum_{m=1}^{28} \frac{\Delta A_m}{28} = \sum_{m=1}^{28} \frac{|A_m - A_{m+1}|}{28} =: MA \text{ (moving average)} \quad (3.5)$$

in order to compare that to the difference of the current two triangle areas. This idea is similar to that of the *QxSens* algorithm, but instead of setting up a minimum and maximum criteria for the length difference of the admittance squares $|\Delta Y^2|$, we use the area difference between two triangles that are spanned with a bundle of three admittance vectors. Finally, this method turns out to have more detection sensitivity, because small changes in the phase angle can be recognised far better in the increase of the triangle area and therefore the control of frequency step width improves immensely, especially with optimized empirical found parameters for this algorithm. Incidentally the length of the chord $|\vec{Y}_n - \vec{Y}_{n-1}|$ is an equivalent option to the area change in order to increase the resonance peak detection.

”Second derivative” slope criteria for resonance peak detection

The evidence from these studies suggests a range for the slope rate related to the admittance and the angular speed in the locus curve. Whereas the triangle area represent the change in \vec{Y} , the difference between two current areas can be seen as ”second derivative”, which inclined a higher phase angle- and resonance detection sensitivity. Let us now define two slope criteria that uses the moving average (equation 3.5) of the last 30 data points during a measurement in order to increase or decrease the frequency step width.

Decrease of Δf by 50%, when: $\boxed{\Delta A > 4 \cdot MA}$

Increase of Δf by 10%, when: $\boxed{\Delta A < MA}$

The parameters presented here where the result of empirical studies with a variety of common ceramic type piezoelectric sensors as well as quartz crystal resonators. When the area change is greater than the minimum rising slope of $4 \cdot MA$, that means we are approaching a resonance peak, then the frequency step width will be decrease in this case by 50% thereby increasing the frequency resolution in the relevant range. Moreover the current frequency will be set back twice the unaltered step values and the measurement rescans this range with lower step size. On the contrary the steps will be increased by 10%, when the area difference in the locus curve is smaller than MA, hence allowing the algorithm to scan the spectrum between resonances faster. Whereas the *QxSens* software implemented the enhancement and reduction of the frequency increment by 20%, the area detection method puts a great value upon maximizing the point density around resonances, thereby preferring to change step ranges unequally.

Necessity of a well-defined "Noise-level"

An important requirement for the previously defined slope criteria in particular the increase of frequency step width to work, is that the hardware has statistical minimal fluctuations in admittance measurements. These small deviations are part of the noise level, which is around $10\mu S$ for the *Impedance Analyzer 16777k*. Therefore, when approaching a resonance peak, the condition of $\Delta A < MA$ is only triggered and the step size increased by 10%, because of small random variation in the measurements. In other words the steps would never be increased between resonances for an ideal hardware with zero noise until the resonance frequency is reached. The explanation for this is given as follows. Once the real- and imaginary part of the admittance become positive (see first quadrant of the locus in figure 3.19(b)), e.g. at early beginnings of new resonances or between two of them, their values will increase strictly monotonically in a world with no noise, therefore never allowing the area difference become smaller than MA until the f_S is passed. In this thought experiment the positive semi-circle would be scanned with high frequency resolution till the resonance frequency and the negative part with very higher step sizes.

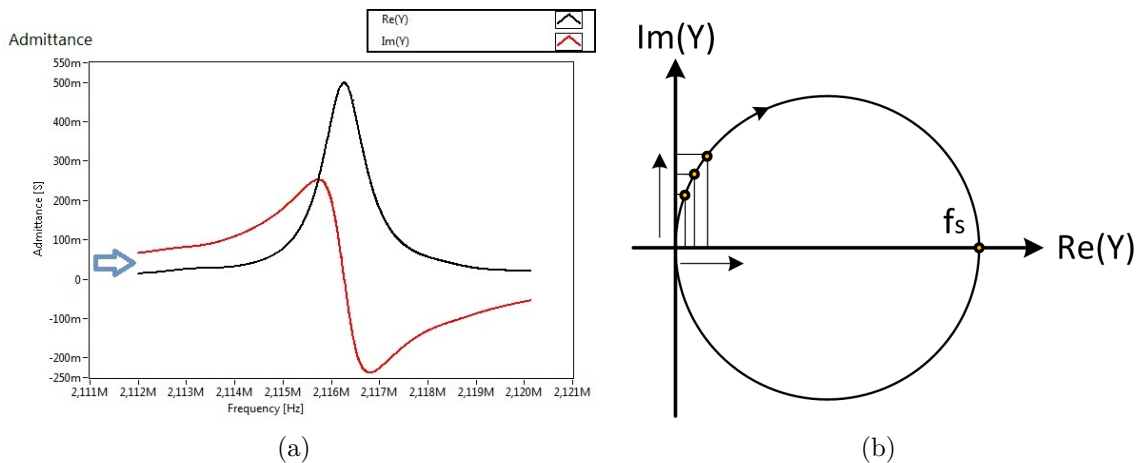


Figure 3.19: The diagrams illustrate the strict monotonic increase of admittance values up until f_S , when the noise level would be zero

In order to avoid the effect described above, we will introduce a so called "Noise-Level", which will be a third input parameter next to the minimum and maximum frequency step width that the user has to specify. The recommended value is $10\mu S$ and will eliminate the randomness of step width increase at the rising part of a resonance peak. For the frequency increment algorithm that means we have to set up an additional criteria, so that the noise-level is well-defined.

Increase of Δf by 10%, when:

$$\Delta G := |G_n - G_{n-1}| < \text{"Noise - Level"} (10\mu S)$$

Here the conductance difference $\Delta G := |G_n - G_{n-1}|$ between two current measurement values is sufficient enough to compare the "Noise-Level". It is important to

point out this comparison criteria has to be validated prior to the other two criteria comparing the area difference in the locus to MA (Moving average), which will also be explained in detail in the are detection algorithm flow chart in figure 3.21. A distinctive measurement example for a quartz crystal sensor ($f_s = 5.9985MHz$) is presented in figure 3.20 to visualize the problem with random increase of Δf at the beginning of a resonance peak. The input parameters are $\Delta f_{Min} = 10Hz$ and $\Delta f_{Max} = 1kHz$. The changes in the frequency step width can be seen with the second y-axis on right side of both diagrams.

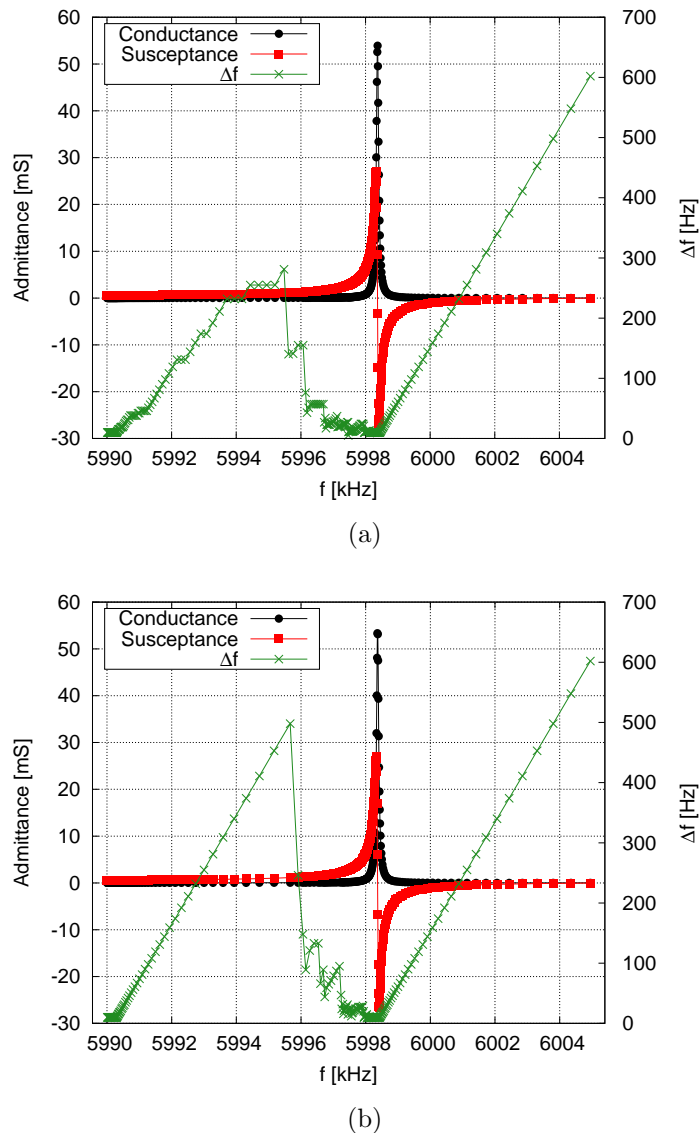


Figure 3.20: Demonstration of the noise influence for step width increases with a measurement of a quartz crystal resonator; (a) Without "Noise-Level" implementation; (b) "Noise-Level" comparison with $10\mu S$

If we compare the graph in figure 3.20(a), whereby the above comparison is not considered, with the measurement in figure 3.20(b) with the "Noise-Level" of

$10\mu S$, we see a distinct difference in the positive gradient of the frequency step width. The first diagram illustrates a random, ill-defined and smaller slope rate, when approaching the resonance peak, where as the second clearly demonstrates a much higher and steady increase in Δf in the frequency ranges around the resonance peaks. Moreover, this idea leads to an decrease in measurement time, in this example of about five seconds. Incidentally in case of hardware improvements that would reduce the noise, the algorithm will work consistently because of the "Noise-Level" input parameter.

Flow chart of the area detection algorithm

The foregoing discussion has attempted to find universal criteria for the resonance peak detection. Let us now bring together all aspects by describing the flow chart of the area detection algorithm. First a list of all input parameters, which will occur is presented.

$$\boxed{fStart; fStop; \Delta fMin; \Delta fMax; "Noise - Level"}$$

Basically the algorithms first performs 30 measurements with the minimal frequency step width ($\Delta fMin$) in order to have enough data to build the moving average. This is ensured by the second query, which can be seen in the flow chart in figure 3.21. When the index is greater than 30, the absolute difference between the current and the last conductance values is calculated and compared to the "Noise-Level". If it is smaller than e.g. $10\mu S$. then change is within the noise and the step can be increased by 10%. In the no-case the absolute area difference is build (see. fig. 3.18) and furthermore the moving average (MA) for the last 30 data points computed. Now we have two possibilities depending on the are in admittance spectrum. When approaching a resonance peak the area difference ΔA will be grater than the four times MA leading to a set-back of the current frequency by twice the current step increment Δf and reducing Δf by 50%. In the other case, whereby passing a resonance, when the area differences become smaller than MA, the current frequency stays unaltered and Δf is increased by 10%. The next step in both cases the step width is coursed into the of $\Delta fMin$ and $\Delta fMax$, avoiding the step size become zero or infinite. The last procedure just adds the adjusted step to the current frequency, which will be also altered, when a reduction took place. The algorithm stops, when the current frequency exceeds the stop frequency $fStop$.

Because of the alteration of the current frequency by two times the current step width, it is possible that the frequency back jump can be greater then the last saved frequency values. Therefore the first query at the beginning of the flow chart makes sure, that all values within the last 10 data points are deleted, when it is greater than the current. In other words, the measurement data will be saved in an ascending frequency order.

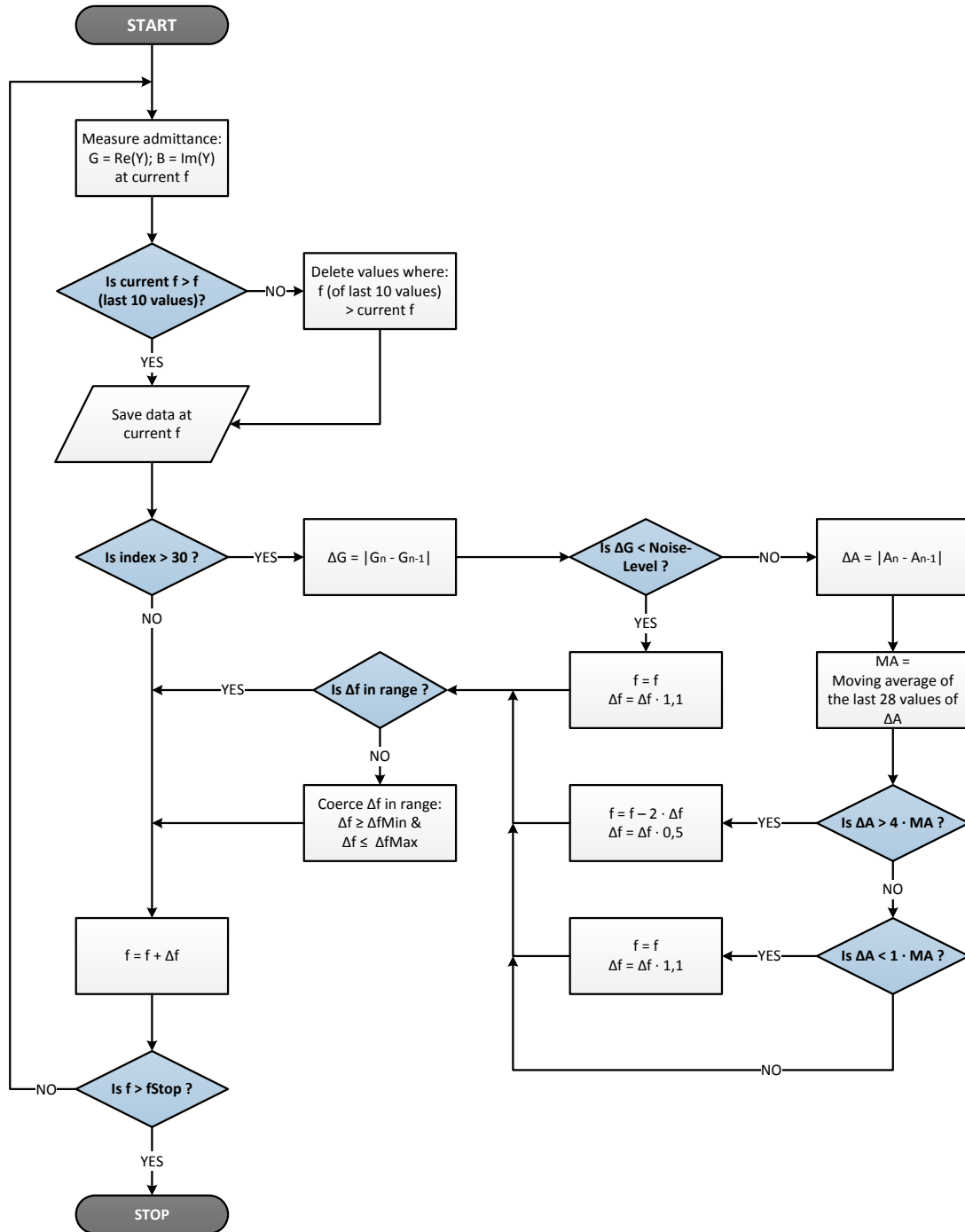


Figure 3.21: This flow chart describes the frequency step optimization for the area detection algorithm; the moving average are build for 30 values in comparison to the 15 in the *QxSens* algorithm

Measurement examples

To demonstrate the improvements in the resonance detection and frequency resolution with the new concept of the area detection algorithm, two measurements

examples of piezoelectric resonators with different quality factors will be given. The first is again an admittance scan of a ceramic type PZT at a frequency range from $2 - 2.2MHz$ (fig. 3.22) and the second is the spectrum of a quartz crystal sensor between 5.995 and $6.005MHz$ (fig. 3.23). Each example contains also the results with the *QxSens* system and for comparison reasons the minimum and maximum frequency steps remained the same ($\Delta f_{Min} = 10Hz$ and $\Delta f_{Max} = 1kHz$). The diagram in figure 3.22(a) for instance depicts two resonance, whereby the one with the conductance amplitude of $5mS$ has Q -factor of 2000. One can interpret the graph in several ways. Firstly it shows very well that the step size Δf is reduced when approaching resonance to the minimum values of 10 Hz at the relevant domains and increased to the maximum of 1 kHz between resonances. Secondly, according also to the locus diagram in figure 3.22(b) the frequency resolution or point density around resonances increased immensely compared to the measurement of the *QxSens* algorithm in figure 3.22(d) for ceramic type sensors.

Similar observations, but not with so large distinctions in the point density, can be seen in the graphs of the quartz resonator in figures 3.23(a) through (d). The reason for that lies in the narrow frequency half width for these type of sensors, whereby the Q -factor amounts to $71.5 \cdot 10^3$.

The results given here prove that this resonance detections concepts fulfils the requirements set out in the in beginning and therefore the area detection algorithm was chosen to be implemented in the demo software of the *Impedance Analyzer 16777k*.

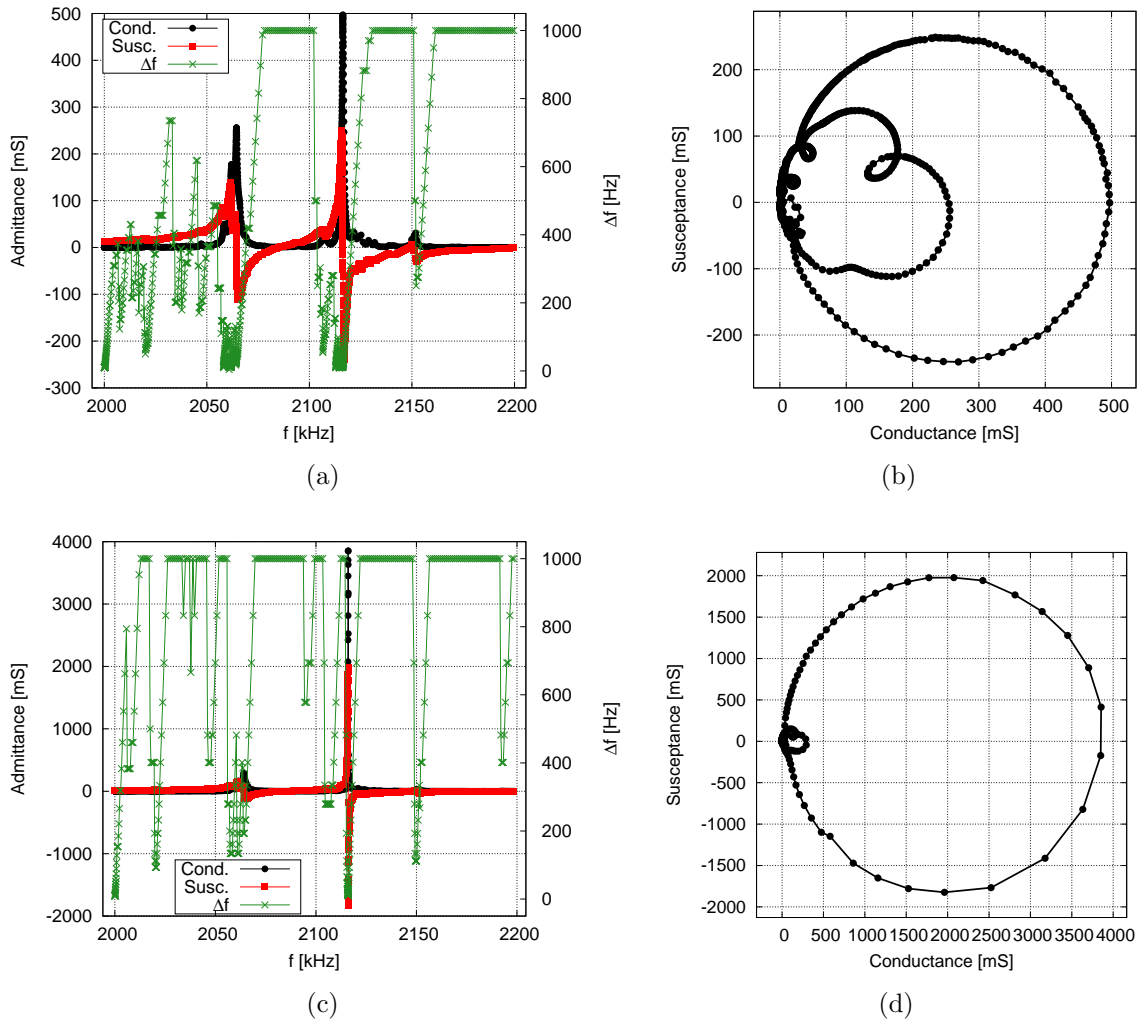


Figure 3.22: Admittance scan of an ceramic type sensor between 2 and 2.2 MHz measured with the area detection algorithm implemented in the demo software of the *Impedance Analyzer 16777k* (a) and (b); *QxSens* system (c) and (d)

3.4 Locus-fit and accurate data evaluation

The second main goal of this work was to implement a fitting procedure that would take the measured conductance data as well as the susceptance data into account, in order to increase the accuracy for the calculated values such as the characteristic frequencies f_s , $f_{-1/2}$, $f_{+1/2}$, the quality factor Q and the equivalent circuit parameters. In other words admittance circles of resonances has to be fitted in the locus diagram of the measured data, since there the real- and imaginary part of the admittance are presented. In this section we first refer to the current fitting procedure of the original software of the *Impedance Analyzer 16777k*, which only uses the conductance data where a Lorentz function is fitted into the measured points. Then we give an alternative solution based on the works of [5], [10] and [11], whereby the basics are outlined in chapter 2.3. Here a detailed description of the locus-fit pro-

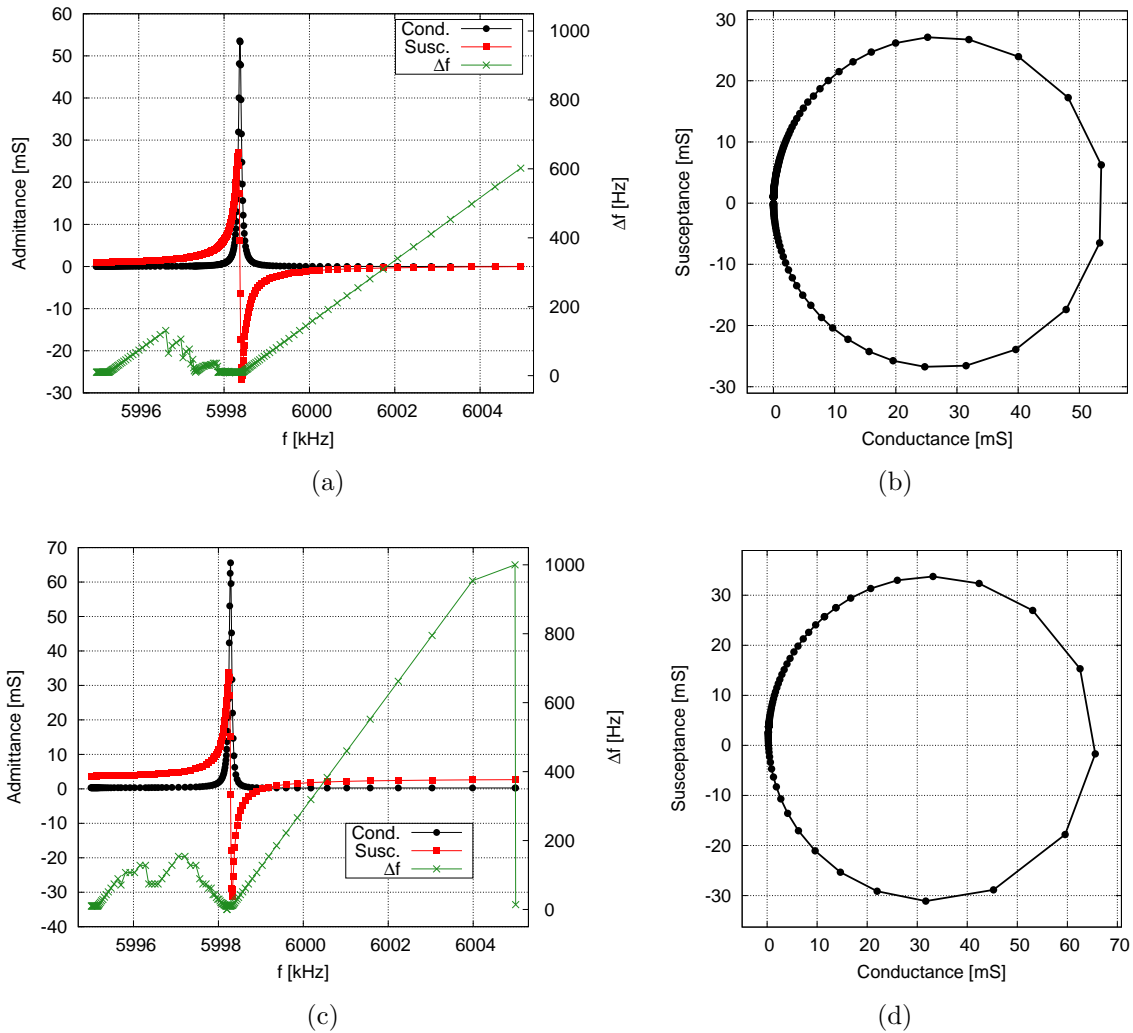
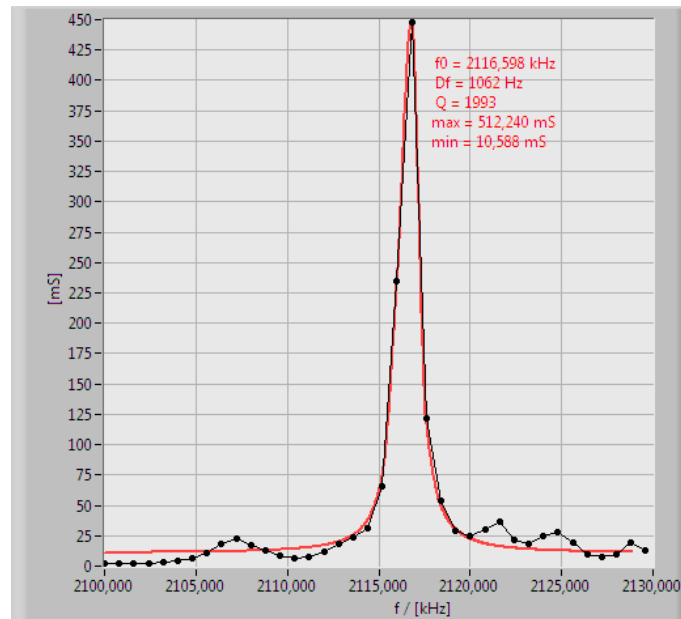


Figure 3.23: Admittance scan of a quartz sensor with the resonance frequency at 5.9985MHz , measured with the area detection algorithm implemented in the demo software of the *Impedance Analyzer 16777k* (a) and (b); *QxSens* system (c) and (d)

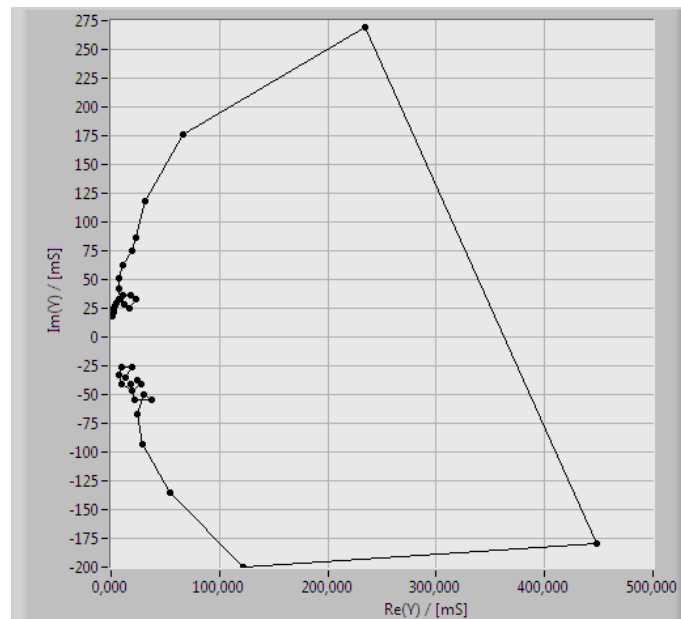
cedure implementation will be specified. Moreover, since an admittance spectrum, especially one of a ceramic type piezoelectric sensor may consist of many main harmonic resonances as well as its an-harmonic peaks, a simple method for analysing each resonance with the Locus-Fit feature will be presented, that will be part of the measurement software.

In figure 3.24(a) an example with the fitting feature of the original SinePhase software is presented, whereby the resonance frequency f_s , the frequency half width (Df) and the quality factor are calculated with the method of fitting a Lorentz function into the data, as well as the minimum and maximum values of the conductance determined. As we can see very well in the locus digram of this measurement, the resonance in this case is scanned with low frequency resolution, therefore lacking enough data points within the resonance half width. In this method, by only taking the conductance into account, the accuracy may be lower since a lot of information

between data points around the half width of a resonance are missing. On the con-



(a)



(b)

Figure 3.24: The initial fit procedure of the original SinePhase software fits a Lorentz function into the conductance data (a); Locus diagram (b)

trary, by using the alternative variation of fitting an admittance circle into the data, the missing measurement points do not have a big consequence on the accuracy of the calculations, since a circle can be defined in the worst case by three data points. We will now give a step by step description of the Locus-Fit, that was implemented

and present measurement examples in the end of this section.

The simplest method for the software user to analyse a specific resonance is to select a frequency range of the measured admittance spectrum, where the resonance of interest is included and judging by visual inspection is the maximum resonance within that area. The algorithm therefore searches always for the resonance with the highest conductance value and uses the corresponding frequency figure as an estimated resonance frequency figure. It is important to emphasize here that the procedure always performs the Locus-Fit for the maximum resonance in the selected area of the spectrum. Since the admittance spectra are scanned with the area detection algorithm with high frequency resolution for relevant resonances, this approach offers the big advantage to analyse each resonance separately, simply by giving the user a tool to zoom in and out within the measured admittance spectrum, thus avoiding rescans of specific domains of interest. The features to enable the data range selection will be described in chapter 4.2.

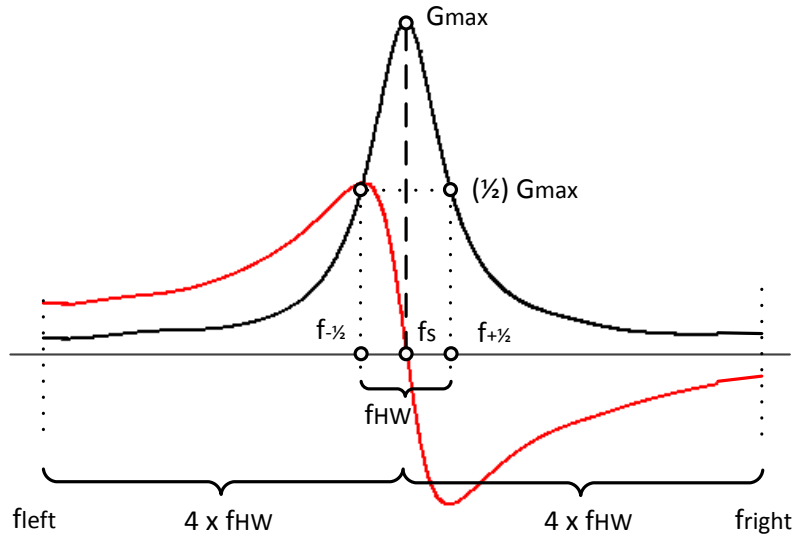


Figure 3.25: Illustrates the determination of the estimated frequency half width f_{HW} and the overall data interval for the Locus-Fit procedure

When the maximum resonance is found, then the algorithm determines automatically an other specific frequency interval within which the corresponding admittance data of that peak will be selected for the Locus-Fit calculations. A good definition is the range

$$\begin{aligned} f_{left} &\leq f \leq f_{right} \\ f_s - 4f_{HW} &\leq f \leq f_s + 4f_{HW} \end{aligned} \quad (3.6)$$

which is eight times the frequency half width of the resonance under consideration.

This data interval is large enough for eliminating statistical errors of the measurement. The estimated band of f_{HW} is defined as

$$f_{HW} = f_{+1/2} - f_{-1/2} \quad (3.7)$$

and determined by searching for the first two frequencies, where their conductance figures are smaller than half of the found conductance maximum (see fig. 3.25).

Calculation of the admittance circle centre and radius

After selecting the measured data of a relevant area of interest, the first step in calculating the wanted parameters is to minimise the difference of the radii of the associated admittance circle. As is outlined in chapter 2.3, we first compute the quantities a to e defined as

$$a = \sum GB - \sum G \sum B/n \quad (3.8)$$

$$b = \sum B/n \left(\sum G^2 + \sum B^2 \right) - \sum B^3 - \sum G^2 B \quad (3.9)$$

$$c = \left(\sum B \right)^2 / n - \sum B^2 \quad (3.10)$$

$$d = \sum G/n \left(\sum G^2 + \sum B^2 \right) - \sum G^3 - \sum GB^2 \quad (3.11)$$

$$e = \left(\sum G \right)^2 / n - \sum G^2. \quad (3.12)$$

whereby the summation is done over the number of data points, denoted here as n . These minimising formulae are then inserted into the equations for determining the centre coordinates (G_c/B_c) of the admittance circle that may be fitted into the data points [11].

$$G_c = \frac{ab + cd}{2(ce - a^2)} \quad B_c = \frac{ad + eb}{2(ce - a^2)} \quad (3.13)$$

This leads then to the determination of the fitted admittance circle radius

$$Y_{radius} = \left[\frac{1}{n} \left(\sum G^2 + \sum B^2 + n(G_c^2 + B_c^2) - 2(G_c \sum G + B_c \sum B) \right) \right]^{1/2} \quad (3.14)$$

and incidentally leading to the calculation of the first equivalent circuit parameter

$$R_1 = \frac{1}{2Y_{radius}} \quad (3.15)$$

The parallel capacitance can then be calculated from the susceptance offset of the circle centre B_c and the estimated value of $f_s = \text{Max}(G)$.

$$C_p = \frac{B_c}{2\pi f_s} \quad (3.16)$$

Extending the Butterworth-Van-Dyke model

If we take a look at a schematic fit of an admittance circle, such as in figure 3.26(a), we can see the deviation of the centre (Y_p) on the conductance axes by the value of G_p . The offset in the susceptance by $B_c = B_p$ can be explained by the parallel capacitance of the sensors electrodes, but since G_p represents the real part of an admittance due to the measurements system spurious effect, the Butterworth-Van-Dyke model must be expanded by including a parallel resistor R_p as the reciprocal of the deviation G_p in the equivalent circuit. Thus defining it as

$$R_p = \frac{1}{G_p} \quad (3.17)$$

whereby the calculation will only be performed for positive values of G_p . It may occur that the circles small deviation is in the negative conductance direction, which has no physical explanation. This can be indicated as systematic errors of the measurement device and therefore in these cases no figure for R_p will be computed.

Shift of the circle centre and simplification of the second minimisation

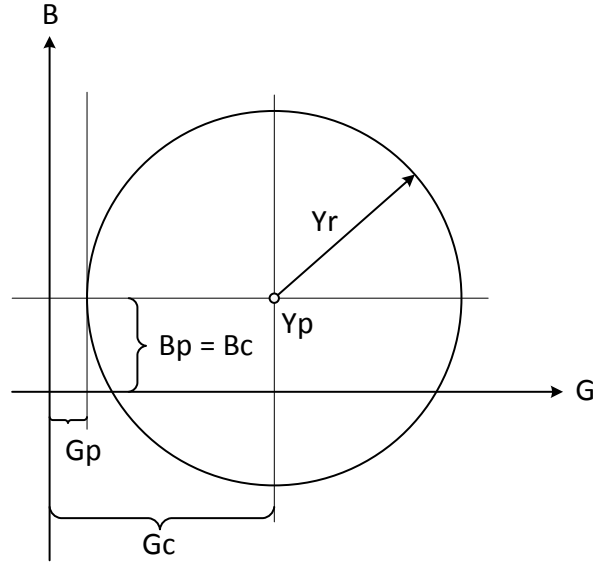
By considering the equations of the second minimisation outlined in chapter 2.3, we can recognise that most terms are dependent on the deviation of the circles centre, in particular on G_p and B_p .

$$\begin{aligned} u_i = & \boxed{-\sum B^3 f^i - \sum G^2 B f^i} \\ & + B_p \left(3 \sum B^2 f^i + \sum G^2 f^i \right) \\ & + 2G_p \sum G B f^i - (3B_p^2 + G_p^2) \sum B f^i \\ & - 2B_p G_p \sum G f^i + (B_p^3 + G_p^2 B_p) \sum f^i \end{aligned} \quad (3.18)$$

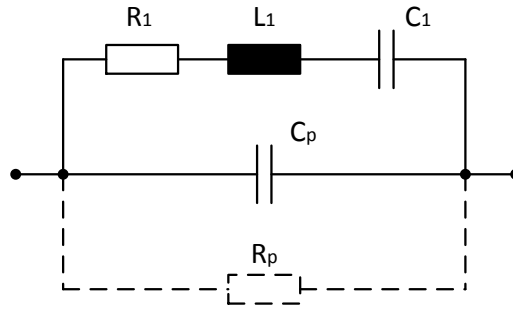
$$\begin{aligned} v_i = & \boxed{\sum G^4 f^i + \sum B^4 f^i} - 4G_p \sum G^3 f^i - 4B_p \sum B^3 f^i \\ & + 6G_p^2 \sum G^2 f^i + 6B_p^2 \sum B^2 f^i - 4G_p^3 \sum G f^i \\ & - 4B_p^3 \sum B f^i + G_p^4 \sum f^i + B_p^4 \sum f^i + \boxed{2 \sum G^2 B^2 f^i} \\ & + 2G_p^2 B_p^2 \sum f^i + 2G_p^2 \sum B^2 f^i + 2B_p^2 \sum G^2 f^i \\ & - 4B_p \sum G^2 B f^i - 4G_p \sum G B^2 f^i \\ & - 4G_p B_p^2 \sum G f^i - 4G_p^2 B_p \sum B f^i + 8G_p B_p \sum G B f^i \end{aligned} \quad (3.19)$$

for $i = 0, 1$ and 2 .

Since all data values are stored and easily computable, a simple subtraction of G_p and B_p from all measured data values within the fit procedure, leads to a drastic



(a)



(b)

Figure 3.26: Schematic admittance circle Locus-Fit centre at (G_c/B_c) (a); extending the Butterworth-Van-Dyke model by R_p (b)

simplification of the formulae (3.18) and (3.20). Hence, resulting to

$$u_i = \boxed{-\sum B^3 f^i - \sum G^2 B f^i} \quad (3.20)$$

$$v_i = \boxed{\sum G^4 f^i + \sum B^4 f^i} + \boxed{2 \sum G^2 B^2 f^i} \quad (3.21)$$

for $i = 0, 1$ and 2

whereby G_p and B_p become zero, when the admittance circle is shifted into the origin (see fig. 3.27). Furthermore, the offset of B_p is calculated for each data point with the corresponding frequency values since C_p was determined in the first minimization step.

$$B_p = 2\pi f_{data\ point} C_p \quad (3.22)$$

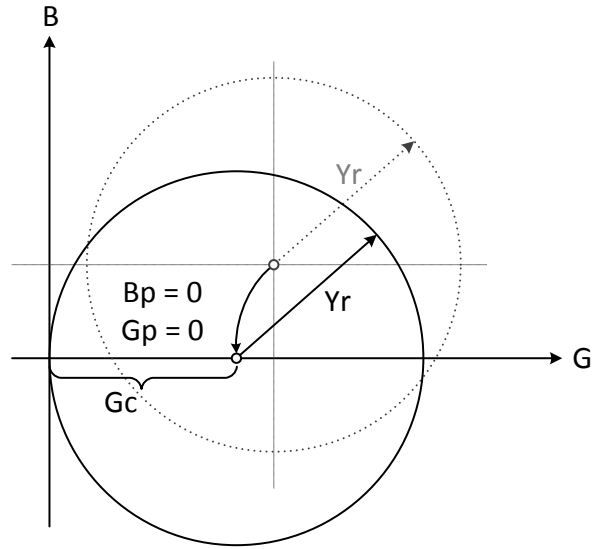


Figure 3.27: Shifting the admittance circle into the origin by subtracting G_p and B_p from every data point

Using the simplified expressions u_i and v_i we can now compute the remaining parameters of interest in the following way

$$f_s = \frac{u_1 v_1 - u_0 v_2}{u_1 v_0 - u_0 v_1} \quad (3.23)$$

$$C_1 = \frac{1}{\pi f_s} \frac{v_0 v_2 - v_1^2}{u_1 v_1 - u_0 v_2} \quad (3.24)$$

$$Q = \frac{1}{2\pi f_s C_1 R_1} \quad (3.25)$$

$$L_1 = \frac{1}{4\pi^2 f_s^2 C_1} \quad (3.26)$$

Locus-Fit plot

Once the parameters of the equivalent series circuit are determined, we can now calculate their admittance values. Since the spurious components C_p and R_p are eliminated by the shift of the circle, we are left with the motional arm of the circuit in figure 3.26(b), consisting of R_1 , L_1 and C_1 . Using the same frequency range of

$8f_{HW}$ and predefined step width, the admittance can be given as

$$Y = G + jB = \frac{R_1}{R_1^2 + X^2} + j \frac{-X}{R_1^2 + X^2} \quad (3.27)$$

$$G = \frac{R_1}{R_1^2 + \left(\omega L_1 - \frac{1}{\omega C_1}\right)^2} \quad (3.28)$$

$$B = -\frac{\omega L_1 - \frac{1}{\omega C_1}}{R_1^2 + \left(\omega L_1 - \frac{1}{\omega C_1}\right)^2} \quad (3.29)$$

$$(3.30)$$

with $\omega = 2\pi f$. In order to plot the admittance circle calculated with the parameters resulting from the Locus-Fit over the measured data in the locus graph, each value must be shifted back by adding G_p to the conductance and B_p to the susceptance. This leads to the correction of

$$Y_{plot} = G_{plot} + jB_{plot} \quad (3.31)$$

$$G_{plot} = G + G_p \quad (3.32)$$

$$B_{plot} = B + B_p = B + 2\pi f C_p \quad (3.33)$$

$$(3.34)$$

whereby B_p must be newly computed with the new frequency figures. Furthermore, the remaining characteristic frequencies $f_{-1/2}$ and $f_{+1/2}$ are determined by

$$f_{-1/2} = f(\text{Max}(B)) \quad (3.35)$$

$$f_{+1/2} = f(\text{Min}(B)) \quad (3.36)$$

Thus the algorithm searches for the corresponding frequencies for maximum and minimum of the susceptance, which are the top and bottom points on the Locus-Fit circle. These values can only be determined with high accuracy, when the frequency resolution for the calculated fit are chosen high. A good choice to determine the smallest step for the plot calculation is

$$\Delta f = \frac{8f_{HW}}{50000} \quad (3.37)$$

This means that for each resonance under consideration the Locus-Fit plot will have fifty-thousand data points to overlay over the measured data. The memory usage and in further consequence the file-size is around a few mega byte, hence justifying the high resolution of the plot data.

Flow chart of the Locus-Fit algorithm and Locus-Fit example

All the described steps to evaluate accurate parameters for each resonance of the measured admittance spectrum can be summarized in the Locus-Fit flow chart in figure 3.28. Moreover the algorithm recognises, when a fit procedure is unsuccessful

due to lack of data, to small frequency range or influence of mode couplings in the resonance and notifies the user with an error message. Another feature is that the plot calculations will only be executed, when there are changes in fit parameters for the same resonance, therefore avoiding unnecessary computing.

A demonstration of the Locus-Fit algorithm can be given with the measurement and calculation results in figure 3.29 for a resonance of a ceramic type sensor at $2.1MHz$. As the locus diagram illustrates an admittance circle could be fitted into the measured data even due too big frequency steps only one value was available within the resonances frequency half width (see fig. 3.29(b)). The calculated characteristic frequencies results in a resonance frequency of $2116.526kHz$, a quality factor of 1834 and a frequency half width of $1151Hz$. The equivalent circuit parameters and the representation of spurious effects can be found on the right of the locus curve. The results of the Locus-Fit are then plotted over the conductance and susceptance data separately in the graph of admittance versus the frequency and figure 3.29(a) shows that the calculation fit the data very accurately for the selected frequency range of 8 times the estimated frequency half width.

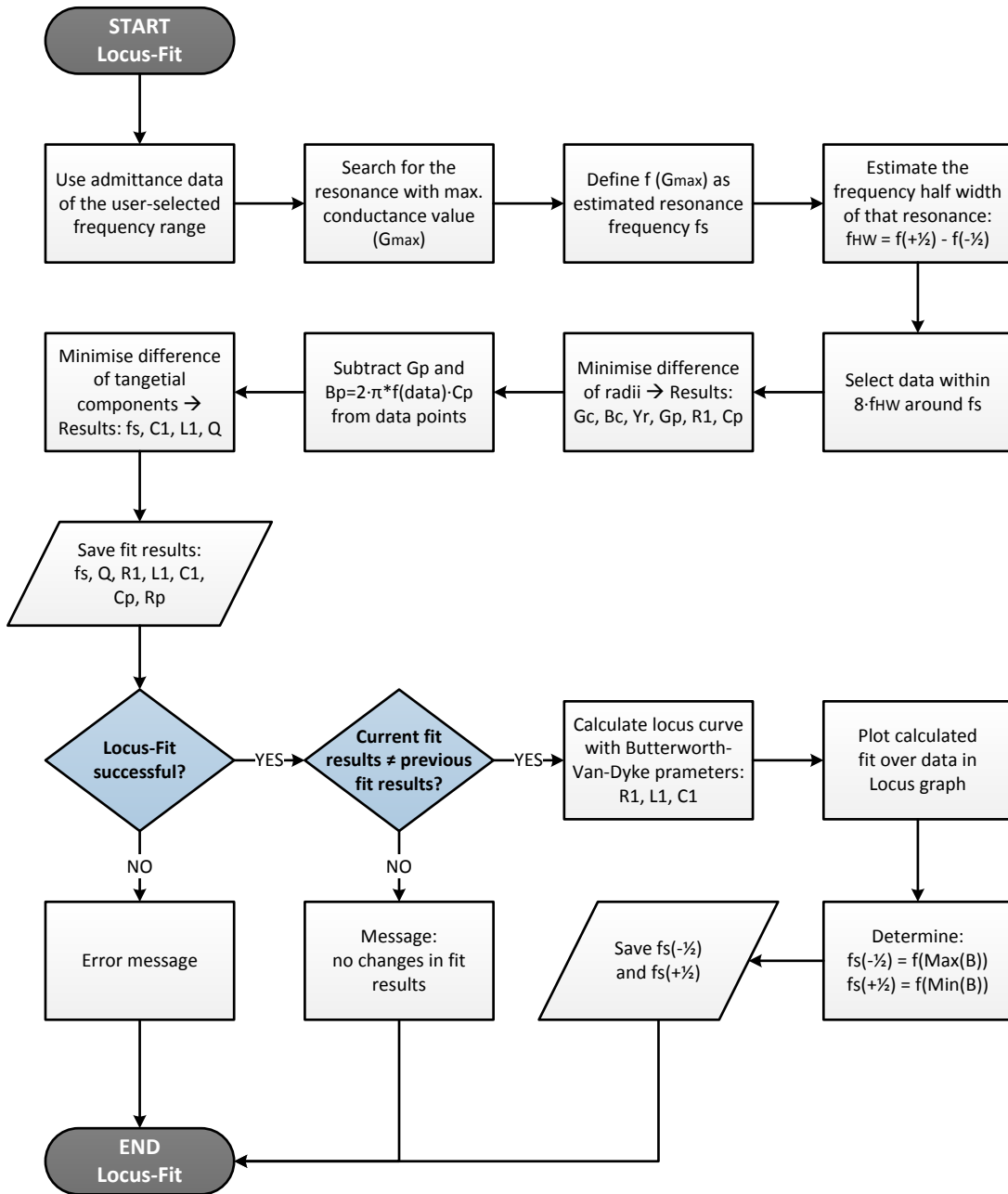
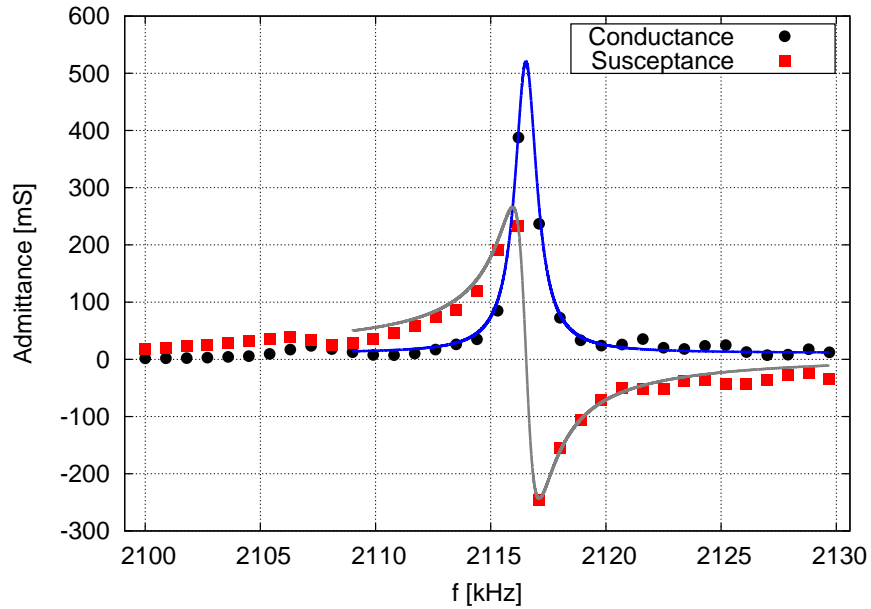
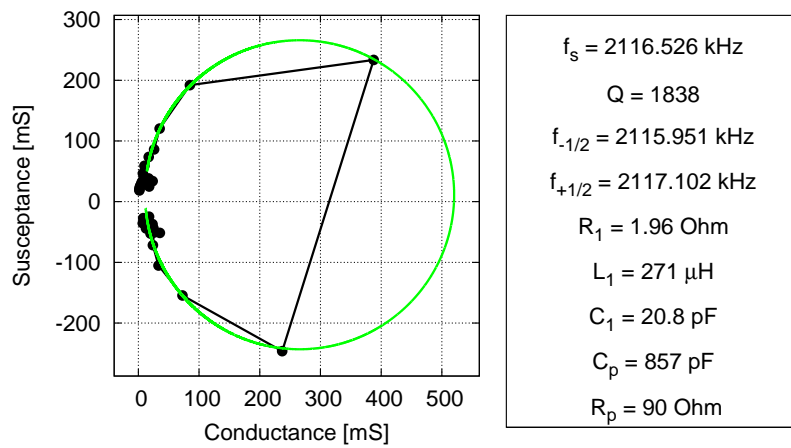


Figure 3.28: Flow chart of the Locus-Fit algorithm



(a)



(b)

Figure 3.29: Demonstration of the Locus-Fit algorithm for a ceramic type resonator with too high frequency steps; (a) Fit of the admittance plot based on the results of the Locus-Fit; (b) Locus-Fit with the calculated parameters

Chapter 4

Admittance scan software

A great deal was written about the methods for the resonance peak detection with the dynamic frequency step change and the Locus-Fit algorithm in the previous chapter. Our focus is now on the implementation of the described methods, which was realised in the graphical programming software LabVIEW®. Firstly, this chapter will present an overview of the admittance scan software by giving a state diagram and the data flow chart of the two important procedures "Measure" and "Locus-Fit". Secondly, the software interface will be discussed briefly and a user manual will guide through all relevant features. As part of that some usability aspect will be addressed as well.

4.1 Software state diagram and procedures

4.1.1 Overview

Apart from the "Start"-and "End"-state, the implemented admittance scan software has an overall number of seven states. An overview of them and their particular transitions are illustrated in figure 4.1. After the program is executed it begins with the "Connect" state, where the connection with the *Impedance Analyzer 16777k* will be established and stays there unless the correct hardware was found. Then the first measurement continuous immediately after the "Initialization" into the main status of "Measure". Here the actual frequency step algorithm based on the area detection method is performed and the measured admittance values are stored in a admittance spectrum graph and locus diagram. Once the current frequency is higher than the stop frequency then the "Wait" is next step in the diagram, where five different states are possible. First we can perform a "Locus-Fit" for the measured spectra, resulting into the list of calculated fit-parameters, or start a new measurement with new scan parameters, as well as new sensors, which closes the loop at the "Initialization" state. For each new measurement all graphs and fit results are deleted and the measurement time set to zero. The other group of states are the "Export admittance data" state and "Export Locus-Fit results", where in both the corresponding data can be stored in a data file. Any visual inspection by zooming in and out within the measured admittance graph does not change the state

of "Wait". Lastly in the "End" status the hardware will be released and the program closed.

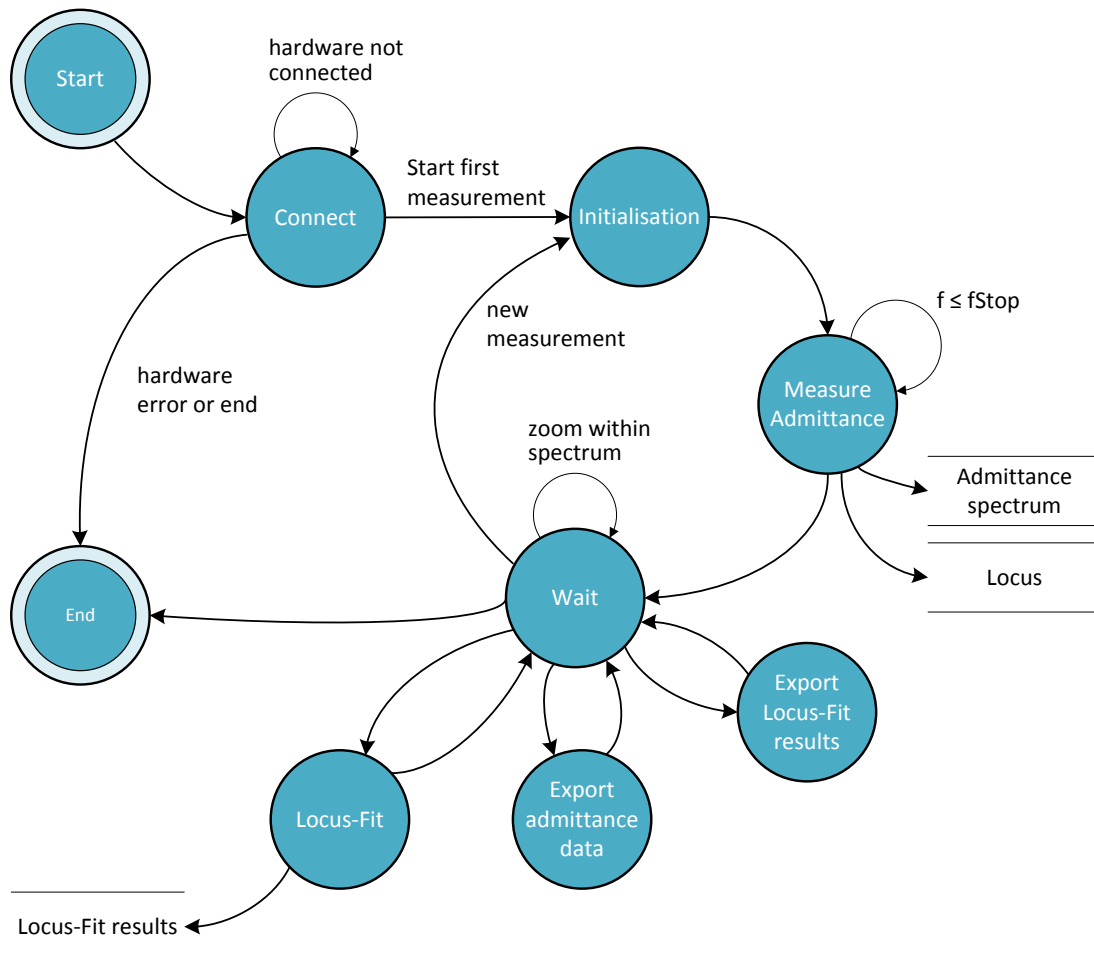


Figure 4.1: State diagram of the admittance scan software

4.1.2 Measurement procedure

Since only in two states, data is produced and saved, we want now look firstly upon the data flow chart of the measurement procedure (see fig. 4.2). There are two scan modes, linear and dynamic mode. The first uses the minimum frequency step Δf_{Min} as a constant. In the second mode, the step optimization using the area detection algorithm, varies the steps between the range of Δf_{Min} and Δf_{Max} . The delay time avoids transient effects of the measurement and is alongside with the current frequency value the most important input parameter for the hardware to measure the admittance accurately. When the data is available, they are corrected by the probe compensation module and saved in an ascending frequency order in

the data array. The results of the measurement procedure are the graphs, where the conductance and the susceptance are plotted versus the frequency in an admittance graph. The second representation of the data is the locus diagram.

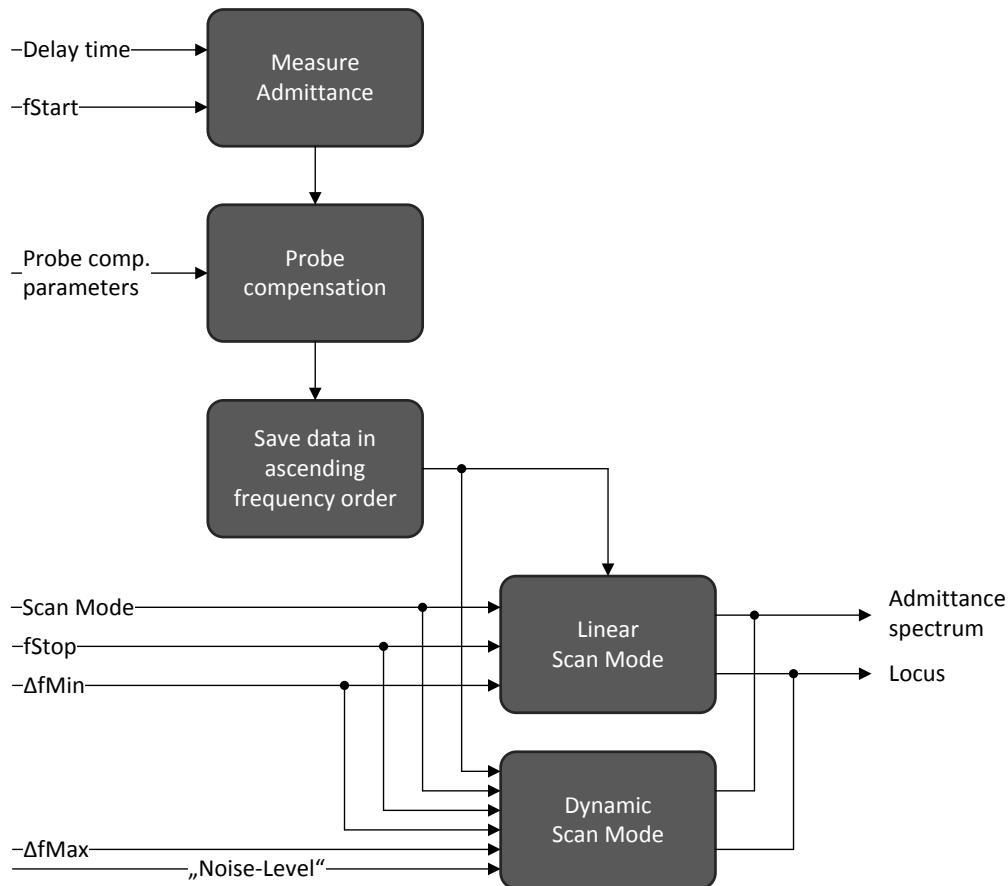


Figure 4.2: Data flow diagram of the measurement procedure within the state "Measure"

4.1.3 Locus-fit procedure

This procedure uses the frequency range selected from the user by zooming within a measured admittance spectrum and their corresponding admittance values to narrow the data range to eight times the estimated frequency half width around a resonance. Figure 4.2 shows an overview of the data flow of the fit calculation. The so called radial fit module results in the parameters R_1 , R_p and C_p . With the information of the admittance circle centre (G_p/B_p) the data points are moved to the origin and the tangential part of the fit procedure calculates the remaining parameters f_s , C_1 , L_1 and Q . With the characteristic values of the Butterworth-Van-Dyke equivalent

circuit the data for the Locus-Fit plot and the half width frequencies $f_{-1/2}$ and $f_{+1/2}$ are determined.

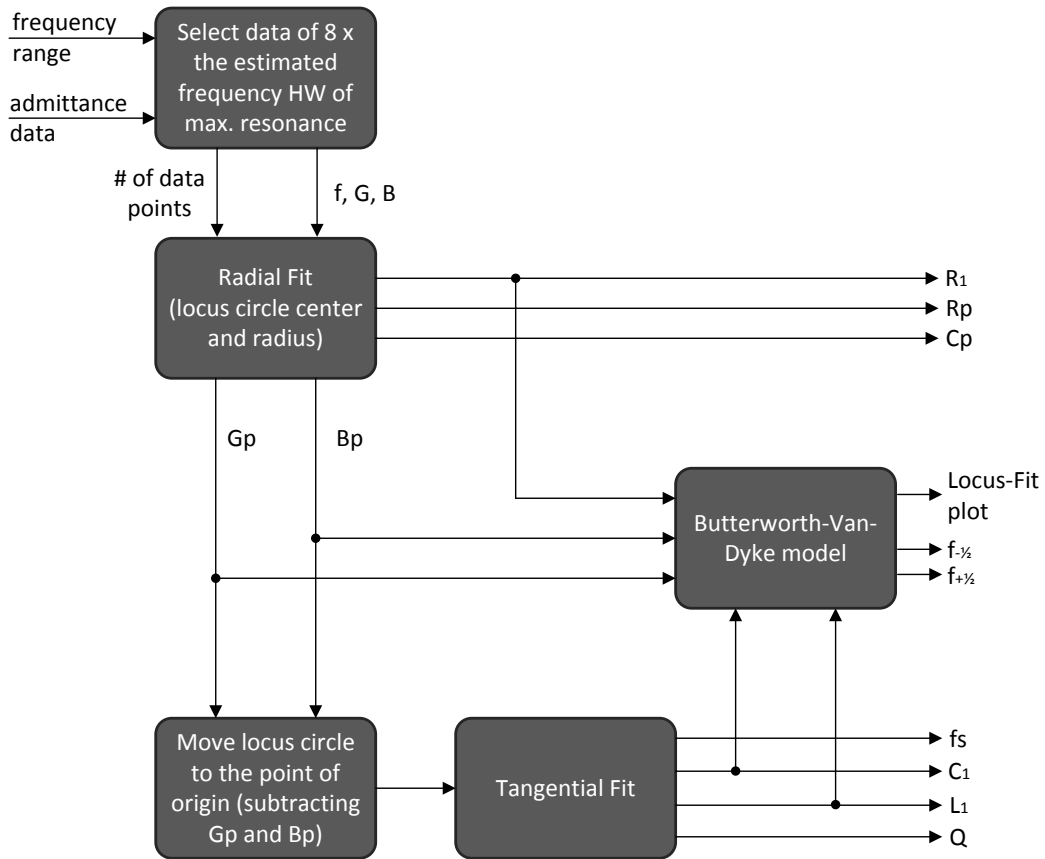


Figure 4.3: Data flow diagram of the Locus-Fit procedure within the state "Locus-Fit"

4.2 Software user interface

In this section we now introduce the software user interface of the admittance scan software that was based on the demo version of the original SinePhase software for the *Impedance Analyzer 16777k*. As we can depict from figure 4.4, the input parameters, such as the frequency ranges, "Noise Level" or the values for probe compensation, are located on left side, where as the measurement results are displayed in the two graphs in the center of the interface. Right below the admittance and locus diagram are the current frequency range displayed and the four buttons for features as for instance Locus-Fit, range selection or data export possibilities. At the bottom there is a color coded list of the fit results, which corresponds with

resonances in the locus graph. Next to that is the Butterworth-Van-Dyke equivalent circuit diagram extended with the resistor R_p .

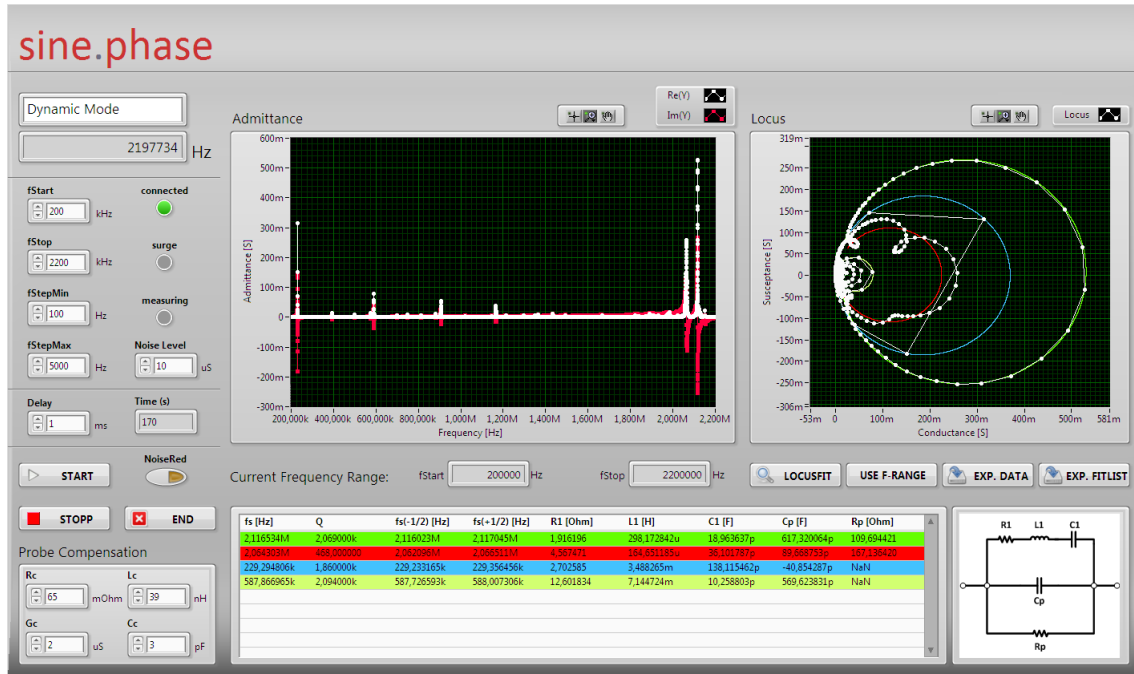
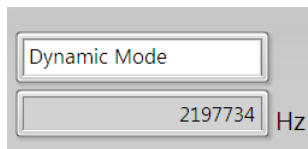


Figure 4.4: User interface of the admittance scan software based on the demo version of SinePhase

4.2.1 User manual

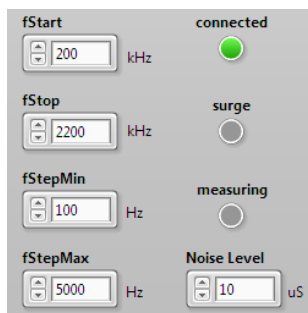
After executing the software it searches automatically for the *Impedance Analyzer 16777k* and tries to build a connection. This is only possible, when it is not connected to the original software of SinePhase. Therefore, multi use of the device with different applications is not possible. When a error free connection could be established the "Start"-button is enabled and "connected" LED is set to green. A measurement can then be started after selecting the scan mode in the pull-down menu in the upper left corner and all the input parameters entered. The delay time is important for transient effects and must be chosen depending on the magnitude of the quality factor of the sensor under test. The parameters for the probe compensation can be given by fields in the lower left corner, and must be determined for every frequency range of interest. It is important to point out here that their determination feature must first be done with the original software of SinePhase (see SinePhase "Impedance Analyzer 16777k - User manual 2.2" [7]). In other word theses parameters must be found for each type of resonator and frequency band prior to using this admittance scan software. Since the algorithms of the present work will be incorporated in the original software of SinePhase in their next release, it didn't make sense to implement the probe compensation feature here. When the proper range of minimum and maximum frequency step width (Δf_{Min} and Δf_{Max}) was found in the dynamic scan mode, it starts with 30 measurements for

building the moving average and continuous with the step size change depending on the admittance spectrum and number of resonances. After the scan is finished the user can select an certain frequency range and perform a Locus-Fit for the maximum resonance in that area. The measurement can be stopped prematurely during measurements and the data still used for analyses. This way the user does not have to wait till the stop frequency is reached in case the range was chosen to big. The measurement time is also displayed for each scan and is also a good indication how well the input parameters of Δf_{Min} and Δf_{Max} are chosen. For even more reduction of noise the so called noise reduction button ("Noise Red") can be activated, which performs an averaging of several measurements for each frequency and leads to longer overall measurement time. The flowing screen shots will give more information on all aspect of the user interface.



Scan-mode and current frequency

The first box is an pull down menu, where the two scan modes "Linear Mode" and "Dynamic Mode" can be chosen. The second field is just for displaying the current frequency during measurements. The maximum resolution is 1 Hz.



Frequency input parameters, "Noise Level" and hardware status LEDs

Start- and Stop frequency is self-explanatory, but "fStepMin" stands for Δf_{Min} and "fStepMax" for Δf_{Max} , which are the main parameters for the dynamic scan mode. The "Noise Level" is set by default to $10\mu S$ and defines a fixed noise level to avoid random increases of the frequency steps (see chapter 3.3.4).



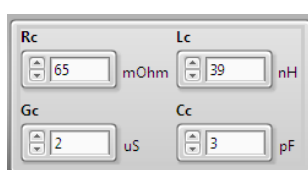
Delay time and measurement time

The delay time is to avoid transient effects and can be set to these values: 1 ms, 10 ms, 30 ms, 100 ms. The measurement time keep track of the overall time for each admittance scan.



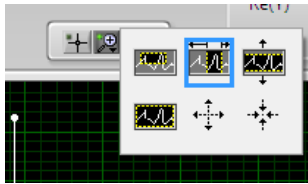
Program control buttons and noise reduction

The "Start"- and "Stop"- button starts and stops a new measurement. The "End"- button ends the hole program. The noise reduction increases accuracy by averaging over several measurement values, but on the contrary increases the scanning time.



Probe compensation parameters

The determination of these parameters must be done for each frequency range with the original admittance software from SinePhase, but the actual correction is of course implemented within the present work.



Zoom features

Each graph has a pallet of several zoom function in order to select analyse certain areas of the measured admittance more closely. They are located in middle above the diagrams.



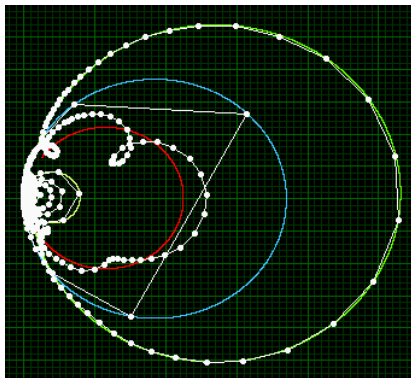
Locus-Fit, frequency range selection and data export

The Locus-Fit and the data export are self explanatory, but the "USE F-RANGE"- button uses the current frequency range in the admittance graph and pre-set the start- and stop frequency as new input parameters to increase the usability.

fs [Hz]	Q	fs(-1/2) [Hz]
2,116534M	2,069000k	2,116023M
2,054303M	458,000000	2,052095M
229,294806k	1,860000k	229,233165k
587,866965k	2,094000k	587,726593k

List of resonance fit results

Here the results of all fitted resonance are stored and can be exported in a data file. The background color of each row has the corresponding color as the plotted fit in the locus graph in order to distinguish resonances.



Current frequency range

This range is updated zooming within an area of the admittance graph.

4.2.2 Usability aspects

There are two main aspects regarding the good usability of this program. Firstly, the admittance- and the locus graph are linked in such a way, that it only shows

the data points that are zoomed in the admittance diagram. The second point is that, when a certain area of the admittance graph is chosen, then the Locus-Fit will always be calculated for the resonance with the highest conductance value, i.e. the maximum resonance for that range. Both makes this software a great tool to analyse the admittance spectra and let the user keep track of data very intuitively.

Chapter 5

Results and Discussion

In this chapter a series of admittance measurements of two ceramic type PZTs and three quartz crystal resonators will be presented. All these sensors are measured with the three impedance measurement systems introduced within the course of this work. The first is the *Impedance Analyzer 16777k* with the area detection and the "Locus-Fit" algorithms. We will summarize and denote this system as "SinePhase" in the results. The second is the *QxSens* method and the third device is the *Agilent 4395A*, which will be used as a reference system in order to evaluate the quality and improvements of the resonance detection algorithm as well as the accuracy of the locus-fit parameters.

5.1 Ceramic type PZT

5.1.1 PIC 255

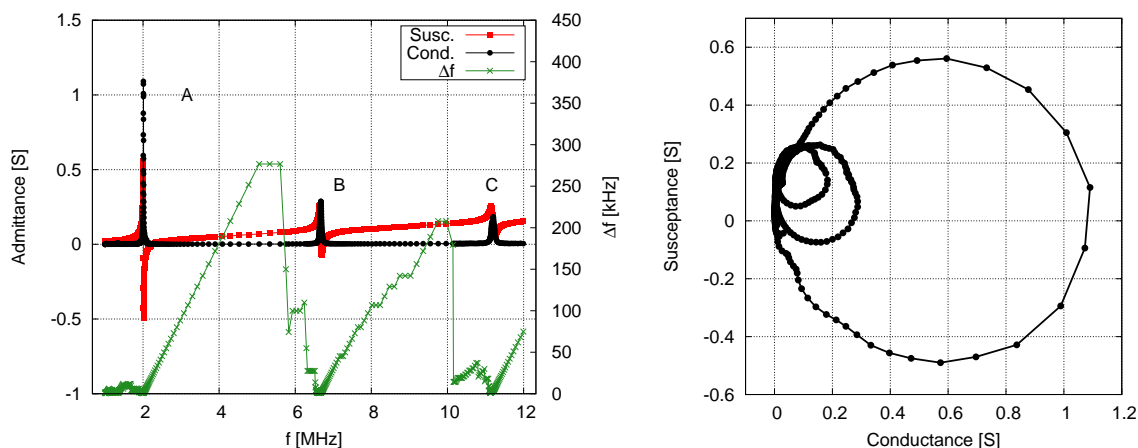


Figure 5.1: Overall admittance spectrum of the PIC 255 measured with the "SinePhase" system in dynamic scan mode; measurement time amounts to 69s

The PIC 255 specimen is a ceramic type sensor made of a modified piezoelectric ceramics material by the company PI Ceramic GmbH with low quality factor and

optimized for actuator applications under dynamic conditions (i.e. for force and acoustic pick ups) [15]. The three resonances A-C from the overall spectrum (fig. 5.1) from $1MHz - 12MHz$ are measured separately and will be presented below.

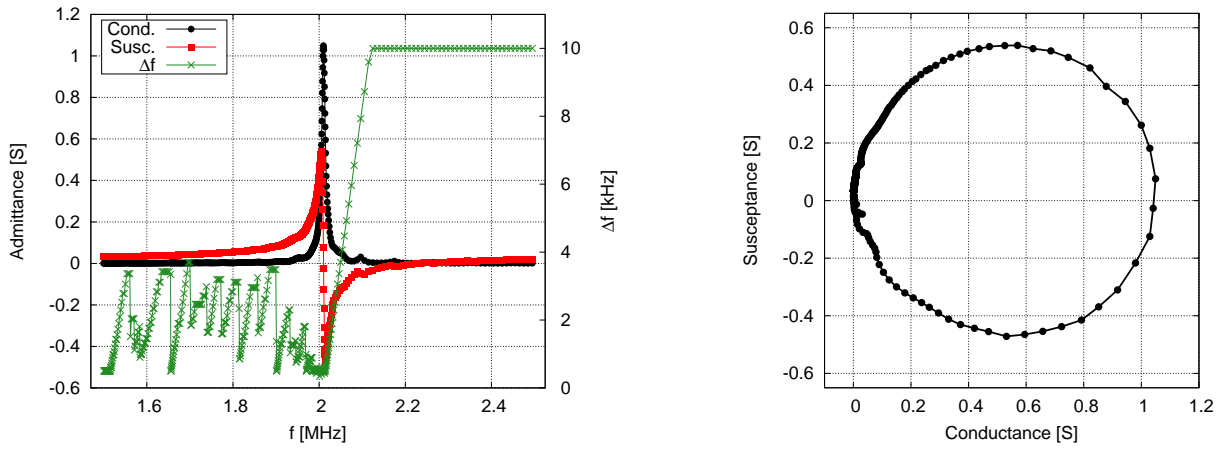
PIC 255 - Measurement input parameters

Overall spectrum:				
$f_{Start} = 1MHz \quad f_{Stop} = 12MHz$				
	Δf_{Min}	Δf_{Max}	Delay time	Probe comp. parameter
SinePhase	1 kHz	300 kHz	10 ms	$R_c=75 \text{ m}\Omega \quad L_c=36.8 \text{ nH}$ $G_c=7 \text{ }\mu\text{S} \quad C_c=2.68 \text{ pF}$
Resonance A				
$f_{Start} = 1.5MHz \quad f_{Stop} = 2.5MHz$				
	Δf_{Min}	Δf_{Max}	Delay time	Probe comp. parameter
SinePhase	500 Hz	10 kHz	10 ms	$R_c=50 \text{ m}\Omega \quad L_c=38 \text{ nH}$ $G_c=5 \text{ }\mu\text{S} \quad C_c=3.4 \text{ pF}$
QxSens	500 Hz	10 kHz	10 ms	internal comp. $R_C=22\Omega$
Agilent	282.5 Hz	8.158 kHz	internal	probe length 100 mm
Resonance B				
$f_{Start} = 6.15MHz \quad f_{Stop} = 7.15MHz$				
	Δf_{Min}	Δf_{Max}	Delay time	Probe comp. parameter
SinePhase	500 Hz	10 kHz	10 ms	$R_c=75 \text{ m}\Omega \quad L_c=37.4 \text{ nH}$ $G_c=2 \text{ }\mu\text{S} \quad C_c=2.7 \text{ pF}$
QxSens	500 Hz	10 kHz	10 ms	internal comp. $R_C=22\Omega$
Agilent	322.1 Hz	8.173 kHz	internal	probe length 100 mm
Resonance C				
$f_{Start} = 10.7MHz \quad f_{Stop} = 11.7MHz$				
	Δf_{Min}	Δf_{Max}	Delay time	Probe comp. parameter
SinePhase	500 Hz	10 kHz	10 ms	$R_c=85 \text{ m}\Omega \quad L_c=36.6 \text{ nH}$ $G_c=7 \text{ }\mu\text{S} \quad C_c=2.68 \text{ pF}$
QxSens	500 Hz	10 kHz	10 ms	internal comp. $R_C=22\Omega$
Agilent	432.9 Hz	7.209 kHz	internal	probe length 100 mm
Further input parameters				
	Overall spec.	Resonance A	Resonance B	Resonance C
SinePhase	$10 \text{ }\mu\text{S}$	$10 \text{ }\mu\text{S}$	$10 \text{ }\mu\text{S}$	$10 \text{ }\mu\text{S}$
"Noise Level"				

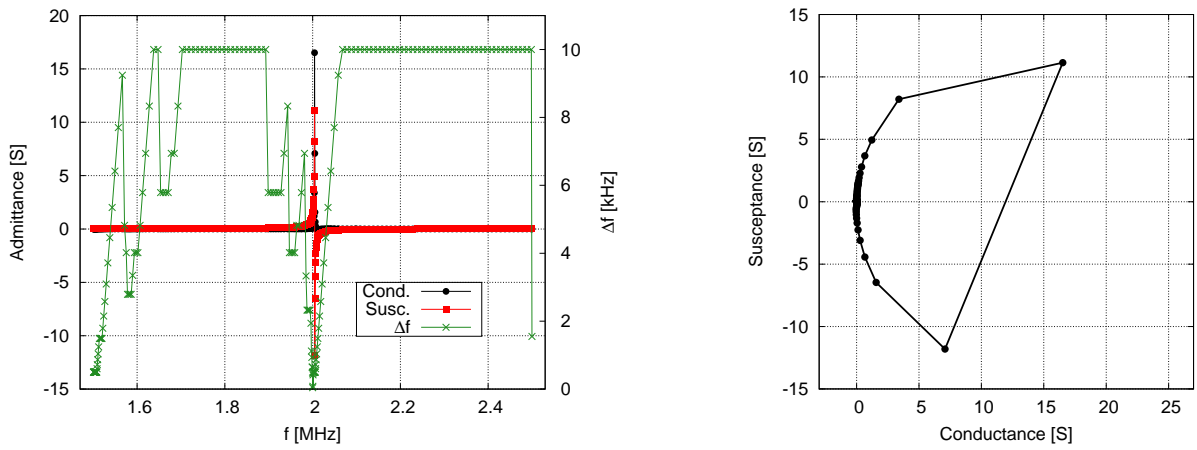
Table 5.1: Summary of the applied input parameters for the PIC 255

PIC 255 - Admittance measurements and fit results

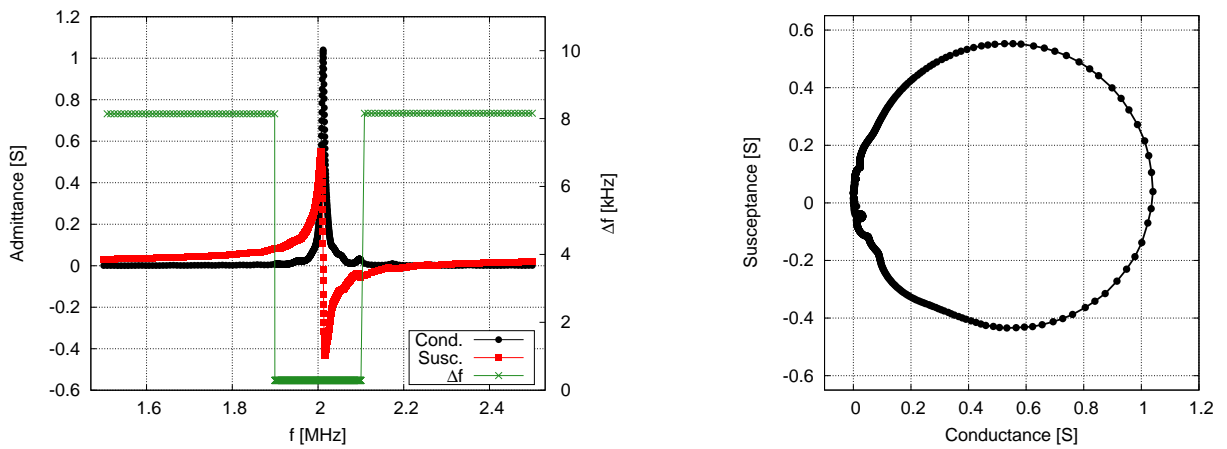
PIC 255 - Resonance A



(a) Impedance Analyzer 16777k (SinePhase)



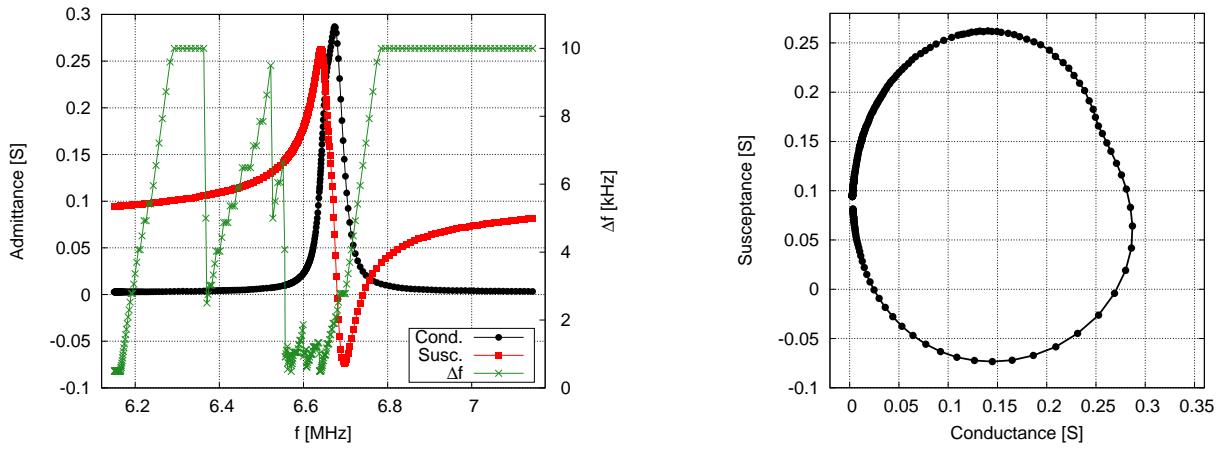
(b) QxSens



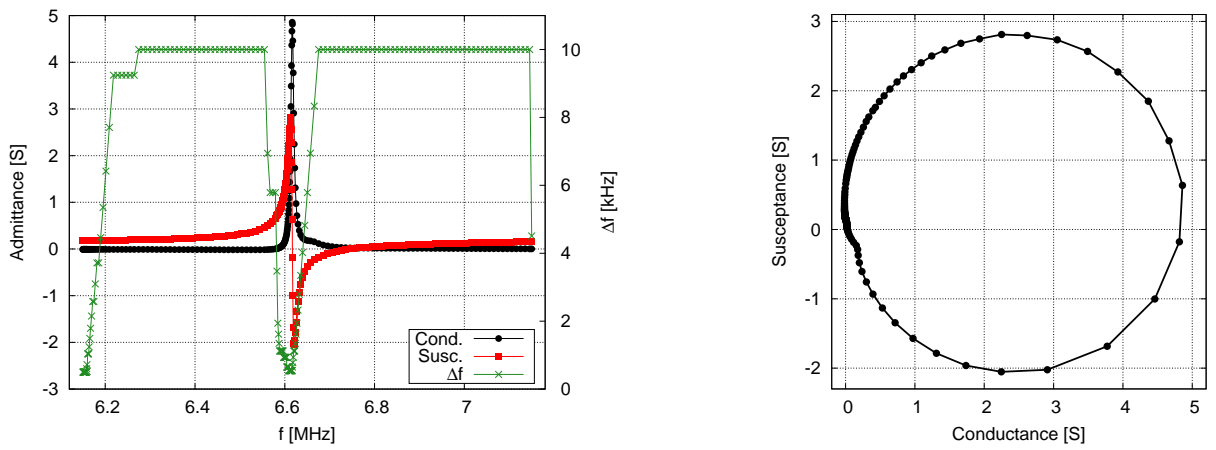
(c) Agilent 4395A

Figure 5.2: Admittance scan of PIC 255 - Resonance A at 2 MHz

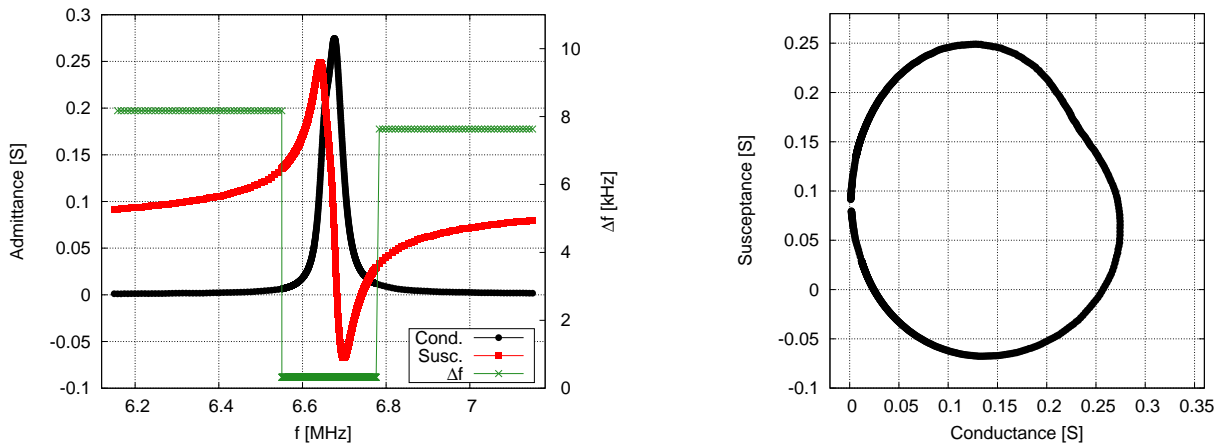
PIC 255 - Resonance B



(a) Impedance Analyzer 16777k (SinePhase)



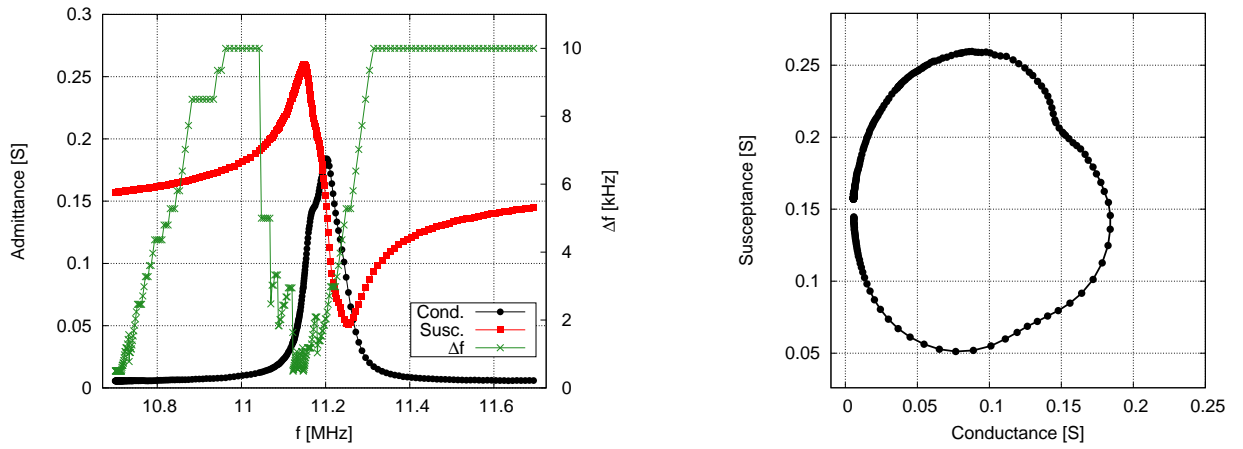
(b) QxSens



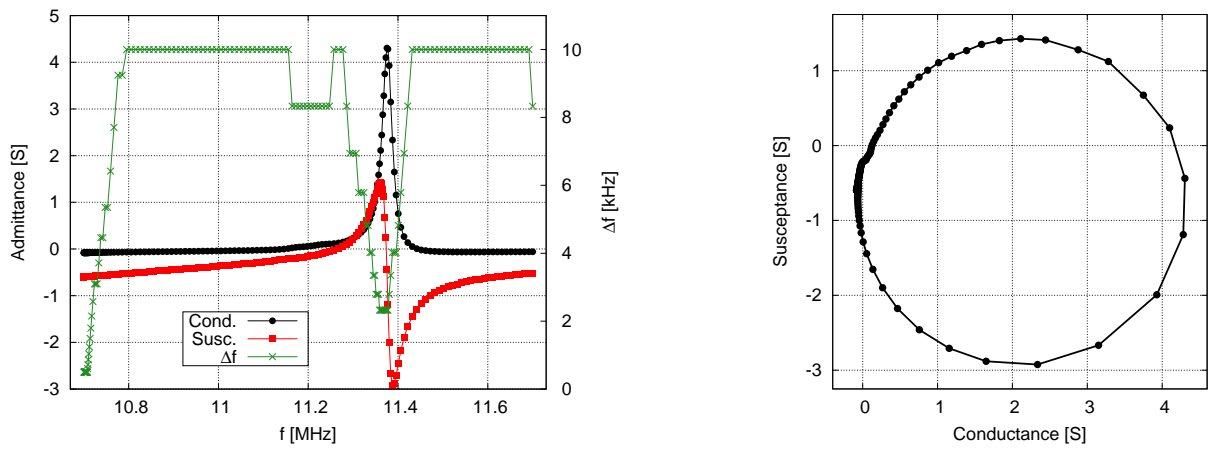
(c) Agilent 4395A

Figure 5.3: Admittance scan of PIC 255 - Resonance B at 6.67 MHz

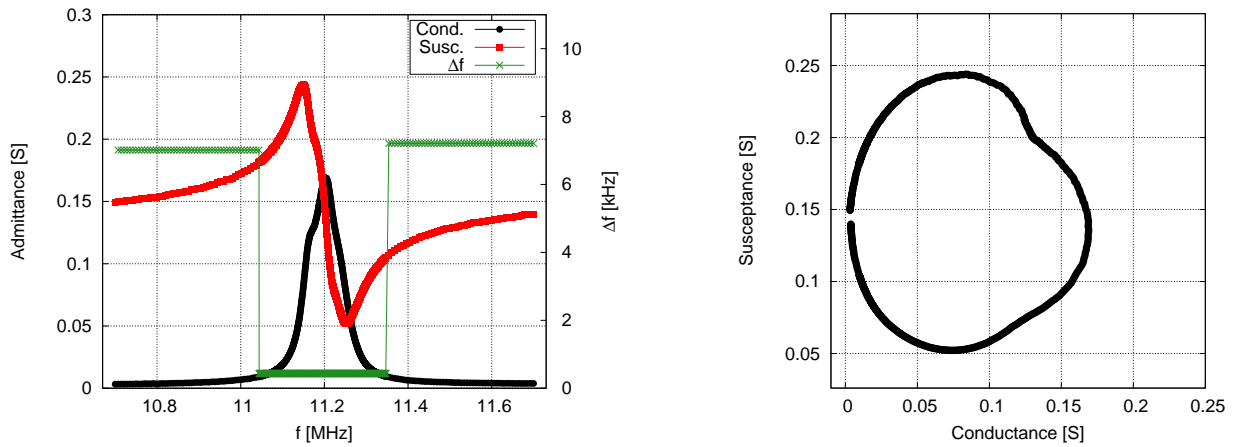
PIC 255 - Resonance C



(a) Impedance Analyzer 16777k (SinePhase)



(b) QxSens



(c) Agilent 4395A

Figure 5.4: Admittance scan of PIC 255 - Resonance C at 11.2 MHz

Resonance A					
	SinePhase	QxSens	Agilent 4395A	SinePhase rel. error [%]	QxSens rel. error [%]
G_{max} [S]	1.409	16.518	1.041	35	1487
f_s [MHz]	2.010143	2.005800	2.011988	0	0
Q	197	334	202	-2	65
f_{HW} [kHz]	10.186	-	9.965	2	-
R_1 [Ω]	1	0	1	0	-100
L_1 [μ H]	15.4	1.1	15.4	0	-93
C_1 [pF]	406	5900	406	0	1353
C_p [nF]	2.8	-38.5	1.8	56	-2239
R_p [Ω]	36.2	-	-	-	-
Time [s]	40	6	42	-5	-86
Resonance B					
	SinePhase	QxSens	Agilent 4395A	SinePhase rel. error [%]	QxSens rel. error [%]
G_{max} [S]	0.287	4.858	0.274	5	1673
f_s [MHz]	6.669537	6.616769	6.676136	0	-1
Q	130	865	122	7	609
f_{HW} [kHz]	51.205	-	54.537	-6	-
R_1 [Ω]	3.3	0.2	3.1	6	-94
L_1 [μ H]	10.2	4.3	12.6	-19	-66
C_1 [pF]	55.7	135.6	45.2	23	200
C_p [nF]	2.3	8.9	2.1	10	324
R_p [Ω]	-	-	-	-	-
Time [s]	25	5	45	-44	-89
Resonance C					
	SinePhase	QxSens	Agilent 4395A	SinePhase rel. error [%]	QxSens rel. error [%]
G_{max} [S]	0.184	4.303	0.169	9	2446
f_s [MHz]	11.197215	11.375779	11.201743	0	2
Q	123	410	115	7	257
f_{HW} [kHz]	90.686	-	97.482	-7	-
R_1 [Ω]	5.4	0.2	5.9	-8	-97
L_1 [μ H]	9.4	1.3	12.4	-24	-90
C_1 [pF]	21.4	148.7	16.3	31	812
C_p [nF]	2.2	-10.6	2.1	5	-605
R_p [Ω]	23.1	-	-	-	-
Time [s]	24	3	43	-44	-93

Table 5.2: PIC 255 - Fit results and error deviations relative to the reference system *Agilent 4395A*

5.1.2 PIC 181

The PIC 181 specimen is a lead zirconate lead titanate material also from the company PI Ceramic GmbH with an extremely high quality factor, which is designed for use in high-power acoustic applications and proved to be successful in piezomotor drives [15]. In the overall scan (fig. 5.5), whereby the hole frequency range of the SinePhase device is used, we can depict seven resonances. Three of them are specifically chosen because of their high quality factors for ceramic type resonators, which lies here in the order of magnitude of 10^3 . They are denoted by the characters *A* through *C* and their individual admittance measurements will be presented in the following graphs.

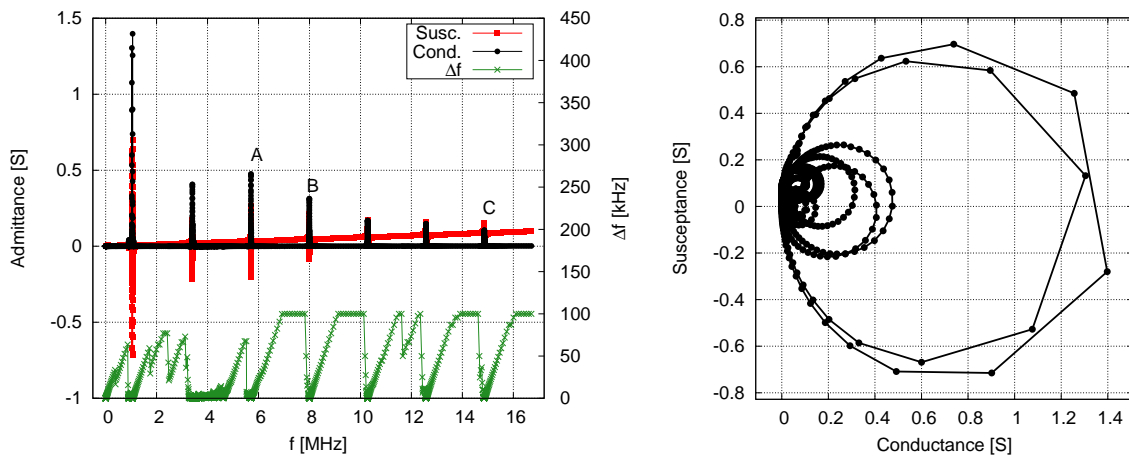


Figure 5.5: Overall admittance spectrum of the PIC 181 measured with the "SinePhase" system in dynamic scan mode; measurement time amounts to 125s ($\approx 2min.$)

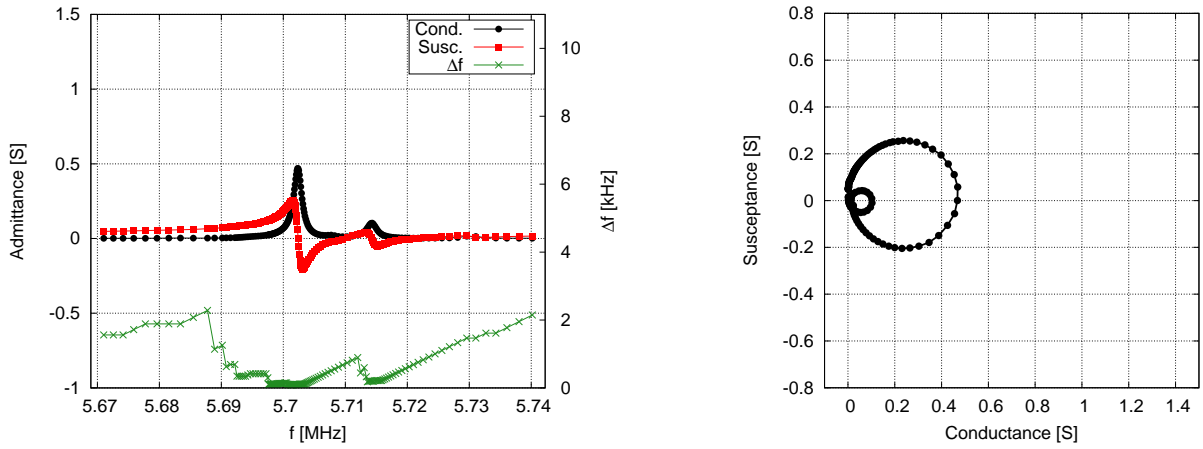
PIC 181 - Measurement input parameters

Overall spectrum:				
	$f_{Start} = 1kHz$		$f_{Stop} = 16.777MHz$	
	Δf_{Min}	Δf_{Max}	Delay time	Probe comp. parameter
SinePhase	100 Hz	100 kHz	1 ms	$R_c=70\text{ m}\Omega$ $L_c=36.8\text{ nH}$ $G_c=1\text{ }\mu\text{S}$ $C_c=2.8\text{ pF}$
Resonance A				
	$f_{Start} = 5.2MHz$		$f_{Stop} = 6.2MHz$	
	Δf_{Min}	Δf_{Max}	Delay time	Probe comp. parameter
SinePhase	100 Hz	10 kHz	1 ms	$R_c=44\text{ m}\Omega$ $L_c=36.7\text{ nH}$ $G_c=0\text{ S}$ $C_c=2.9\text{ pF}$
QxSens	100 Hz	10 kHz	1 ms	internal comp. $R_C=22\Omega$
Agilent	287.1 Hz	8.158 kHz	internal	probe length 100 mm
Resonance B				
	$f_{Start} = 7.5MHz$		$f_{Stop} = 8.5MHz$	
	Δf_{Min}	Δf_{Max}	Delay time	Probe comp. parameter
SinePhase	100 Hz	10 kHz	1 ms	$R_c=82\text{ m}\Omega$ $L_c=36.8\text{ nH}$ $G_c=8\text{ }\mu\text{S}$ $C_c=2.9\text{ pF}$
QxSens	100 Hz	10 kHz	1 ms	internal comp. $R_C=22\Omega$
Agilent	284.3 Hz	8.183 kHz	internal	probe length 100 mm
Resonance C				
	$f_{Start} = 14.3MHz$		$f_{Stop} = 15.3MHz$	
	Δf_{Min}	Δf_{Max}	Delay time	Probe comp. parameter
SinePhase	100 Hz	10 kHz	1 ms	$R_c=95\text{ m}\Omega$ $L_c=36.3\text{ nH}$ $G_c=3\text{ }\mu\text{S}$ $C_c=2.8\text{ pF}$
QxSens	100 Hz	10 kHz	1 ms	internal comp. $R_C=22\Omega$
Agilent	227.1 Hz	9.643 kHz	internal	probe length 100 mm
Further input parameters				
	Overall spec.	Resonance A	Resonance B	Resonance C
SinePhase "Noise Level"	$50\text{ }\mu\text{S}$	$10\text{ }\mu\text{S}$	$10\text{ }\mu\text{S}$	$10\text{ }\mu\text{S}$

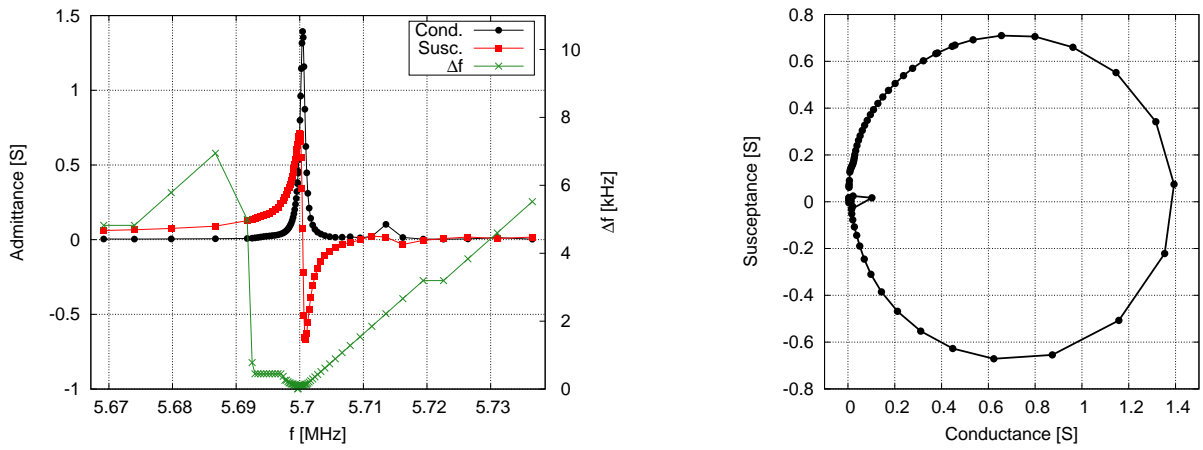
Table 5.3: Summary of the applied input parameters for the PIC 181 sensor

PIC 181 - Admittance measurements and fit results

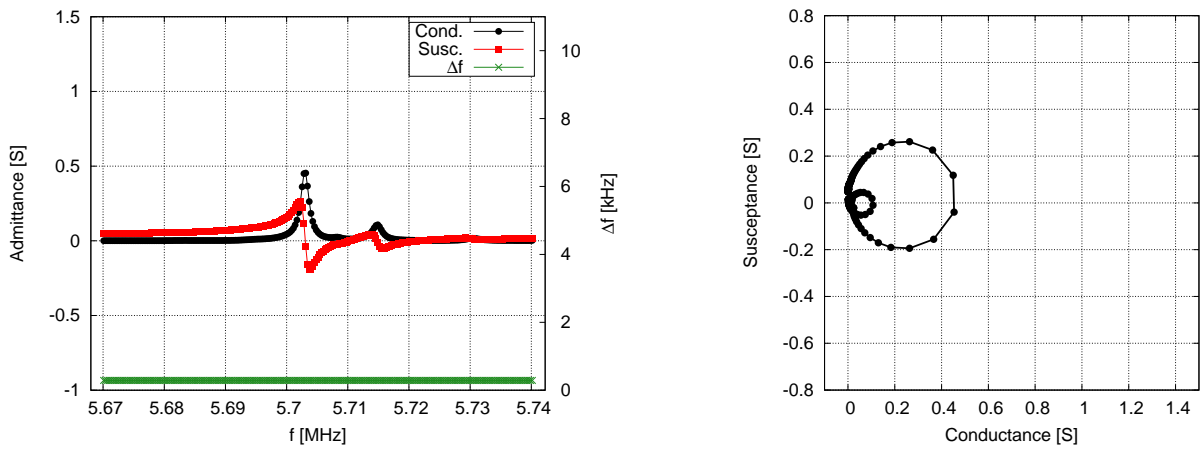
PIC 181 - Resonance A



(a) Impedance Analyzer 16777k (SinePhase)



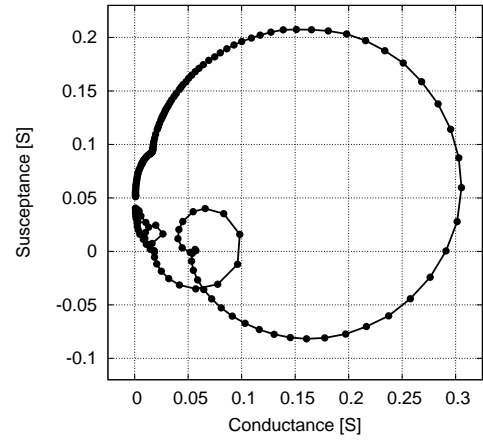
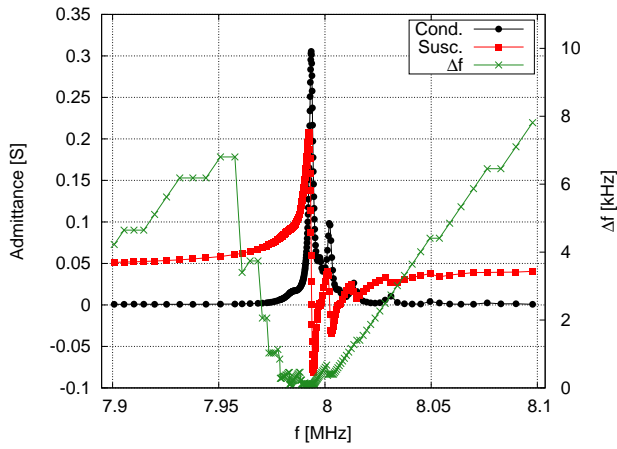
(b) QxSens



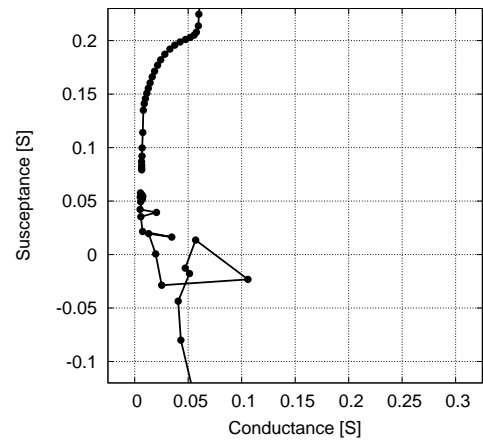
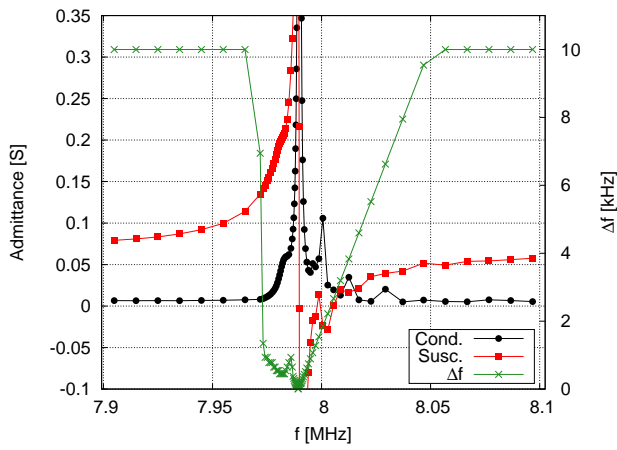
(c) Agilent 4395A

Figure 5.6: Admittance scan of PIC 181 - Resonance A at 5.7 MHz

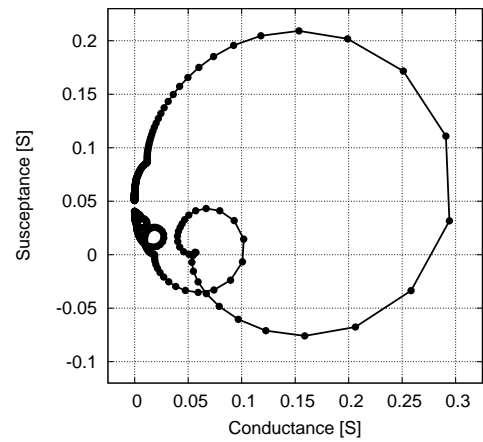
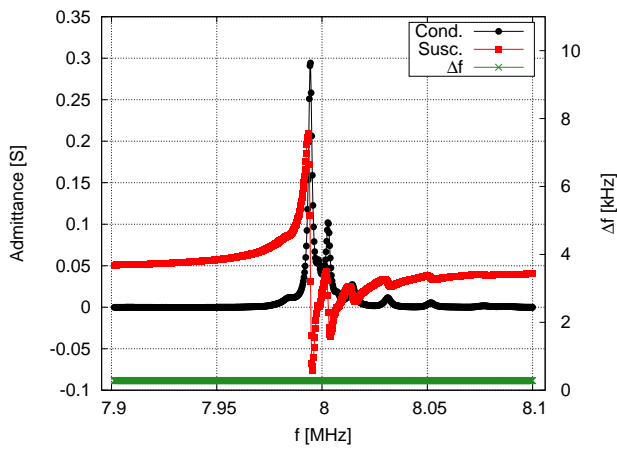
PIC 181 - Resonance B



(a) Impedance Analyzer 16777k (SinePhase)



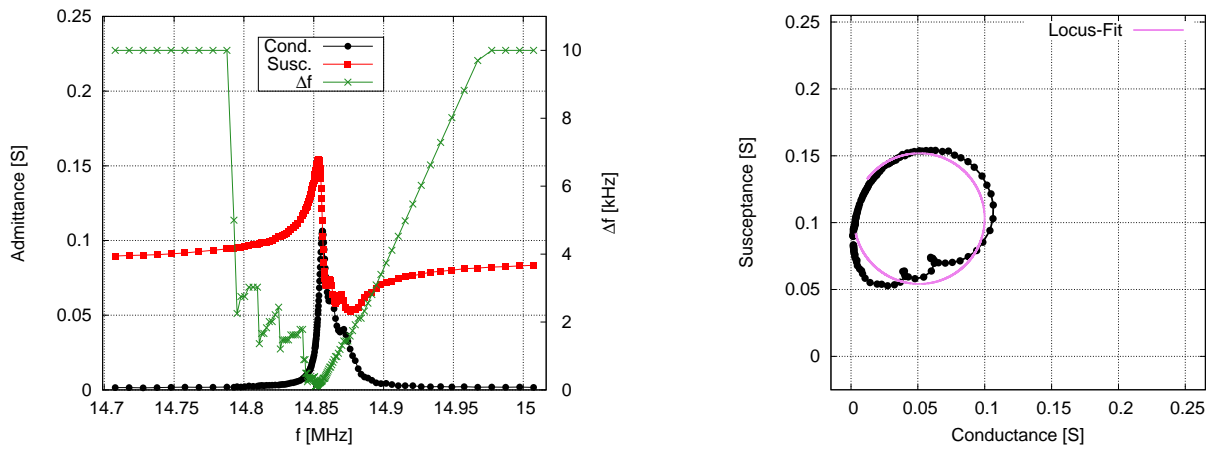
(b) QxSens



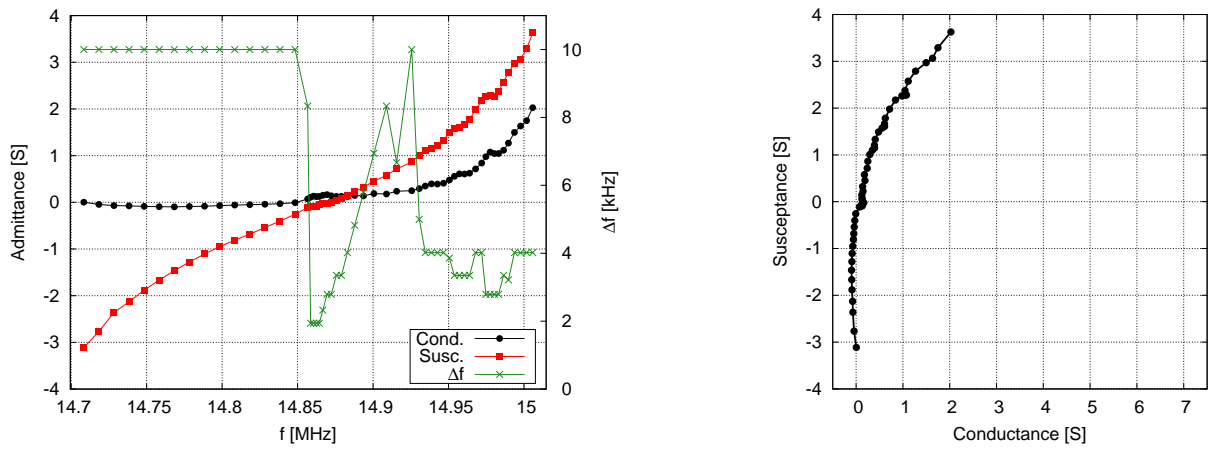
(c) Agilent 4395A

Figure 5.7: Admittance scan of PIC 181 - Resonance B at 7.99 MHz

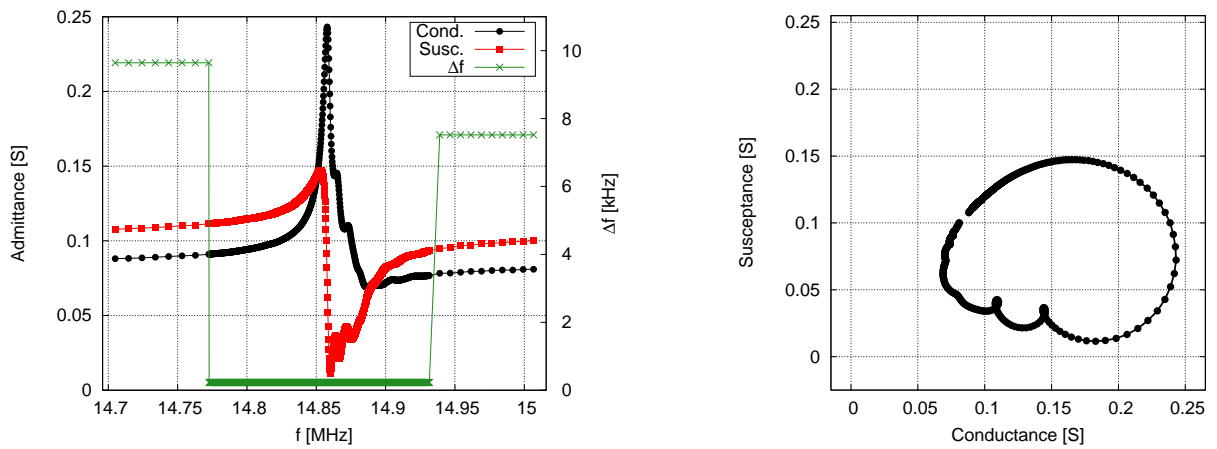
PIC 181 - Resonance C



(a) Impedance Analyzer 16777k (SinePhase)



(b) QxSens



(c) Agilent 4395A

Figure 5.8: Admittance scan of PIC 181 - Resonance C at 14.86 MHz

Resonance A					
	SinePhase	QxSens	Agilent 4395A	SinePhase rel. error [%]	QxSens rel. error [%]
G_{max} [S]	0.469	1.394	0.454	3	207
f_s [MHz]	5.702326	5.700451	5.703121	0	0
Q	3365	6074	3343	1	82
f_{HW} [kHz]	1.695	-	1.706	-1	-
R_1 [Ω]	2.2	0.7	2.2	0	-68
L_1 [μ H]	203.9	122.1	209.5	-3	-42
C_1 [pF]	3.8	6.4	3.7	3	73
C_p [nF]	0.754	0.517	0.635	19	-19
R_p [Ω]	125.6	-	-	-	-
Time [s]	23	8	43	-47	-81
Resonance B					
	SinePhase	QxSens	Agilent 4395A	SinePhase rel. error [%]	QxSens rel. error [%]
G_{max} [S]	0.305	1.349	0.296	3	356
f_s [MHz]	7.993508	7.9897589	7.994530	0	0
Q	3651	6635	3769	-3	76
f_{HW} [kHz]	2.189	-	2.121	3	-
R_1 [Ω]	3.5	0.7	3.5	0	-80
L_1 [μ H]	256.2	99	254.8	1	-61
C_1 [pF]	1.5	4	1.6	-6	150
C_p [nF]	1.4	1.23	0.67	109	84
R_p [Ω]	48.7	-	-	-	-
Time [s]	18	4	43	-58	-91
Resonance C					
	SinePhase	QxSens	Agilent 4395A	SinePhase rel. error [%]	QxSens rel. error [%]
G_{max} [S]	0.106	13	0.243	-56	5250
f_s [MHz]	14.858316	15.025994	14.857906	0	1
Q	829	448	676	23	-34
f_{HW} [kHz]	17.902	-	21.973	-19	-
R_1 [Ω]	10.2	0.1	5.4	89	-98
L_1 [μ H]	0.3	122.1	26.8	-99	356
C_1 [pF]	1.3	366.8	4.3	-70	8430
C_p [nF]	1.1	-16.3	1.3	-15	-1354
R_p [Ω]	477	-	-	-	-
Time [s]	14	5	43	-67	-88

Table 5.4: PIC 181 - Fit results and the error deviations relative to the reference system *Agilent 4395A*

5.2 Quartz crystal resonators

The next type of specimen are quartz crystal resonators with high quality factors ($\approx 10^5$) and low frequency tolerance ($\pm 20ppm$). These are the so called HC49 type U crystals, which indicates the shell size. The resonance frequencies are chosen in a way that three areas of the overall frequency range of the SinePhase device ($1kHz - 16.777MHz$) could be verified by measurements.

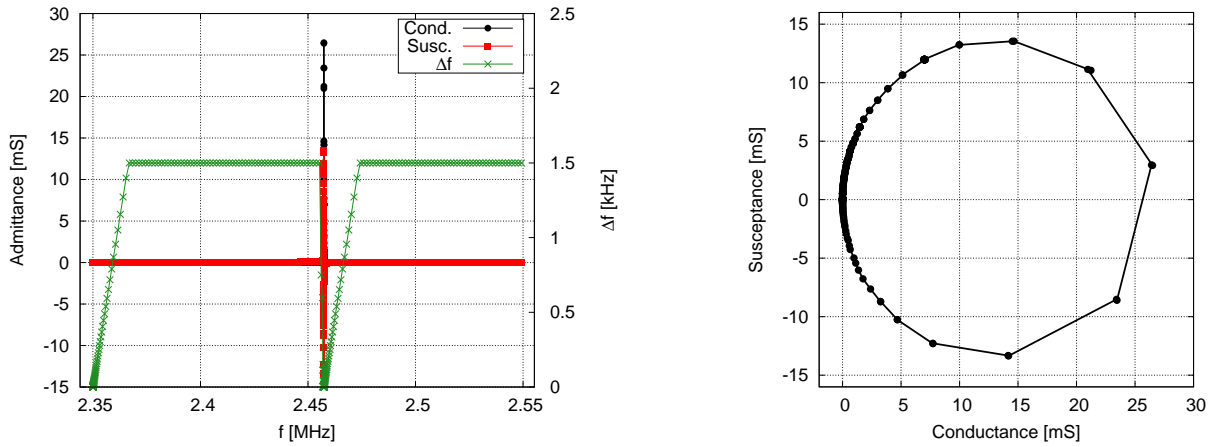
Measurement input parameters

Quartz A				
$f_{Start} = 2.35MHz$ $f_{Stop} = 2.55MHz$				
	Δf_{Min}	Δf_{Max}	Delay time	Probe comp. parameter
SinePhase	1 Hz	1.5 kHz	100 ms	$R_c=101 m\Omega$ $L_c=61.3 nH$ $G_c=10 \mu S$ $C_c=3.91 pF$
QxSens	1 Hz	1.5 kHz	100 ms	internal comp. $R_C=22\Omega$
Agilent	0.05 Hz	2.191 kHz	internal	probe length 3.4 mm
Quartz B				
$f_{Start} = 6.3MHz$ $f_{Stop} = 6.5MHz$				
	Δf_{Min}	Δf_{Max}	Delay time	Probe comp. parameter
SinePhase	1 Hz	7 kHz	10 ms	$R_c=130 m\Omega$ $L_c=58.7 nH$ $G_c=3 \mu S$ $C_c=5.55 pF$
QxSens	1 Hz	7 kHz	10 ms	internal comp. $R_C=22\Omega$
Agilent	6.7 Hz	2.027 kHz	internal	probe length 3.4 mm
Quartz C				
$f_{Start} = 14.5MHz$ $f_{Stop} = 16.777MHz$				
	Δf_{Min}	Δf_{Max}	Delay time	Probe comp. parameter
SinePhase	1 Hz	75 kHz	10 ms	$R_c=150 m\Omega$ $L_c=53 nH$ $G_c=0 S$ $C_c=3.3 pF$
QxSens	1 Hz	75 kHz	10 ms	internal comp. $R_C=22\Omega$
Agilent	10.6 Hz	30.4 kHz	internal	probe length 3.4 mm
Further input parameters				
	Quartz A	Quartz B	Quartz C	
SinePhase "Noise Level"	$10 \mu S$	$10 \mu S$	$10 \mu S$	

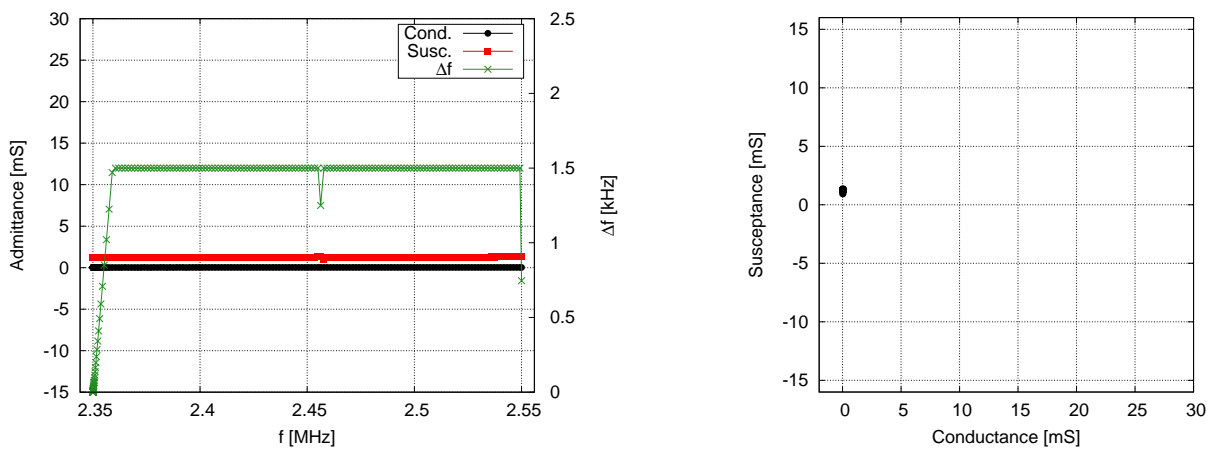
Table 5.5: Summary of the applied input parameters for the quartz crystal resonators A-C

Quartz crystal resonators - Admittance measurements and fit results

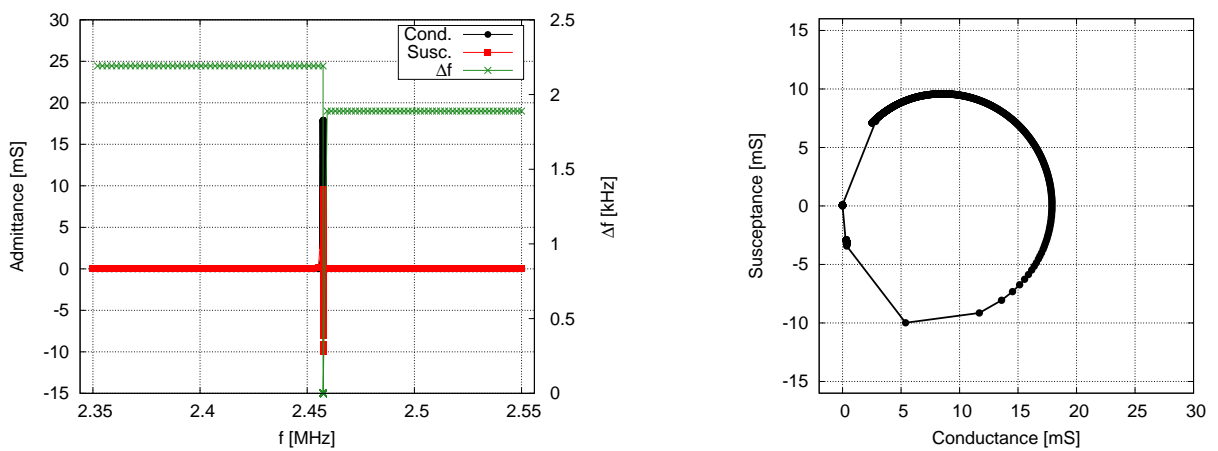
Quartz A



(a) Impedance Analyzer 16777k (SinePhase)



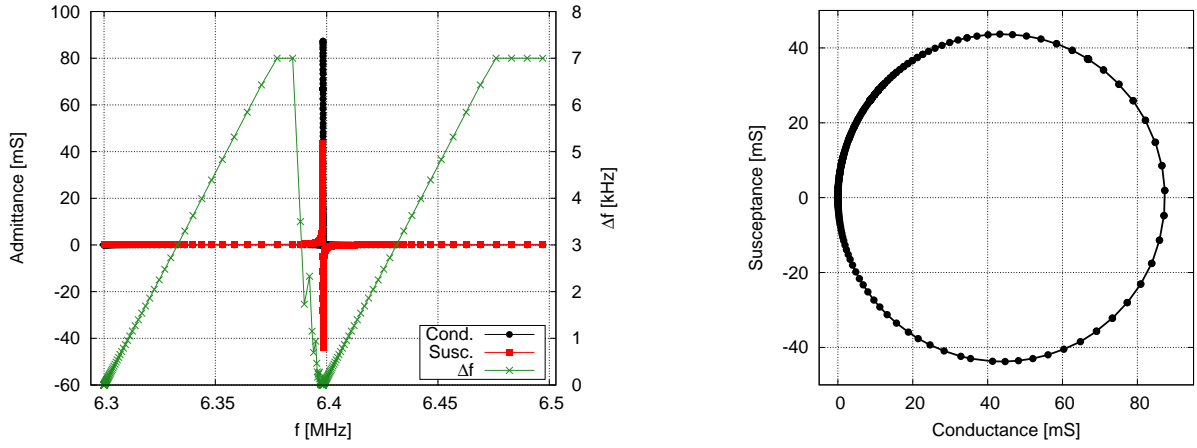
(b) QxSens



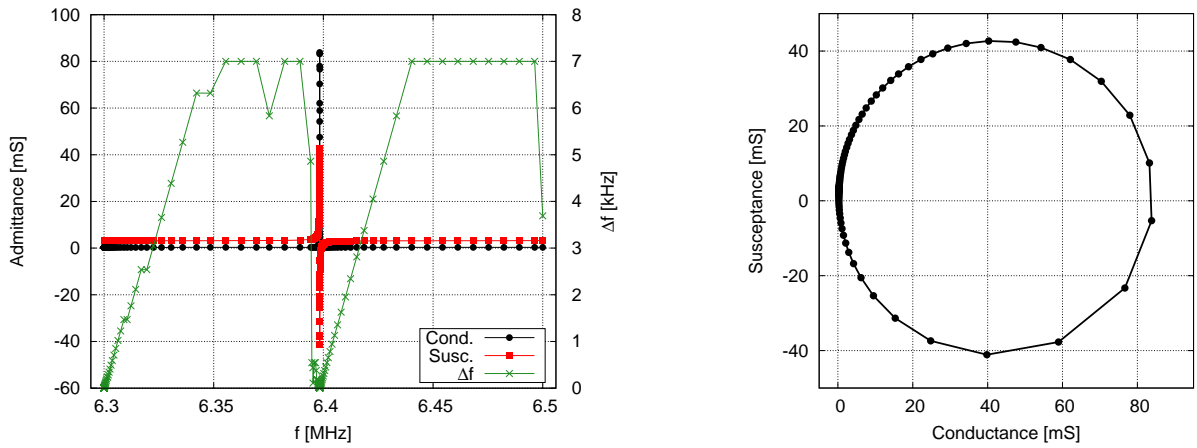
(c) Agilent 4395A

Figure 5.9: Admittance scan of quartz A at the resonance frequency of 2.457 MHz

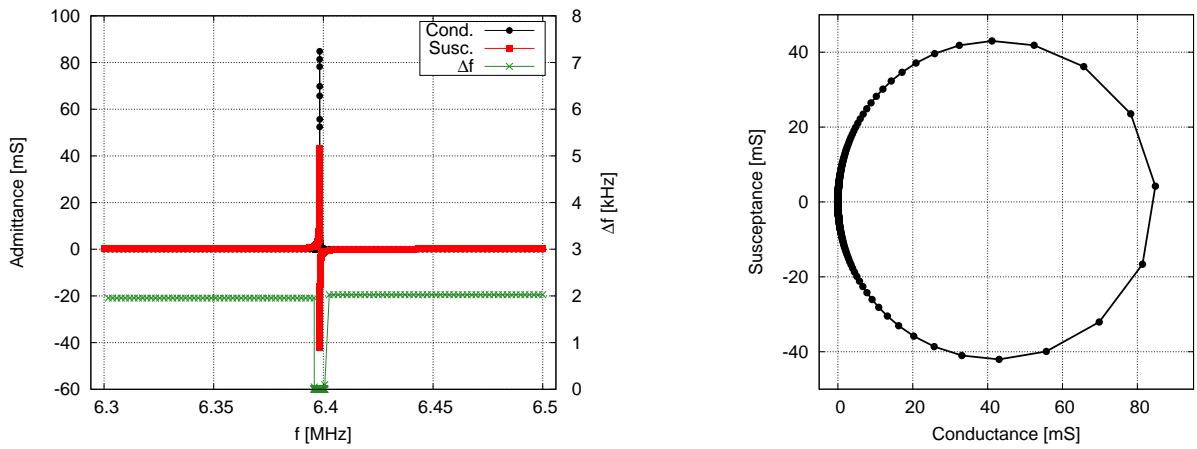
Quartz B



(a) Impedance Analyzer 16777k (SinePhase)



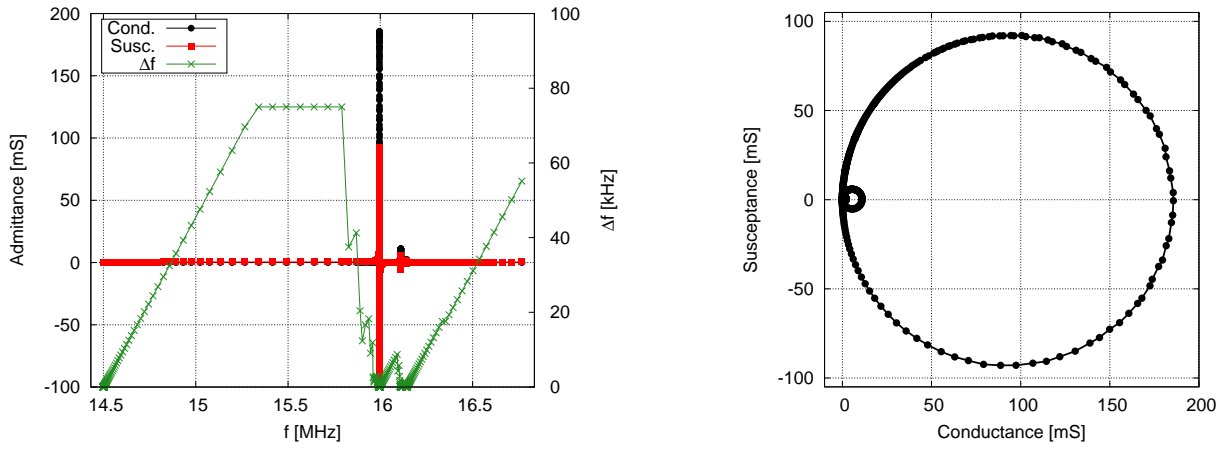
(b) QxSens



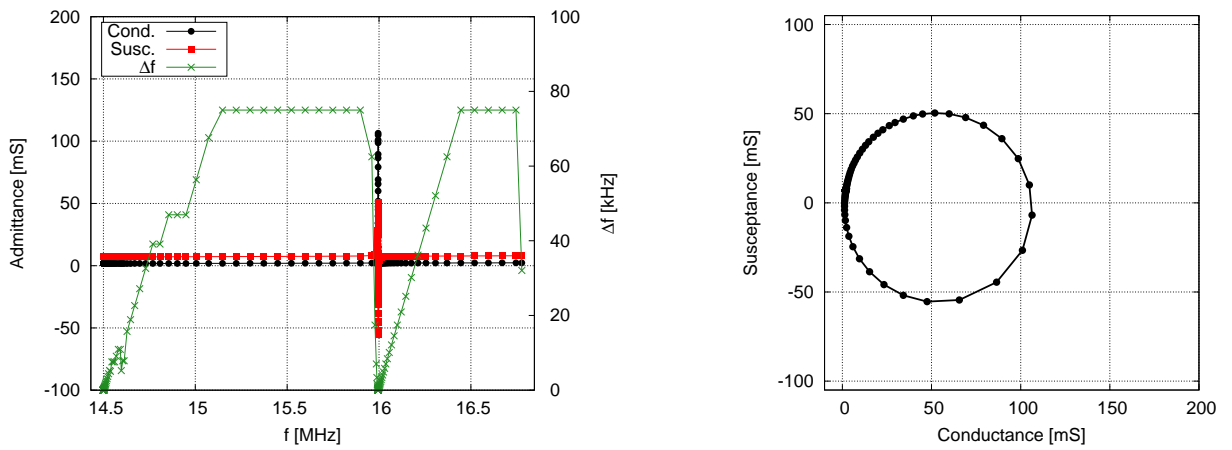
(c) Agilent 4395A

Figure 5.10: Admittance scan of quartz B at the resonance frequency of 6.4 MHz

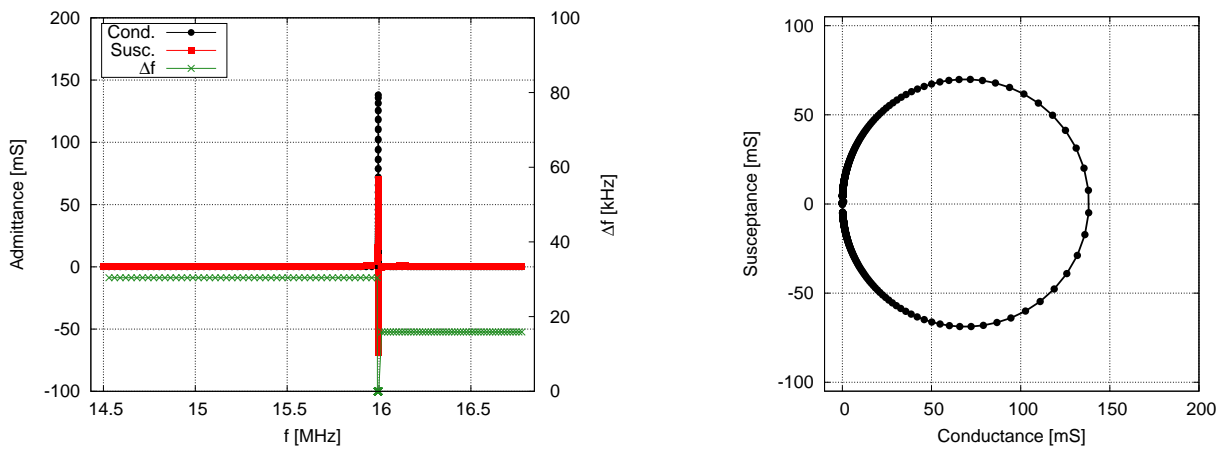
Quartz C



(a) Impedance Analyzer 16777k (SinePhase)



(b) QxSens



(c) Agilent 4395A

Figure 5.11: Admittance scan of quartz C at the resonance frequency of 16 MHz

Quartz A					
	SinePhase	QxSens	Agilent 4395A	SinePhase rel. error [%]	QxSens rel. error [%]
G_{max} [mS]	26.5	-	17.9	48	-
f_s [MHz]	2.457413	-	2.457419	0	-
Q	268310	-	162340	65	-
f_{HW} [Hz]	9	-	15	-40	-
R_1 [Ω]	37.2	-	47.5	-22	-
L_1 [mH]	646.4	-	500.2	29	-
C_1 [fF]	6.5	-	8.4	-23	-
C_p [pF]	7.3	-	59.3	-88	-
R_p [k Ω]	-	-	-	-	-
Time [s]	136	22	45	202	-51
Quartz B					
	SinePhase	QxSens	Agilent 4395A	SinePhase rel. error [%]	QxSens rel. error [%]
G_{max} [mS]	87.3	83.8	84.7	3	-1
f_s [MHz]	6.398369	6.398314	6.398314	0	0
Q	122150	100887	119860	2	-16
f_{HW} [Hz]	52	-	53	-2	-
R_1 [Ω]	11.4	11.9	11.7	-3	2
L_1 [mH]	34.7	29.9	35.3	-2	-15
C_1 [fF]	17.8	20.7	11.5	55	80
C_p [pF]	-1.2	19.7	3.9	-131	405
R_p [k Ω]	59.8	-	-	-	-
Time [s]	68	6	45	51	-87
Quartz C					
	SinePhase	QxSens	Agilent 4395A	SinePhase rel. error [%]	QxSens rel. error [%]
G_{max} [mS]	185.7	106.4	138.2	34	-23
f_s [MHz]	15.995472	15.995005	15.995314	0	0
Q	91534	43402	68655	33	-37
f_{HW} [Hz]	175	-	233	-25	-
R_1 [Ω]	5.4	9.4	7.2	-25	31
L_1 [mH]	4.9	4.1	5	-2	-18
C_1 [fF]	20.1	24.3	20	1	22
C_p [pF]	-4.9	-26	4.4	-211	-691
R_p [k Ω]	5.9	-	-	-	-
Time [s]	91	6	45	102	-87

Table 5.6: Fit results and the deviations relative to the reference system *Agilent 4395A*

5.3 Discussion

Further aspects about the admittance measurement systems

Since there is no possibility to determine the real values of the characteristic parameters of a resonators under test, the *Agilent 4395A* was chosen as a reference device to compare the results of the area detection algorithm and the Locus-Fit procedure with those of the *QxSens* measurement system. It is important to emphasize that the *Agilent 4395A* only have the ability of measuring 801 data points for each frequency range, regardless of the band width size. Therefore in order to have high point densities around resonances with this reference device, the frequency range of interest can be spilt into several segments, whereby the resonance is within a segment with the highest number of points. Hence in the above measurements the frequency range was divided into three ranges, whereby the area of resonance contained 701 data points and the left and right segment to the resonance only 50 points each. Moreover, this can only be applied when the information of the exact resonance frequency is found first. That means the dynamic frequency scan of the SinePhase system must be used to obtain the right frequency range.

The data of the fit results such as the equivalent circuit parameters are not an average of many measurements, rather the results of one single measurement. Nevertheless the reproducibility of each scan was verified consistently with all devices and all sensors under test. Let us now turn to the discussion of each specimen's findings.

Ceramic type sensor PIC 255

It can be seen from the overall admittance chart in figure 5.1, that the area detection algorithm found three distinct resonances within the frequency span from 1 MHz - 12 MHz, which are denoted as *A*, *B* and *C*. The measurement time for such a wide range lies at 69s for a delay time parameter of 10ms. The data here provides high point densities in the range of relevant resonances. The change in frequency steps (Δf), which can be seen from the second y-axes on the right side of the overall admittance diagram, shows a constant increase between resonances almost up to the maximum step width of $\Delta f_{Max} = 300kHz$ (see tab. 5.1) and a rapid decrease down to the minimum value of $\Delta f_{Min} = 1kHz$, when approaching a relevant resonance peak. An important observation is, that the slope for the decrease is higher than the one for the increase to avoid skipping relevant segments of the spectrum.

When one compares the admittance- and locus graph of the resonances *A*, *B* and *C* from the SinePhase system with those of the Agilent reference device, one can see very similar data plots in terms of conductance and susceptance values (see fig. 5.2, 5.3 and 5.4). This findings can be confirmed by the fit results in table 5.2. The numbers show very small deviations of the SinePhase data from those of the Agilent system for the resonance frequency f_s , *Q* factor, frequency half width f_{HW} and the equivalent circuit parameters R_1 , L_1 and C_1 , which incidentally amounts to zero for resonance *A*. Furthermore, the measurement time of the SinePhase device is also less than the sweep time of the Agilent system. On the contrary the data of the QxSens

measurements seem to suggest errors in the calculation of the admittance values, as well as the fit parameters. In general the conductance and susceptance figures are between 15 and 20 times the values of the other two measurement systems. As we can see from the table 5.2 the PIC 255 has very low impedance values for R_1 , which lies between 1Ω and maximal 6Ω . The kernel electronics of the *QxSens* measurement system is based on a voltage divider principal and measures the voltage drop of the series resistor R_C , which has a fixed value of 22Ω . This leads to high voltage drops on the resistor rather the resonator under test and therefore measuring inaccurate values for the admittance. Here we can see very well the limits and inflexibility of the *QxSens* system, because even when we used smaller series resistors for R_C , the current would become to high and may damage the sensor. Furthermore, several noteworthy results were also that for resonance *A* despite the low Q factor and high frequency half width of $10kHz$, the point density around the resonance was not sufficient enough with the *QxSens* device. The huge differences in the locus curves compared to the other devices in *B* and *C* can be easily depicted for the *QxSens* diagrams. Lastly, although the measurement time amounts to maximal $6sec.$, the enormously large deviations in the fit data, which for example in *C* is 2% for the resonance frequency (the most important quantity), demonstrates that the *QxSens* system is not reliable for measuring the PIC 255 ceramic sensor.

The separation of the frequency range into three segments with different number of data points, explains the high point densities in the locus curves of the Agilent graphs and leads to relatively small frequency steps from $200Hz$ up to $400Hz$ within resonances (see. tab. 5.1).

Ceramic type sensor PIC 181

The admittance spectrum in figure 5.5 is also measured with the SinePhase system and demonstrates the overall possible frequency range for that device ($1kHz - 16.777MHz$). The input parameter for the maximum frequency step Δf_{Max} was chosen $100kHz$ and is 1000 times the number of the minimum value of $100Hz$. Despite this great dynamic range, the point density around all seven detected resonances is high enough to perform the Locus-Fit procedure in the overall spectrum to get accurate results. As can be depicted from the admittance diagram and locus, the circles are getting smaller in diameter and the influence of the parallel capacitance C_p moves them up at higher frequencies, hence leading to the increase of susceptance. Therefore resonance *C* serves as a good example, where the imaginary part does not cross zero and still the area detection algorithm works accurate enough to decrease the frequency step width to the minimum value. The measurement time for the hole spectrum amounts to just over two minutes for a delay time of $1ms$ (see. tab. 5.3). It is important to emphasise here that the "Noise Level" was set to $50\mu S$, therefore leading to more tolerance in conductance changes. Taking into account that for more segments of the scan the frequency step width was increased, the measurement time decreases as a result. That means the "Noise-Level" parameter can be used to reduce the measurement time. Let us now turn to the findings of the three specific resonances also denoted as *A*, *B* and *C*. The implications of the

visual inspection of resonance *A* and *B* (fig. 5.6 and 5.7) illustrates once again very similar measurements for the SinePhase and Agilent devices. This can be verified by the numbers from table 5.4, which shows that the relative error lies with a few percentage for the fit results. The last resonance example *C* reveals that the form of the locus curve is similar to the one of the Agilent, but it seems to be rotated 45° to the left and is smaller in the admittance values for the SinePhase measurement. Moreover, the resonance contains mode couplings and the Locus-Fit, which is also plotted in the locus diagram in this case (see fig. 5.8(a)), yields relative high deviations. This can be explained by the high influence of spurious effects at high frequencies, which is at approximately $15MHz$ in this example. The results of the present study demonstrates again that the admittance values of the QxSens system tend to have to high admittance values. The cause here is again the big ratio between the kernel electronics series resistor R_C and the low-ohmic values of R_1 for the PIC 181. For resonance *A* and *B* the maximum conductance values (G_{max}) is three and four times the figures for the other devices respectively. The data for *C* reveals an even greater difference, whereby the values diverges so far that it becomes 130-fold the peak values of the compared systems. According to the fit data the relative errors are also enormous for the *QxSens* system and again the last resonance deviates by 1%. These findings show the limits and low flexibility of the voltage divider principal used in the *QxSens* method. It reveals that the resistance value ranges of an unknown sensors resonance must be known in advance in order to optimise the resistor R_C for the kernel electronics in the *QxSens* measurement system, which of course is a big disadvantage, despite the low measurement time. On the contrary the results show that the SinePhase system is much more flexible in its measurement principal and does require any hardware changes. The only requirement is the probe compensation (cable compensation) prior to a measurement, which is performed with the user software.

Quartz crystal resonators

The delay time of $100ms$ (see tab. 5.5) for quartz *A* seem to suggest a very high quality factor. The choice of the minimum frequency step of $1Hz$, which is the highest frequency resolution, indicates this. The difference of the step widths input parameters amounts to a factor of 1500 and as can be seen from figure 5.9(a) the dynamic scan mode is able to track the resonance peak very well. Furthermore, the collected set of data points around the resonance is enough to perform an accurate fit. Several noteworthy results from the fit data in table 5.6 for quartz *A* are the very high quality factor of $2.7 \cdot 10^5$ with the SinePhase system, the very low values of $9Hz$ for the frequency half width, which makes the scan very challenging considering the frequency range of $200kHz$ and that the QxSens measurement could not find the resonance with the same input parameters. The cause for the last finding could be the similar slope rates for the increase and decrease of the frequency step widths in the QxSens method. However the deviations between the SinePhase results and the Agilent are substantially high. Since the quality factor for the Agilent fit is smaller than that for the SinePhase, one explanation could be an inaccurate segmenting

of the frequency range (see fig. 5.9(c)), which led to an irregular point density within the resonance half width.

The measurements for quartz *B* at the resonance frequency of $6,4\text{MHz}$ are for the first time in this study very similar for all devices, as can be seen in the spectra in figure 5.10. The gap between Δf_{Min} and Δf_{Max} is even higher in this case (7500). Nevertheless, the quality factor still amounts to $1.2 \cdot 10^5$ at a resonance half width (f_{HW}) of approximately 50Hz and a frequency range of 200kHz (tab. 5.5). The smaller delay time of 10ms was enough to consider the settling time of the crystal oscillator and therefore avoid transient effects. When one compares the admittance spectra from figure 5.10(a) and 5.10(b), one can see very well that the slope rates for the step width increase (Δf) is higher for the QxSens system than for the SinePhase algorithms, which is a major factor for the big differences in the measurement time. However the data for quartz *B* in table 5.6 shows once again that the SinePhase measurements are far closer to the values of the Agilent reference system.

The last quartz crystal resonator *C* has his resonance frequency at 16MHz , which is at the edge of the possible frequency range of the SinePhase measurement device. The remarkable finding here is that despite the relative wide scan range of approximately 2.7MHz for a resonance with the frequency half width of 175Hz , the area detection algorithm as well as the QxSens method could detect the resonance peak with high point density despite the very large difference of $7.5 \cdot 10^4$ between Δf_{Min} and Δf_{Max} . Moreover due to the fact that the gradient of the first method is smaller, the SinePhase device could also detect a smaller neighbouring resonance, whereas the QxSens skipped over that peak. All locus figures reveal quite noticeable differences in the amplitude of the conductance, which can again be the results of spurious effects and the different methods of probe compensation. Due to the fact that quartz resonators have longer settling time and therefore the delay time must be set higher, the measurement time is higher for the SinePhase system than the other two devices, but still in a very acceptable range considering the high frequency resolution.

Chapter 6

Conclusion and Recommendations

We opened this work by noting that the algorithm implemented in *QxSens* software did not reveal the same results, when programmed for the *Impedance Analyzer 16777k* from SinePhase, because the point density around resonances was too low and for some input parameters it was stuck in an endless loop. Several attempts, such as the "Zero-crossing" method, whose trigger was the interception of the susceptance with the x-axis at the resonance frequency and the idea of monitoring the admittance phase angle for a certain value had to be discarded due to the weakness of considering the influence of the parallel capacitance at high frequency ranges. In order to detect resonances with various quality factors and mode couplings if need be, the importance of detecting the change in phase angle of the admittance vector was crucial to develop the idea behind the area detection algorithm, which calculated the area difference between two triangles spanned with three admittance vectors. This solved also the critical problem of considering the displacement of the admittance circle to higher susceptance areas due to the spurious effects of the parallel capacitance. Since the area change detection in the locus diagram was almost not affected by a shift of the circle centre by B_p , this algorithm has proven to be successful also at high frequency ranges. Furthermore, the concept of comparing the area difference of the last two triangles in the locus curve with the moving average of the last 28 differences, defined two slope criteria for detecting resonance peaks. These decision rules for increasing and decreasing the frequency steps during an admittance scan were found by empirical tests with various piezoelectric sensors and further to make sure not to skip relevant resonances the rising gradient was chosen smaller than the falling slope rate.

The implemented "Locus-Fit" works very accurately and can fit a circle into the measured data even, when there is only one measurement point within the frequency half width of a resonance. The comparison of the fit results such as the equivalent circuit parameters with the reference device *Agilent 4395A* in chapter 5 confirms the high accuracy and consistency of this fit algorithm.

The arguments given above prove that the *Impedance Analyzer 16777k* from SinePhase combined with the area detection- and "Locus-Fit" software fulfil the requirements set out in the beginning of this work. It offers first and foremost a truly mobile, low-cost and easy to use measurement system to plot admittance

spectra of various piezoelectric sensors with a dynamic scan algorithm at similar accuracy as the commercial impedance analyzer *Agilent 4395A*. A further distinguish advantage of this program is a user-friendly implementation for analysing, inspecting and calculating fit parameters of all resonances contained in the scanned spectra.

One important application that could be developed based on the resonance detection algorithm is a time tracking algorithm of the resonance frequency and quality factor. As stated in the introduction a change in those two characteristic quantities can be used to calculate physical measured variables such as viscosity, temperature, density of liquids, film thickness, etc [1]. Depending on the frequency range and the type of sensor used, the tracking software must be able to detect changes in the admittance spectra due to the changes of the specific physical quantity in the magnitude of seconds. Furthermore, a database of characteristic curves can be stored for each type of sensor and measured parameter, which could be used to compute the above physical quantity and also be able to trace the changes of that variable in time.

Bibliography

- [1] **Nowotny H., Benes E.**
General one-dimensional treatment of the layered piezoelectric resonator with two electrodes;
J. Acoust. Soc. Am., **Vol. 82**, No. 2, August 1987, pp. 513-521
- [2] **Schnitzer R.**
Development of a microprocessor controlled multi-channel measurement system for resonant piezoelectric sensors;
Thesis (PhD), Vienna University of Technology, 2006
- [3] **Fritscher G.**
Ultrasonic enhanced IR sensor;
Thesis (Bac), Vienna University of Technology, 2011
- [4] **Gröschl M.**
Ultrasonic Separation of Suspended Particles - Part I: Fundamentals;
ACUSTICA, **84**, 1998, pp. 432-447
- [5] **Schmid M., Benes E., Sedlaczek R.**
A computer-controlled system for the measurement of complete admittance spectra of piezoelectric resonators;
Meas. Sci. Technol. **1**, 1990, pp. 970-975
- [6] **Agilent Technologies**
*Agilent 4395A Network/Spectrum/Impedance Analyzer
Operational Manual;*
Agilent Technologies Japan, Ltd., 2001
- [7] **sine.phase**
*Impedance Analyzer 16777k
User Manual 2.2;*
sine.phase instrumentation technology, Revision 91102
- [8] **Arnau Vives, A**
Piezoelectric Transducers and Applications;
2nd ed. Springer-Verlag Berlin Heidelberg, 2008, pp. 63-72

- [9] **Holland R., EerNisse E.P.**
Accurate measurement of coefficients in a ferroelectric ceramic;
IEEE Trans. Ultrason., **SU-16**, 1969, 173-81
- [10] **ANSI/EIA**
Standard methods for measurement of the equivalent electrical parameters of crystal units, 1 kHz to 1 GHz;
EIA Standard 512 (Washington DC: Electronic Industries Association), 1985
- [11] **Williamson J. R.**
An improved method for measuring quartz crystal parameters;
IEEE Trans. Ultrason. Ferroelec. Freq. Contr., **UFFC-34**, 1987, pp. 681-9
- [12] **IEEE**
Definitions and methods of measurement for piezoelectric vibrators;
IEEE Standard, **No 177**, (New York: IEEE) equivalent to ANSI C83.17, 1970
- [13] **sine.phase website**
Z-Check 16777k impedance analyzer [online];
SinePhase Instruments GmbH, [viewed 23/12/2112].
Available from: <http://www.impedanceanalyzer.info/>
- [14] **Kliche T.**
Evaluation of Admittance Spectra of Resonant Piezoelectric Crystals;
Master thesis, Vienna University of Technology, 2008
- [15] **PI Ceramic website**
Advanced Piezo Materials, for Standard and OEM Components and Assemblies [online];
PI Ceramic GmbH, [viewed 25/01/2113].
Available from:
http://www.piceramic.com/piezo_materials_1.php